SAND79-7116
Unlimited Release
Printed January 1980

Category UC-66c

WELLBORE AND SOIL THERMAL SIMULATION FOR GEOTHERMAL WELLS: COMPARISON OF GEOTEMP PREDICTIONS TO FIELD DATA AND EVALUATION OF FLOW VARIABLES*

PART II REPORT

Gary R. Wooley
Enertech Engineering and Research Co.
Houston, Texas 77098

ABSTRACT

A better understanding of downhole temperatures in a geothermal well will improve many aspects of well design. This report presents the results of testing and application of the computer code GEOTEMP, which predicts these downhole temperatures.

*Work performed under Sandia Contract No. 13-0212; sponsored by U.S. Department of Energy, Division of Geothermal Energy.

3,4

DISCLAIMER

Table of Contents

I Summary

A. Objective

Downhole temperatures are a necessary part of the design of any well for drilling, completion, and injection or production. In geothermal wells, downhole temperatures are more difficult to determine than in petroleum wells, and are more important for design because of the extreme conditions. A better understanding of temperatures in a well is needed to improve casing selection, cement design, drilling fluid formulation, packer selection, and many other aspects of well design.

A computer code called GEOTEMP has been developed to predict downhole temperatures in geothermal wells. This report presents the results of testing and application of the code. There are two objectives to the effort described herein:

1. Test GEOTEMP to establish its capability to accurately predict downhole temperatures.

2. Determine the importance of certain well variables on downhole temperatures.

B. Work Description

This report presents two applications of GEOTEMP which provide the calculations needed to meet the above objectives. First, the results of testing GEOTEMP predictions with analytical solutions and with field temperature data are presented. And second, sensitivity studies establish the importance of certain well variables on downhole temperatures.

An exact analytical solution for radial transient heat conduction is plotted for comparison to GEOTEMP predictions. Good agreement is achieved between computer calculation and exact solution, and convergence of GEOTEMP predictions is demonstrated as time step size is reduced. In addition, convergence of solutions is shown as the vertical grid spacing is reduced for an example well. These calculations demonstrate that the energy balance equations are formulated and coded properly.

Another test of GEOTEMP is performed by comparing predictions to field temperature data. Existing temperature data was obtained for several wells from both the petroleum and geothermal industries. Two sets of data from each industry are reported, GEOTEMP predictions are plotted, and interpretations of similarities and differences are presented. Good agreement between measurements and predictions is obtained, and some very interesting differences are interpreted. The ability to accurately compute downhole temperatures for field conditions demonstrates that the important physical phenomena are accounted

for in the model.

Having established GEOTEMP's ability to accurately compute temperatures, the code is used to evaluate the importance of seven well variables with regard to downhole temperatures. All seven variables are investigated for injection, production, forward circulation, and reverse circulation. Sensitivities are presented for each variable with two plots, a transient bottom-hole temperature (surface temperature for production), and a steady temperature-depth profile. These curves are plotted for two values of each variable.

C. Conclusions

Calculations presented in this report establish many important results. Some general conclusions are presented based on code testing, and numerous specific conclusions result from the sensitivity studies. Code testing establishes the following conclusions:

1. Improved well design can be achieved with a better understanding of downhole temperatures in a well. Applications include cementing, logging, casing design, drilling fluid formulation and many others.

2. A computer model is needed to accurately predict the full range of transient downhole temperatures in a well. Field measurements do not provide complete data, and simple calculations do not account for the many factors affecting downhole temperatures.

3. GEOTEMP can accurately predict downhole temperatures in a flowing well. Good agreement between predictions and field data demonstrates capability.

Many detailed conclusions may be drawn from the numerous sensitivity studies, but only the more decisive conclusions are presented here. These apply to the well conditions of the calculations, 4-1/2" tubing, 9-5/8" casing, 5000 foot well, 10 lb/gal fluid entering the well at the surrounding earth temperature, and at a flow rate of 200 gal/min for circulation and 1000 BPD for production and injection. The same conclusions can also be extended to other well conditions, if carefully applied. Following are the conclusions resulting from the sensitivity study:

4. Flow rate is important for all flowing conditions. At low rates fluid temperature parallels the undisturbed geothermal temperatures, and at high rates the fluid travels through the well with essentially no change in temperature. The impact of flow rate is reduced in deeper wells.

5. Inlet temperature plays an important role in determining downhole temperatures for high rate wells, but for low

rate wells fluid soon reaches the temperature of the surrounding earth, regardless of the inlet. The effect of inlet temperature is reduced in deeper wells.

6. Fluid density can effect downhole temperatures, but not dramatically. During circulation with low inlet temperatures, lighter fluids produce cooler downhole temperatures. However, during injection the reverse is true.

7. Fluid plastic viscosity has only a small impact on downhole temperatures. During production and injection the effect is negligible in a range of 15 to 50 centipoise. During circulation more viscous fluids result in slightly cooler downhole temperatures.

8. Undisturbed formation temperature gradient has a very strong influence on downhole temperatures. Circulating at 200 gal/min, with a gradient of 2.6°F/100 ft the bottom hole fluid temperature is 40°F higher than with a gradient of 1.1°F. The deeper the well, the more important this variable becomes. But at high rates the importance of this variable is reduced.

9. Thermal conductivity of the soil surrounding a well has only a small effect on downhole temperatures. For a 5000 foot well with circulation at 200 GPM, the bottom hole temperature changes 5°F for a range of thermal conductivity from 0.5 to 4.0 BTU/hr ft °F. During production and injection this temperature change is even smaller. The impact of soil thermal conductivity is increased for deeper wells and lower flow rates.

10. Well depth strongly influences downhole temperatures under all flowing conditions. Of course, deeper wells have warmer flowing fluid temperatures. During injection, total well depth does not effect fluid temperatures at any particular depth, but for production and circulation total well depth is important to fluid temperatures at every position in the well.

D. Recommendations

Based on the results presented in this report and on experience gained through applications of GEOTEMP, the following recommendations are made for further study:

1. Improve GEOTEMP to handle simultaneous gas and liquid flow. Flowing fluids may contain air, CO_2, steam, or other gases. Air, mist, and foam drilling are important applications.

2. Extend GEOTEMP to include flashing of liquid into gas. Flashing can occur in the return stream of a circulating liquid, and in production fluid.

3. Expand GEOTEMP to provide more flexibility. Improvements include variable flow area, deviated holes, more complex geothermal gradients, variable fluid loss depth, and others.

4. Apply GEOTEMP to specific well histories to provide downhole temperatures during drilling, completion, and production.

5. Develop correlations for graphical representations of GEOTEMP results. Under certain conditions computer calculations may be replaced with readings from a graph, chart, or table.

II Introduction

A. Background

High temperatures occuring in geothermal wells influence many aspects of well design including

- design of casing cements
- thermal expansion and contraction of tubing and casing
- formulation of drilling fluids
- interpretation and design of well logs.

An improvement in predicting downhole temperatures will naturally improve well design.

Determining downhole temperatures is a difficult task, made complex by the large number of variables that influence temperatures. Wells drilled in hostile environments, such as geothermal wells, require accurate information on downhole temperatures, but understanding temperatures is complicated by the extreme conditions. Many temperature recording devices have been developed, but measurements provide only isolated data points for a quantity dependent on both time and position. Also, the effect of a specific variable on downhole temperatures is difficult to isolate with measurements.

Therefore, a means of predicting downhole temperatures for specific conditions would be valuable. Early attempts at such calculations involved simple analytical formulations or correlations of experimental data. However, subsequent experience revealed that a computer code is necessary to properly account for the complex nature of heat transfer in and near a flowing well. Several computer codes have been developed for specific applications, but most were developed by major oil companies and are not available for public use. Those that are available are not very flexible, and do not accurately model highly transient flow, [1].

B. Project Review

In June 1978, Enertech Engineering and Research Co. contracted with Sandia Laboratories to provide a flexible and easy to use

computer code capable of predicting downhole temperatures in transient flowing geothermal wells. There were four basic objectives of the study.

1. Develop a thermal simulator for computing downhole temperatures

2. Acquire field temperature data for flowing and shut-in conditions

3. Test computer code with analytical solutions and field data

4. Establish sensitivity of downhole temperatures to important well variables.

GEOTEMP is the result of objective 1. It is a computer code to predict downhole temperatures in geothermal wells. Development of the code has been documented during the course of the study, but a summary of its construction is presented here. Code development was completed in December 1978, and a Part I report was presented to Sandia documenting the first phase of the work, [2]. More details are available in a technical paper describing the code and applications, [3]. GEOTEMP was operational in December. Although not in its final form the code did possess all of the necessary capabilities. During January of 1979 the code was "cleaned up" for other users, and a user manual was prepared. A deck of computer cards for GEOTEMP and a user manual with input formats, example printouts, and a fortran listing of the code were presented to Sandia at the end of January, [4].

Objective 2 was satisfied with data presented in the Part I report and in subsequent monthly progress reports. Field temperature data has been acquired from geothermal and petroleum wells for both flowing and shut-in conditions. These data provide well descriptions, flow histories, and surface and downhole temperature measurements.

Many petroleum industry sources have been contacted to obtain field temperature data. Major and independent producing companies, service companies, and the American Petroleum Institute have all been contacted. Data has been reviewed for drilling, shut-in, circulating, injecting, and producing wells. Petroleum industry companies contacted include the following:

1. Schlumberger
2. Halliburton
3. Dresser Industries
4. Gulf Oil
5. IMCO Services
6. Kirby Petroleum

Some of these contacts provided excellent data for comparison to computer predictions, some claimed to have data but would not release it, and others simply did not have satisfactory data.

Considerable effort was made to obtain field temperature data from operators of geothermal wells. In view of the relatively few number of geothermal wells compared to the vast petroleum industry experience, there is a much smaller base from which to obtain data. Yet, on the other hand, many of the geothermal projects tend to be research oriented, so more precise data is likely to be recorded. Our search for data revealed temperature records on several wells. Although there are complex temperature histories to be interpreted, some useful data has been derived.

Contact has been made with several geothermal operating companies including the following:

1. Battelle Northwest
2. Republic Geothermal
3. Los Alamos Scientific Laboratories
4. General Crude

Some useful temperature records have been obtained, some data is not complete enough to simulate, and other companies simply did not have any data.

This document provides results to satisfy objectives 3 and 4 presented above. Field temperature data has been compared to GEOTEMP predictions for the well conditions when data were recorded, and the results are presented in Section III. In addition, GEOTEMP calculations are used to determine the importance of certain flow variables on downhole temperatures during circulation, injection, and production. Results of the sensitivity studies are described in Section IV.

C. GEOTEMP Description

There are basically three components of wellbore thermal simulators - flowing stream, well completion, and formation. Figure 1 is a well schematic showing the three components. The relative importance of each component depends on the particular application and the desired result. For example, to predict surface temperatures in high rate production wells, such as geothermal wells, the formation calculation is much less important than the flowing stream calculation.

Several methods have been used in the past to compute flowing stream temperatures. Many early models assumed constant temperatures in the flowing fluid, or used experimentally deter-

mined correlations to compute temperatures. Later studies performed a steady state analysis to estimate fluid temperature, followed by models employing a pseudo steady state scheme, whereby the temperatures in the flowing stream are assumed to be steady at each time step. Recent models have included the full transient response of the flowing stream. For short time periods, the transient response is very important, such as for drilling and cementing operations, or for production and injection startup

Resistance to heat transfer exists between the flowing fluid and the earth. During drilling in an open hole, the resistance results simply from the convection coefficient between the drilling fluid and the formation. However, when circulating inside casing, or during production and injection, the heat transfer resistance is more complex. Indeed, some well completions use this resistance to advantage with varying methods of insulation.

Figure 1 shows that heat must pass through several materials to travel from flow stream to the formation. Moreover, the resistance to heat flow varies with depth as casing is set, introducing steel, cement, and annular fluids where there once was earth. Some previous work has neglected the wellbore resistance, but more recent efforts have indicated a trend to detailed analyses of the well components.

In the earth, heat is transferred both radially and vertically by conduction. Early attempts to model wellbore temperatures assumed a constant undisturbed geothermal temperature in the earth, or employed an analytical solution to the steady state or transient radial heat conduction problem. Later models included numerical solutions to transient radial heat flow, or both radial and vertical conduction.

A grid system has been selected whereby three temperatures are computed in the wellbore at each depth. Mathematical cells are constructed with radial boundaries at three locations, the well centerline, the outside surface of the drill pipe or tubing, and the wall of the open hole or the outside of the largest casing string. Such a grid is illustrated in Figure 2 and shows the three wellbore temperatures. The centerline of the third cell is located at the well/soil interface.

Temperature nodes are located at the centers of the cells. The first node is for the fluid in the drill pipe or tubing, which gives the flowing production, injection or circulating fluid temperature, or simply a temperature at the center of the well during shut-in. The second node is located to compute annular fluid temperature during circulation. The third node serves as an interface between the wellbore and soil calculations

by being located at the boundary between the two regions.

Vertical heat conduction is neglected in the wellbore. Cell dimensions in the wellbore and the presence of vertical convection in the flowing streams make vertical conduction negligible. Each cell is selected to be several hundred feet long and is generally a few inches to a few feet in radial width. A length to width ratio of 100 to 1000 clearly allows a much greater path to radial heat flow. Moreover, the vertical temperature gradients are generally less than the radial temperature gradients for most applications. Finally, for a flowing stream the vertical forced convection transports heat at a much faster rate than vertical conduction.

Nodal points in the soil are located at the same vertical positions as those in the wellbore. Cell length should be small enough to permit acceptable grid refinement to realistically model a well, yet sufficiently long to avoid unnecessary calculations by employing too many grid points. Experience indicates that 100 to 500 feet is a reasonable compromise. Two rows of soil cells are placed below the maximum depth for fluid flow in the well. One provides a transient response of the soil below the bottom of the well, and the second serves as a fixed temperature boundary.

In the radial direction temperature gradients are much greater near the well, so nodal locations are concentrated in this region. A program routine has been written to generate the radial positions of the nodes. Cell width is exponentially increased with radius to produce a grid as illustrated in Figure 3. The exponent chosen is determined from the specified maximum radius and number of radial points. Selection of the maximum radius and number of nodes requires some understanding of the expected rate of radial heat flow. High rates of heat flow should be modeled with a large maximum radius to locate an outside boundary that is sufficiently far from the well to be unaffected by the temperature disturbance caused by the well. Smaller rates of heat flow do not require as large a maximum radius. Similarly, large temperature gradients near a well indicate that many nodes are needed in the radial direction.

There are many solution techniques, of varying degrees of sophistication and speed, available for computing the new temperatures at each new time step. A Gauss elimination direct solution or a Guass-Seidel iteration solution are the two simplest methods to apply, with variations of each available for improving speed or efficiency of solution.

A modified Gauss-Seidel iteration is employed in GEOTEMP to solve for the new temperatures. An energy balance equation is repetitively applied until two successive calculations of

each temperature are sufficiently close. The minimal computation time required for applications of the model does not justify an extensive effort to speed up the process. However, one simple procedure has been applied. Temperatures in the soil converge faster than in the well, so they need not be recomputed with every iteration. A check for local convergence reduces wasted effort in subsequent iterations.

III Testing GEOTEMP Predictions

Accuracy of any computer code must be verified to establish its reliability and to develop the confidence of its users. GEOTEMP has been evaluated with the following tests:

1. Comparison to exact solution
2. Convergence tests
3. Comparison to geothermal production well data
4. Comparison to petroleum circulating well data

Favorable comparisons of computer predictions to exact solutions verify proper formulation of the code, and convergence tests show numerical stability. To check that all the important physical phenomena in a flowing well are included in the model, comparisons are made to field temperature data. Several sets of existing field data have been collected to evaluate the accuracy of the computer model [2]. Four of these data sets are presented here for comparison to model predictions, two from the geothermal industry and two from the petroleum industry.

A. Exact Solutions

GEOTEMP has been tested against an exact solution to a simplified heat conduction problem. The comparison serves two purposes

- compare transient radial conduction analysis to exact solution
- evaluate the importance of time step size on solution accuracy.

By setting the flow rate equal to zero, the flowing stream energy balance reduces to transient radial heat conduction. This simplification has been applied to an exact solution with a fixed temperature T_R at outer boundary R, [5]. Figure 4 illustrates the exact solution temperature profiles at various times, and the thermal simulator predictions at four evenly spaced grid points. At time zero all temperatures are zero, then the temperature T at r = R is increased to T_R. Plotted in Figure 4 are the temperature profiles at three times, showing how the temperature at r = R conducts into the body.

Even though a rather course grid is used in the computer model, an accurate approximation of the exact solution is obtained. Only at early times and where the temperature gradients are large is there a noticeable difference, but a denser grid in the region of large gradients would reduce the difference. It is worth noting that for wellbore thermal simulation the temperature gradients are larger near the well. But Figure 3 illustrates that the grid is more dense near the well, reducing the error revealed in the comparison to exact

solution. For an appropriate grid dimension relative to the temperature gradient, at later times or away from the heat source, Figure 4 demonstrates close agreement between computer and exact solutions.

B. Convergence Tests

Convergence of GEOTEMP solutions with time step size and vertical grid spacing has been verified. There are two objectives to the time step and grid spacing tests. First, numerical convergence must be demonstrated, since it is necessary for a unique temperature distribution to exist. And second, optimum values of time step size and vertical grid spacing can be selected for adequate solution accuracy with minimum computing time.

Consider again the comparison of GEOTEMP calculations to exact solution presented above. Shown in Figure 4 are computer calculations with three time step sizes. Two conclusions can be drawn. First, as a result of the implicit formulation of the energy balance in GEOTEMP, calculation accuracy is not very dependent on time step size. However, a fully implicit solution, independent of time increment, has not been achieved due to the explicit nature of the formulation of fluid properties. Only in the high gradient region at early times does temperature show a dependence on time increment. Refining the grid in this region would reduce the gradient, and therefore the dependence on size of the time step.

Another conclusion that is apparent from Figure 4, is that the GEOTEMP predictions are approaching the exact solution as time step size is reduced. Convergence of temperature predictions with reduced time step size is a necessary feature if the solution is unique. Selecting the proper time step size is a difficult task dependent on well geometry, initial temperatures, grid spacing, and temperature gradients. Generally, for large temperature gradients a small time step is needed. GEOTEMP has a variable time increment defined internally based on a maximum permissible interval. At startup, and whenever flow variables are changed, the time increment is defined as a small fraction of the maximum. The time interval is increased steadily in successive steps until the maximum value is reached, after which the time interval remains constant unless flow varibles are redefined.

Convergence of solution as vertical grid spacing is reduced is demonstrated with an example injection well. Figure 5 shows the well schematic used in this example, a deep 15,900 foot well with a 2-3/8 inch tubing. Fluid is injected in the well at 110^{o}F and a rate of 42 gal/min. Figure 6 shows the transient temperature profiles computed at times from 0 to 8 hours after injection begins. Fluid cools immediately after entering the well, then continuously heats as it travels down the well through the warm earth. Figure 7 shows how the fluid cools with time at three depths, and in Figure 8 the radial temperature distribution at three depths is shown after 8 hours of injection. The cooling influence of the well is obvious, particularly deep in the well.

How these results vary with vertical depth increment is demonstrated in Figures 9-12. At bottom hole, the temperature after 8 hours of injection is not very sensitive to depth increment, as shown in Figure 9. A depth increment up to 2000 feet provides satisfactory results, within 2°F. However, Figures 10 and 11 demonstrate that much smaller vertical spacing is required at shallower depths. At a depth of 8000 feet a spacing of 500 feet is acceptable, but at 2000 feet a 500 foot spacing is questionable. However, for deep wells where temperatures near bottom hole are needed, 500 foot vertical spacing is recommended. Spacings of 200 feet are recommended for applications where more accuracy is needed. Of course, computation time increases as more vertical cells are added to improve accuracy. Figure 12 summarizes the results for depth increments of 200 to 2000 feet. Convergence is evident as the grid spacing is reduced.

Figure 13 provides another check on the sensitivity of results to time step size. Shown here is the computed temperature profile after eight hours of injection for two calculations, one with 6 time steps and one with 24 steps. Previous tests have demonstrated convergence as time step size is reduced. Therefore, the solution with 24 steps should be much more accurate than for 6 steps, yet there is no difference in results except at bottom hole. There is less than 1°F difference in temperatures down to 10,000 feet, and only a 7°F difference at 16,000 feet. With only 6 time increments in an 8 hour period, the computed temperature distribution was very close to the converged solution.

C. Geothermal Production Well Data

Republic Geothermal has supplied two sets of downhole temperature measurements for production and for shut-in conditions in a geothermal well. Three sets of downhole measurements of shut-in temperatures are plotted in Figure 14 to establish the undisturbed geothermal temperature distribution in well #1. The solid line in Figure 14 is the undisturbed temperature distribution adopted in the computer calculations for flowing conditions. These temperatures serve as both initial and boundary conditions. Two geothermal gradients are recognized, a high gradient of 8°F/100 ft from the surface to a depth of 2000 feet, and a more conventional gradient of 2°F/100 feet from 2000 to 8000 feet.

Figure 15 gives the measured and computed temperatures during production of well #1 at 12,000 BPD. Also shown is the undisturbed temperature profile and a casing completion diagram. Production fluid enters the well along the perforations at the undisturbed formation temperatures, then travels up the well through various casings. Although GEOTEMP is not designed for changes in flow area, each section of liner has been analyzed separately to predict temperatures in that section only. For well #1 three sections had to be analyzed. It is evident from Figure 15 that GEOTEMP provides very accurate predictions up to a few hundred feet from the surface. As the production fluid approaches the surface, pressure decreases,

causing high temperature water to flash into steam. Of course, the very low heat capacity of steam causes temperatures to drop rapidly after flashing has occurred. GEOTEMP does not account for the physics of a phase change in the production fluid, and therefore does not predict the rapid temperature drop near the surface. Field data provides only steady-state temperatures recorded in well #1 after 20 hours of production.

Figure 16 illustrates the transient behavior of the fluid temperature at four depths. GEOTEMP predictions demonstrate that there is no change in temperature with time at bottom hole, but temperatures near the surface increase rapidly with production time. At a depth of 1000 feet fluid temperature increases from 160°F before production to more than 300°F less than three hours after production begins. Steady temperature is reached at all depths after six hours of circulation, and comparisons are made to steady temperature measurements after 30 hours of production. It is evident that GEOTEMP provides not only accurate temperatures for long times, but predicts how temperatures traverse from the undisturbed to the steady-state conditions.

Similar comparisons are made for the second Republic Geothermal well. Figure 17 gives the measured shut-in temperatures and adopted computer model of undisturbed initial and boundary temperatures. Again, two geothermal gradients are apparent. From the surface to 2100 feet the gradient is 8.6°F/100 ft, and from 2100 to bottom hole, at 6800 feet, the gradient is 1.8°F/100 ft.

Steady-state production fluid temperatures for a rate of 14,500 BPD are given in FIgure 18, along with the undisturbed temperature profile and casing program. As with well #1, predictions are very accurate in well #2 up to a depth of 1000 feet, where flashing of the hot water into steam begins. The measured bottom hole temperature during production is actually less than the undisturbed measurement at bottom hole, which is unusual, but perhaps attributable to Joule Thompson cooling as fluid passes through the perforations. However, using this bottom hole measurement as a starting temperature, the other temperatures of the production fluid are very accurately predicted, until flashing occurs.

The transient temperature behavior at three depths is given in Figure 19. Rapid heating occurs as production proceeds, until a steady value is reached after five hours. Again, the agreement with steady state measurements after 44 hours of production is excellent, and the computer model provides the transient behavior.

D. Petroleum Circulating Well Data

A cementing temperature study conducted by the American Petroleum Institute provides field data on downhole temperatures in a circulating well, [6, 7]. After drilling was completed, the test

wells were shut-in for an extended period of time, and downhole temperature probes were set. Then circulation was initiated at a controlled flow rate, while measuring surface inlet temperature and one or two downhole temperatures. GEOTEMP predictions for test well conditions have been compared to the downhole temperature measurements while circulating. Two sets of data were selected from five Gulf wells that participated in the API study.

Data extracted from Gulf Well #1 is presented in Table II-1. A 15,375 foot well was circualted for seven hours following 34.5 hours of shut-in. Circulating fluid was an 11.5 lb/gal water based mud, which flowed at 477 gal/min with a well inlet temperature that increased from 92 to 168°F during the test. Bottom hole fluid cooled from 309 to 222°F during the test.

Measured bottom hole circulating temperatures are plotted versus time in Figure 20. The temperature dropped very quickly from 309°F to less than 240°F in one hour, less than 220°F in two hours, then increased back to 222°F after four hours where the temperature stabilizes. Although the temperature plot seems reasonable, two unusual features are noted. First, the beginning temperature of 309°F is less than the expected bottom hole undisturbed temperature based on the measured geothermal gradient. This observation indicates that either the rock surrounding the well has not fully reheated following circulation for drilling, or that some circulation occurred just before the test. The second feature of the data substantiates the assumption of incomplete reheating or prior circulation. Simple intuition predicts that the bottom hole circulating temperature should asymptotically approach an equilibrium value, where the heat carried to bottom by the circulating fluid is balanced by the energy leaving the well with the fluid and by that conducted out into the soil. However, the measured temperature cools below the equilibrium value during the transient period after two hours, which results from the rock near the well being cooler than the rock further away from the well at the same depth. Subsequent investigation of the procedures before the circulation test revealed that a field hand had decided to "clean" the well prior to the API test. Details of flow rate and time during the preliminary clean-up circulation were not available, so this period could not be simulated. But a certain result is that the well and surrounding formation will be cooled below undisturbed temperatures. The effect is to begin the test with cooler than expected temperatures, and to cool too quickly as indicated in Figure 20.

Figure 21 shows the fluid temperature profiles after 0.25 and 7 hours of circulation. After 0.25 hours fluid enters the well at 111°F, cools slightly at depths above 2000 feet deep, then heats steadily to more than 260°F at bottom hole. In the return annulus, fluid heats quickly to nearly 290°F as it leaves bottom hole, then cools steadily to less than 100°F at the surface. At early times, like 0.25 hours, the temperature profiles closely follow the undisturbed geothermal temperatures. Fluid temperature changes more than 160°F from top to bottom of the well. Also plotted is the steady temperature profile after 7 hours of circulation. At later times mud temperatures at shallow depths have increased as a result of

increased mud inlet temperatures and heating by the formation, but near bottom hole cooling has occurred. Formation temperatures change with time, reducing the effect of the formation on fluid temperature, which changes only about 50°F from top to bottom after 7 hours.

Measured data from the second Gulf well is listed in Table III-2. The test well is 13,083 feet deep with two temperature probes, one at bottom hole and another in the return annulus at 11,023 feet. A second temperature data point makes this test well data very useful for comparisons to GEOTEMP. An 11.5 lb/gal water base mud is circulated at 180 gal/min for 3.5 hours with an inlet temperature of 98 to 120°F. Bottom fluid cooled from 229 to 149°F during the test, and at 11,023 feet in the return annulus fluid cooled from 190 to 162°F. These temperature data are plotted in Figure 22. Unlike well #1, bottom hole temperature follows a steady decline curve, but the return annulus temperature is below the undisturbed geothermal value, and initial heating does not occur at start-up of circulation. Initial heating is expected as warm fluid from below flows up past the return annulus probe, before the cooler circulating fluid from above arrives. Closer study of pretest history revealed a well clean-up circulation similar to that described for the previous well. Also, the report for this test well indicated that some very thick or heavy muds were encountered in this well, particularly near bottom. Two special features result from these heavy muds. First, mud build up on the pipe walls increases significantly causing an insulating effect, which is accounted for with a fouling factor. Second, as a result of the heavy mud, it was necessary to wash seven joints of drill pipe near the bottom. However, this circulation occurred at a depth of 12,000 feet, and therefore did not effect the bottom hole value. As a result, the well and nearby surrounding formation above 12,000 feet deep are cooled below undisturbed temperatures at the beginning of the test.

Also plotted in Figure 22 are bottom hole and return annulus temperatures calculated with GEOTEMP. Predictions by the computer code agree very well with measurements at bottom hole. However, in the return annulus, the predicted temperature pattern disagrees with the early time measurements as a result of the circulation before the test. But as the effect of the pre-test circulation fades, the return annulus predictions agree with the measured data. Similar circulation tests in other wells demonstrated the expected pattern in the return annulus of an early increase in temperature followed by a steady decline.

Vertical temperature profiles along the circulation test well are presented in Figures 23 and 24, after 30 minutes and after 3 hours of circulation respectively. Also shown are the undisturbed geothermal temperatures and the measurements at 13,000 feet and 11,000 feet. The agreement between prediction and measurement at 13,000 feet and the previously discussed early disagreement at 11,000 feet are apparent. Figure 24 shows that the fluid temperatures have

moved away from the initial temperature distribution after three hours of circulation. Also, the improved agreement at later times with measured data at 11,000 feet is clear.

Table III-1

Field Temperature Data
Gulf Well #1

Mud - 11.5 lb/gal water base

Flow rate - 477 gal/min

Shut-in prior to circulation - 34.5 hours

Hours of Circulation	BHT, °F @ 15,375'	Mud Temperature, °F Suction	Discharge
0	309	95	92
0.125	290	-	-
0.25	264	-	-
0.5	250	-	-
1.0	234	102	130
1.5	226	-	-
2	218	128	156
3	218	142	164
4	222	149	166
5	222	152	167
6	223	-	-
7	222	-	-

Table III-2

Field Temperature Data
Gulf Well #2

Mud - 11.0-11.5 lb/gal

Flow rate - 180 gal/min

Shut-in prior to circulation - 42 hours
(slight circulation prior to test to wash seven joints of drill pipe)

Hours of Circulation	BHT, °F @ 13,023'	UHT, °F @ 11,023'	Mud Temperature °F Suction	Discharge
0	229	190	90	98
0.25	190	183	-	-
0.5	178	179	-	-
1.0	170	176	96	104
1.5	157	170	-	-
2.0	152	167	100	110
2.5	150	165	-	-
3.0	149	162	112	120
3.5	149	162	-	-

IV Evaluation of Flow Variables

A. Objective

Downhole temperatures in a well are influenced by many variables. Adequately defining these variables for an accurate calculation of temperatures can be difficult, and in some cases impossible. Thus, it is important to define the influence of each variable on downhole temperatures. To establish the importance of a variable, a sensitivity study is performed by computing downhole temperatures in a well with several values of that variable, and with all others held constant. These calculations are not intended to provide temperature predictions for any specific well. There is only the one following basic objective for sensitivity calculations:

> To establish the impact of each variable studied on computing downhole temperatures in a well.

Although the conclusions of sensitivity calculations strictly apply only to the specific conditions employed, the trends defined are generally applicable to other conditions.

Even though there is only one objective to the sensitivity studies, several benefits result. First, an obvious benefit is that the calculations demonstrate which variables have stronger influence on downhole temperatures. Rough estimates and guesses as to the importance of a variable are eliminated. A second useful result of the sensitivity studies is the determination of how much effort is needed to adequately define each variable. In compiling the input data for a GEOTEMP calculation, little effort should be expended trying to accurately define a variable that has only a small impact on downhole temperatures in a well. And the third benefit of sensitivity calculations is to improve intuition, allowing quick decisions to be made with regard to the importance of certain variables on downhole temperatures.

B. Variables Tested

Too many variables are involved in calculation of downhole temperatures to permit a complete sensitivity study of all of them. Therefore, the following seven variables have been selected for study based on their anticipated importance:

1. Fluid flow rate
2. Fluid inlet temperature
3. Fluid density
4. Fluid viscosity
5. Undisturbed earth temperatures
6. Soil thermal conductivity
7. Well depth

The impact of each of these variables on downhole temperatures is calculated for the following four flowing conditions:

1. Forward circulation
2. Reverse circulation
3. Injection
4. Production

Downhole temperatures are computed for two values of each variable. Two plots are presented to illustrate the importance of each variable, one plot of bottom hole temperature (surface temperature for production) versus time, and the second plot of fluid temperature versus depth after five hours. In each plot two curves are given for the two values of a variable used in the calculations. The range of values selected for the seven variables are provided in Table IV-1.

As stated above, results of the sensitivity study can be extended to applications for conditions other than those used in the study, but the conditions of the study are very important. A well configuration with the following four strings of pipe was employed for the sensitivity studies:

tubing	- 4-1/2"	to TD
production casing	- 9-5/8"	to TD
intermediate casing	-13-3/8"	to 3,000' depth
surface casing	- 20"	to 1,000' depth.

Annular spaces between pipes was assumed to be filled with cement and a naturally convecting water based drilling mud.

C. Forward Circulation

The seven flow variables listed in Section IV-B has been tested for their importance on downhole temperatures during forward circulation, and the results are presented in Figures 25-38. Most variables have a significant effect on downhole temperatures, except soil thermal conductivity and fluid plastic viscosity.

Figures 25 and 26 illustrate the importance of flow rate for a well depth of 5000 feet and an inlet temperature of 70°F. Transient bottom hole temperature behavior is plotted in Figure 25 for rates of 100 and 1000 gal/min. At a low flow rate, bottom hole temperature slowly decreases to 107°F after 5 hours. Rapid cooling occurs at the high flow rate of 1000 gal/min, reaching 87°F in one hour.

Figure 26 shows two fluid temperature vs. depth profiles for the two flow rates. At a low rate fluid heats continuously as it travels down the well, following a path just below the undisturbed geothermal gradient. As it nears bottom hole, the fluid heats less rapidly reaching 107°F at bottom hole. High circulation rates do not allow time for the flowing fluid in a well to change

temperature. Figure 26 shows for a flow rate of 1000 gal/min fluid is injected at 70°F, reaches bottom hole at 75°F, then returns to the surface at 72°F. Surrounding earth temperatures have little effect on fluid temperatures in high rate wells.

Effects of inlet fluid temperature on downhole temperatures are illustrated in Figures 27 and 28. Figure 27 shows the change in bottom hole temperature with time for inlet temperatures of 50 and 150°F. With the low inlet temperature, bottom hole fluid steadily cools to 93°F after 5 hours. For an inlet temperature of 150°F, bottom hole temperature decreases along the same path to approximately 115°F after less than an hour. However, bottom hole fluid reheats to approximately 117°F after five hours as a result of the high inlet temperature. The excess cooling at bottom hole results from fluid initially in the well cooling bottom hole before the hot injection fluid reaches bottom. At higher rates excess cooling is magnified.

Figure 28 shows the sensitivity of fluid temperature profile to inlet temperature. Plotted are temperature versus depth for the two inlet temperatures studied, 50 and 150°F, after 5 hours of circulation. Cool fluid heats as it travels down into the well along a path nearly parallel to the surrounding earth temperatures. As the fluid nears bottom hole, the rate of heating decreases to near zero, while the temperature reaches 93°F. Returning fluid in the annulus is warmer at all depths than the injection stream in the tubing or drill pipe. With an inlet temperature of 150°F, the circulating fluid cools rapidly until it approaches the formation temperature. At bottom hole, cooling has vanished and even slight reheating can occur. The return annulus fluid is a few degrees cooler than the descending stream.

Fluid density is evaluated in Figures 29 and 30. Plotted in Figure 29 is bottom hole temperature versus time for 8.3 and 20 lb/gal fluids. Bottom hole temperature decreases more rapidly and to a lower final value with light weight fluid. An 8.3 lb/gal fluid reaches 87°F at bottom hole after 5 hours, and a 20 lb/gal fluid reaches 103°F.

Presented in Figure 30 is the temperature versus depth profiles after 5 hours of circulation for the two densities. Both curves show an increase in temperature with depth as fluid moves down a well, with little heating at bottom hole, and continuous cooling as the fluid returns to the surface. As solids content is increased in a fluid, the density increases and the specific heat capacity decreases. Total fluid heat capacity is the product of specific heat capacity and density, which increases with solids content. Therefore, heavier fluids have a greater heat capacity, and as a result carry more thermal energy. The ability to carry thermal energy up from the earth causes higher temperatures in heavier circulating fluids.

Figures 31, and 32 illustrate the effect of fluid plastic viscosity on downhole temperatures. Bottom hole temperature versus time is plotted in Figure 31 for plastic viscosities of 15 and 50 centipoise. With an inlet temperature of 70°F, the bottom hole temperature steadily decreases from 125 to 79°F for 50 CP and to 87°F for 15 CP. High viscosity fluid tends to insulate the well by decreasing the pipe wall convection coefficient. As a result, the cool fluid is not heated as rapidly by the surrounding earth.

Fluid temperature versus depth profiles are shown in Figure 32 for the two viscosities. Although both plots show an increase in temperature with depth, the insulating effect in the high viscosity fluid is evident. Greater cooling of bottom hole is achieved with a high viscosity fluid.

The importance of undisturbed formation temperature gradient is presented in Figures 33 and 34. Transient bottom hole temperatures are provided in Figure 33 for formation temperature gradients of 1.1 and 2.6°F/100 ft. For a 1.1°F/100 ft gradient, bottom hole temperature begins at 125°F and cools to 98°F after 5 hours. A 2.6°F/100 ft gradient results in a bottom hole temperature of 200°F, which cools to 136°F after 5 hours. Although a high gradient increases bottom hole temperatures significantly, the difference is reduced with time due to the greater cooling for the high gradient.

Figure 34 has the temperature profiles after five hours for each gradient, and the gradients themselves are plotted. Both curves follow nearly parallel to the formation temperature gradient at shallow depths, and approach constant temperature at bottom hole. Much greater heating is evident for a high temperature gradient well.

Soil thermal conductivity has only a small effect on flowing fluid temperatures, if the rates are not too low. Figures 35 and 36 show that the effect is less than 5°F at bottom hole, and is even less at shallower depths. These conclusions apply to the well conditions in the test calculations, and for a range of thermal conductivities from 0.5 to 4.0 BTU/hr ft °F.

The influence of well depth is provided in Figures 37 and 38. As one might expect deeper wells have hotter circulating fluids at bottom hole as shown in Figure 37. A 5,000 foot well starts with a 125°F bottom hole fluid, which drops to 98°F after 5 hours, and for 10,000 feet bottom hole fluid cools from 180°F to 153°F, assuming a constant geothermal gradient.

Figure 38 presents the fluid temperature profiles for a 5,000 and a 10,000 foot well after 5 hours of circulation. Not only are bottom hole temperatures higher, but at all depths, circulating fluid is warmer in the deeper well.

D. Reverse Circulation

Downhole fluid temperatures in a well during reverse circulation have been tested for sensitivity to each of the seven variables presented in Section IV-B. Results of the studies are very similar to those presented above for forward circulation, with two basic differences. First, downhole fluid temperatures tend to be higher during reverse circulation. Fluid is immediately exposed to warm earth temperatures as it enters the well annulus. But conversely, for forward circulation the entering fluid in the tubing or drill pipe is insulated from the surrounding earth by the return annulus stream. A second difference occurs during reverse circulation, for which the return annulus stream is generally cooler than the descending inlet fluid. This trend is opposite to that experienced during forward circulation.

Due to close similarities in downhole temperatures for forward and reverse circulation, interpretations of sensitivity studies for the two flow conditions are similar. Therefore, interpretations presented in this section for reverse circulation are limited to avoid repetition, although the complete set of sensitivity curves are provided. The previous section may be referenced for additional interpretations applicable to both forward and reverse circulation.

Flow rate is evaluated for reverse circulation in Figures 39 and 40. Figure 39 shows that bottom hole fluid cools more rapidly and to a lower temperature at high flow rate. Comparison of Figures 39 and 25 demonstrates that bottom hole temperatures are somewhat higher for reverse circulation than those experienced for forward circulation. Temperature profiles are given in Figure 40.

Figures 31 and 42 present sensitivity of downhole temperatures to inlet temperature. As one might expect, a high inlet temperature yields high downhole temperatures. But the importance of inlet temperature is less for reverse circulation than for forward circulation.

The impact of fluid density on downhole temperatures is provided in Figures 43 and 44. High density fluid has a high specific heat capacity, and therefore shows a greater response to formation temperatures.

Fluid plastic viscosity effects on downhole temperatures are presented in Figures 45 and 46. High viscosity fluid has a low surface convection coefficient at the pipe wall, which insulates fluid from the formation. This insulating effect allows greater cooling at bottom hole.

An important variable for any flowing condition is undisturbed formation temperature. The effects on downhole temperatures during reverse circulation are plotted in Figures 47 and 48 for temperature gradients of 1.1 and 2.6°F/100 ft. As expected, high

earth temperatures cause high fluid tempeartures. Geothermal temperature gradient has a greater influence during reverse circulation than any of the other flow options because exposure of flowing fluid to earth temperatures is greatest.

Figures 49 and 50 illustrate the impact of formation or soil thermal conductivity on downhole temperatures during reverse circulation. The importance of soil thermal conductivity is small, 5°F maximum error, for this 5000 foot deep well. Deeper wells will show a more pronounced dependence on this variable.

Of course, well depth has a strong impact on downhole temperatures during reverse circulation, as illustrated in Figures 51 and 52. Fluid temperatures are greater at every depth in a deeper well.

E. Injection

This section presents results of sensitivity studies conducted for injection. Figures 53-62 illustrate the importance of the seven variables listed in Section IV-B.

Flow rate sensitivities are presented in Figures 53 and 54 for an injection depth of 5000 feet. Bottom hole temperatures as a function of time are plotted for flow rates of 500 and 10,000 BPD. At low rates the bottom hole temperature slowly drops from 125 to 107°F after five hours of injection. Much faster cooling occurs for injection at 10,000 BPD. For this case the bottom hole temperature decreases from 125 to 75°F after only one hour of injection. A steady bottom hole temperature of 73°F is reached in two hours at the higher rate. Figure 54 shows two temperature versus depth profiles, one for each flow rate. Clearly, at high injection rates near maximum cooling occurs. Injection fluid is only 3°F warmer at bottom hole than at the surface. For low flow rate, fluid temperature parallels the undisturbed geothermal gradient to 107°F at bottom hole.

The importance of inlet temperature is defined in Figures 55 and 56. Cooling of bottom hole fluid with time of injection is shown in Figure 55 for two inlet temperatures, 50 and 150°F. Fluid at bottom hole cools steadily from 125 to 111°F within one hour for both inlet temperatures. After one hour inlet temperature has a stronger impact on bottom hole temperature. With an inlet of 50°F, fluid at bottom hole continues to cool steadily to 90°F after five hours. But with an inlet of 150°F, bottom hole temperature decreases only to 110°F after a little more than an hour, and then increases slightly to a steady value of 112°F. The excess cooling at early times is a result of the inlet temperature being greater than the surrounding formation temperature. Before the hot injection fluid reaches bottom hole, cooler fluid initially in the well causes a decrease in bottom hole temperature. But at later times the high temperature injection fluid increases the bottom hole temperature to a steady value. For the conditions of this test the excess cooling phenomena is small, but for other con-

ditions it may be more noticeable. Sensitivity studies for circulation described above demonstrate greater excess cooling at bottom hole with high inlet temperature.

Temperature-depth profiles for the two inlet temperatures are plotted in Figure 56. With an inlet temperature at or below the near surface earth temperature, continuous heating of the injection fluid occurs as it travels to bottom hole. For a 50°F inlet temperature, fluid heats to 90°F at 5,000 feet. When high temperature fluid enters a well, above the surrounding earth temperature, it begins to cool as it travels downhole, but at a decreasing rate. If the inlet temperature and flow rate are sufficiently high, injection fluid decreases continuously to bottom hole. However, if the inlet temperature is above the near surface earth temperature, but is not "too" high, then the fluid temperature will cool below the earth temperature at some depth, and begin to heat from that depth to bottom hole. Figure 56 shows this phenomena with an inlet temperature of 150°F. Injection fluid cools continuously to 111°F at a depth of 3800 feet where it drops below the surrounding earth temperature. Below this depth the fluid stops cooling and begins to heat, reaching 112°F at 5000 feet. A deeper well or a lower flow rate would exaggerate the reheating.

The impact of injection fluid density is illustrated in Figures 57 and 58. Shown in Figure 57 is the transient bottom hole fluid temperature behavior for two fluid densities, 8.3 and 20 lb/gal. Heavier fluid has a greater heat capacity, and therefore requires more time for its temperature to change and carries more heat energy. What this means is that heavier injection fluid changes temperature less as it travels to bottom hole, causing cooler bottom hole temperatures at any time. For a density of 8.3 lb/gal, Figure 57 shows continuous cooling of bottom hole for 125 to 95°F after 5 hours. A 20 lb/gal fluid arrives at bottom hole at a lower temperature than the lighter fluid, reaching 91°F after 5 hours. Significant increase in injection fluid density causes only a 4°F difference in bottom hole temperature after 5 hours.

Figure 58 shows the temperature-depth profiles after 5 hours of injection for the two fluid densities of 8.3 and 20 lb/gal. Fluid continuously heats for both densities as it travels downhole, showing the previously mentioned 4°F difference in bottom hole temperature. The lighter fluid is heated faster by the surrounding earth due to its low heat capacity. Note that the trend is reversed for circulation (see Figures 26 and 44), that is bottom hole temperature is greater for the heavier fluid during circulation. This occurs because during circulation the return fluid carries heat up from the warmer earth below, and the heavier fluid is better at carrying this heat. Since the return stream heats the inlet stream, temperatures are higher for heavier fluids.

Undisturbed geothermal temperature gradient plays an important role in downhole fluid temperatures. Its importance is illustrated in Figures 59 and 60 for gradients of 1.1 and 2.6°F/100 foot. Figure 59 shows the bottom hole temperature versus time. A gradient of 1.1°F/100 foot results in a 125°F bottom hole undisturbed temperature, which cools continuously to 94°F after 5 hours of injection. For a 2.6°F/100 foot gradient, the initial bottom hole temperature is 200°F, and it cools rapidly to 127°F after 5 hours. The higher gradient initially causes a 75°F higher bottom hole temperature (200-125°F), but after 5 hours of injection the difference is reduced to 33°F (127-94°F).

Figure 60 shows the temperature-depth profiles for each gradient, and plots the gradients themselves. Fluid enters the well at the same temperature as the surrounding earth, and heats continuously as it travels downhole. Each plot moves toward a path parallel to the respective undisturbed geothermal temperature gradient. It is clear from these profiles that the higher earth temperature gradient increases the fluid temperature at every depth.

The effect of well depth on downhole temperatures is presented in Figure 61 and 62. As expected, deeper wells have warmer fluids at bottom hole as shown in Figure 61. However, greater cooling in the deeper wells reduces the difference in bottom hole temperatures with time.

Figure 62 presents the fluid temperature profiles for two wells with identical conditions except depth. This figure shows that for injection fluid, temperatures at any depth are not influenced by the depth below. Therefore, the temperature at 5000 feet is the same for a well depth of 5000 feet as for 10,000 feet.

As with production wells, the importance of fluid viscosity on downhole injection temperatures is small. For a plastic viscosity range of 15 to 50 centipoise the bottom hole temperature varied less than 1°F, so no sensitivity plots are provided. These results indicate the direct impact of fluid viscosity on downhole temperatures. Secondary effects such as increased solids buildup on the pipe wall are not accounted for.

Also, the importance of formation thermal conductivity on downhole fluid temperature is negligible. Conductivities from 0.5 to 4.0 BTU/hr ft °F were tested with little change in downhole injection fluid temperatures. The several annuli of fluid, cement, and steel in a well tend to insulate the fluid from the formation, reducing its importance.

F. Production

Tests of flow variables listed above are given in this section for production and are presented in Figures 63-70. Well depth, geothermal gradient, and inlet temperature are directly related for production, so they have not been independently studied.

Results for flow rate are presented in Figures 63 and 64. Surface temperature versus time is plotted for production rates of 500 and 10,000 BPD. At 10,000 BPD the surface temperature increases rapidly from 70 to 120°F in one hour. However, at a production rate of 500 BPD the surface temperature increases much more slowly to a steady value less than 90°F after five hours. At high rates the fluid reaches the surface before it has time to change temperature. Steady production fluid temperature profiles are illustrated in Figure 64. At low flow rates the fluid temperature parallels the undisturbed temperature, while at high rates very little temperature change occurs as the fluid travels to the surface.

Very accurate fluid properties are not necessary for accurate temperature predictions during production. Figures 65 and 66 demonstrate the importance of fluid density on production fluid temperature. It is evident that for the range of density studied, from 8.3 to 20 lb/gal, only a small effect on fluid temperatures is realized. Similarly, a range of plastic viscosity from 15 to 50 centipoise changed fluid temperatures by less than 1°F, eliminating the need for sensitivity curves.

Figures 67 and 68 show the important effect of undisturbed geothermal gradients with the two cases presented for gradients of 2.5 and 4.0°F/100 ft. The difference in surface fluid temperatures for these two cases is given in Figure 67. The higher geothermal gradient, and its effect on bottom-hole temperature, significantly increases the surface temperature from 84 to 103°F after one hour, and from 100 to 140°F after 5 hours. Figure 68 shows the higher bottom-hole temperature resulting from the higher gradient, and shows the effect on steady fluid temperature profile. It is interesting to note how each profile tends to parallel the undisturbed geothermal gradient, as one might expect. For a gradient of 2.6°F/100 ft, the temperature at 5000 feet is 200°F, compared to 125°F for 1.1°F/100 ft. As fluid travels to the surface, the temperature difference decreases, and the rate of decrease is a function of flow rate as described above.

Soil thermal conductivity was studied with the two values presented in Table IV-1. Results demonstrate that this variable, in the range of interest, has little influence on the production fluid temperature. For two values of 0.5 and 4.0 BTU/hr-ft °F, the surface fluid temperatures are different by less than 1°F. Therefore, sensitivity curves have not been plotted.

Production formation depth is evaluated in Figures 69 and 70 for a fixed gradient of 1.1°F/100 ft. Figure 69 shows only a small increase in production temperature, from 100 to 105°F after five hours, for an increase in depth from 5000 to 10,000 feet. How the big difference in bottom hole temperatures, 125 compared to 180°F, dissipates as the fluid travels to the surface is illustrated in Figure 70.

Table IV-1

Range of Values For Flow Variables

Variables	Units	Low Value	High Value
fluid flow rate: circulation production/injection	 gal/min bbl/day	 100 500	 1,000 10,000
fluid inlet temperature	^{o}F	50	150
fluid density	lb/gal	8.3	20.0
fluid viscosity	centipoise	15	50
undisturbed earth temperature gradient	^{o}F/100 ft.	1.1	2.6
soil thermal conductivity	BTU/hr ft ^{o}F	0.5	4.0
well depth	feet	5000	10,000

V References

1. Goodman, M. A. "Wellbore Thermal Simulation - Survey of Existing Capability and Industry Needs and Interest," Final Report to U.S. Energy Research and Development Administration, Geothermal Energy Division, Contract EG 76-C-07-1603, June, 1977.

2. Wooley, G. R., "Wellbore and Soil Thermal Simulation for Geothermal Wells - Development of Computer Model and Acquisition of Field Temperature Data," Part I Report to Sandia Laboratories on Contract No. 13-0212, December, 1978.

3. Wooley, G. R., "Computing Downhole Temperatures In Petroleum And Geothermal Wells," SPE 8441, presented at the Society of Petroleum Engineers of AIME 51st Annual Fall Technical Conference and Exhibition, September 26, 1979, Las Vegas, Nevada.

4. Wooley, G. R., "User's Manual For GEOTEMP - A Computer Code for Predicting Downhole Wellbore and Soil Temperatures In Geothermal Wells," Appendix to Part I Report to Sandia Laboratories on Contract No. 13-0212, January 25, 1979.

5. Carslaw, H. S. and J. C. Jeager, Conduction of Heat in Solids, Oxford Press, London, 1959.

6. Shell, F. and A. Tragesser, "API Is Seeking More Accurate Bottom Hole Temperatures," Oil and Gas Journal, July 10, 1972.

7. Shell, F. and A. Tragesser, "Accurate Bottom Hole Temperatures Are Needed," Presented at the Second Annual Meeting of the Production Division of the American Petroleum Institute, March 6-8, 1972, Houston, Texas.

VI Figures

Figure 1

Wellbore Completion Model

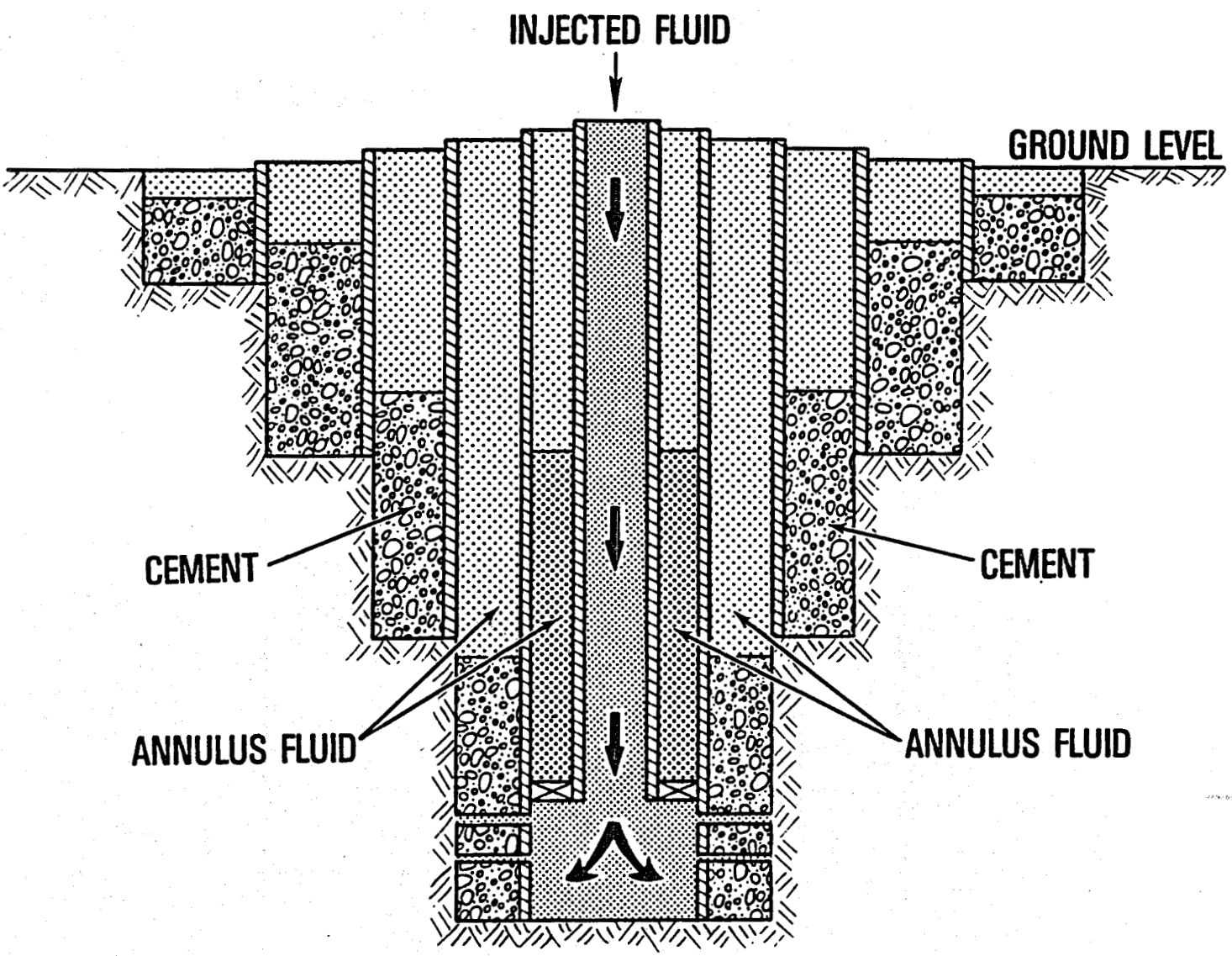

Figure 2

Wellbore Mathematical Cells

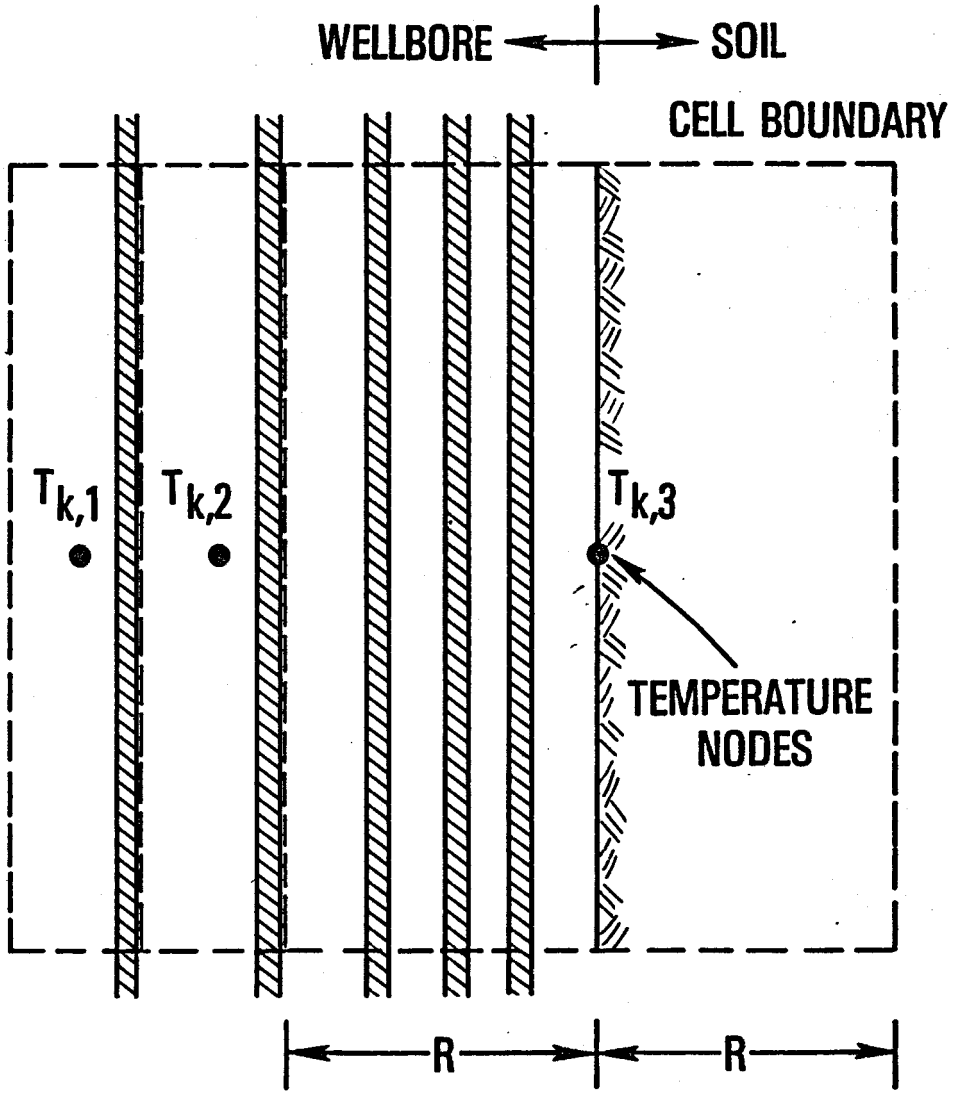

Figure 3

Soil Mathematical Cells

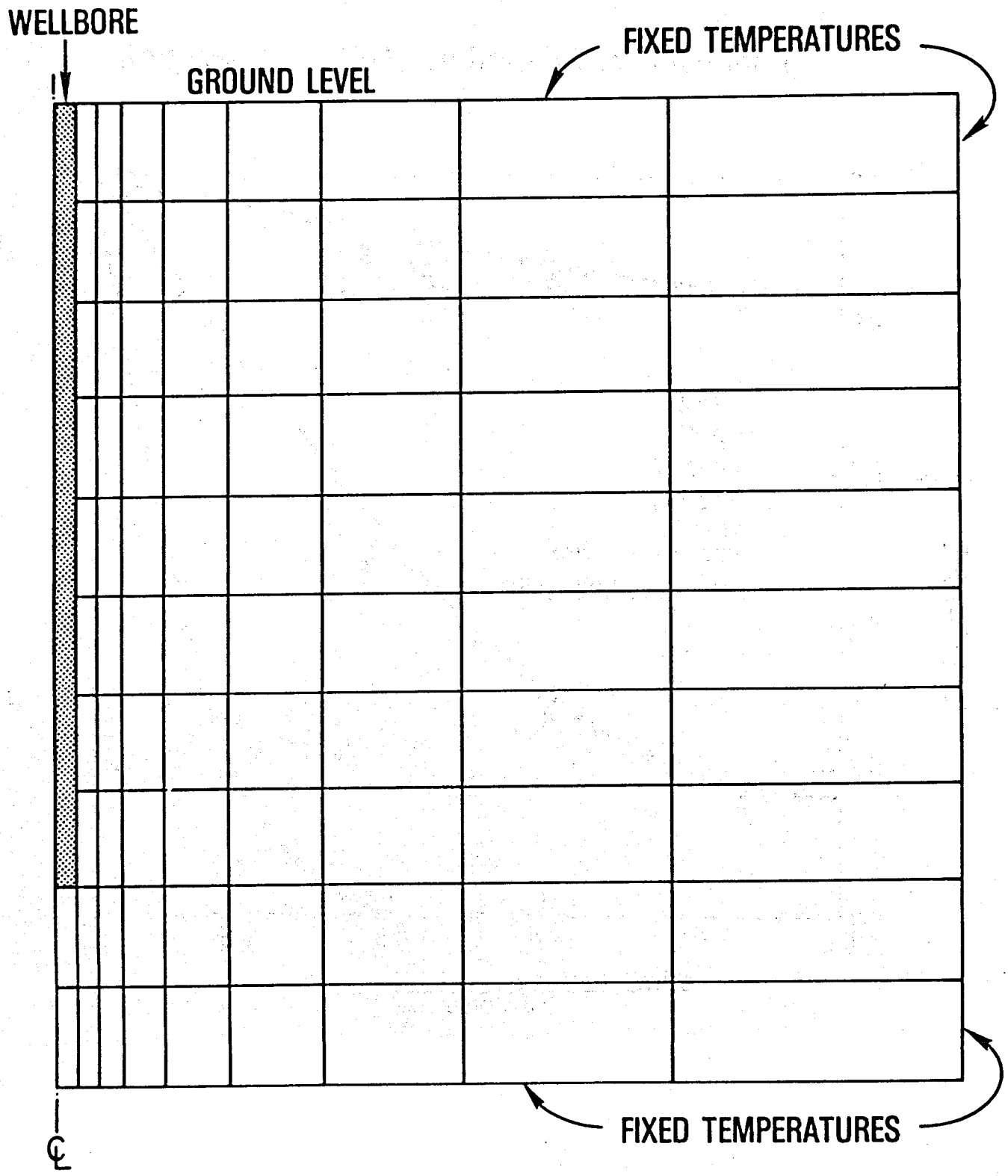

Figure 4

Comparison of Predictions To Exact Solution

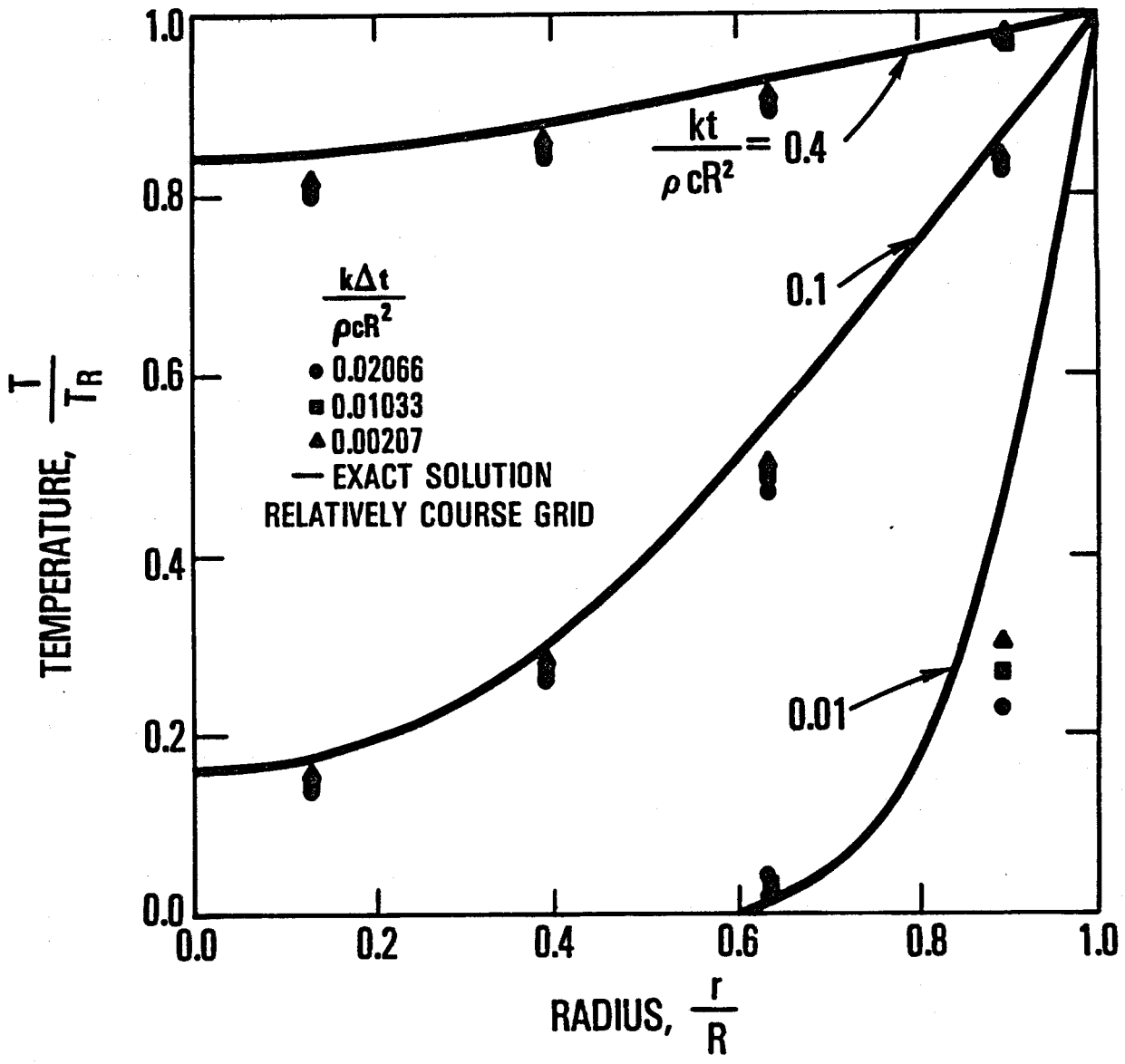

Figure 5

Well Schematic of Example Case For Convergence Test

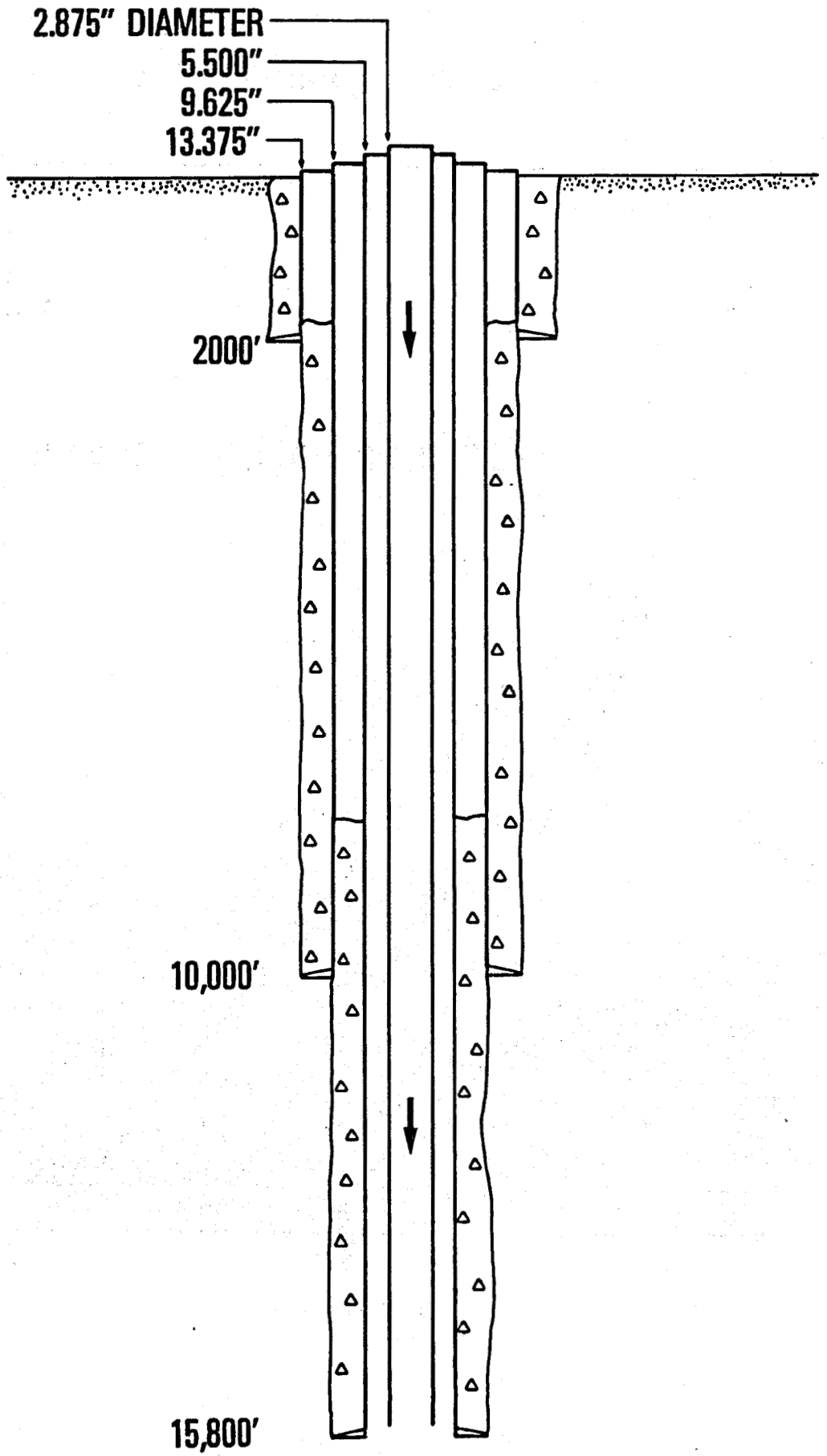

Figure 6

Transient Temperature Profiles

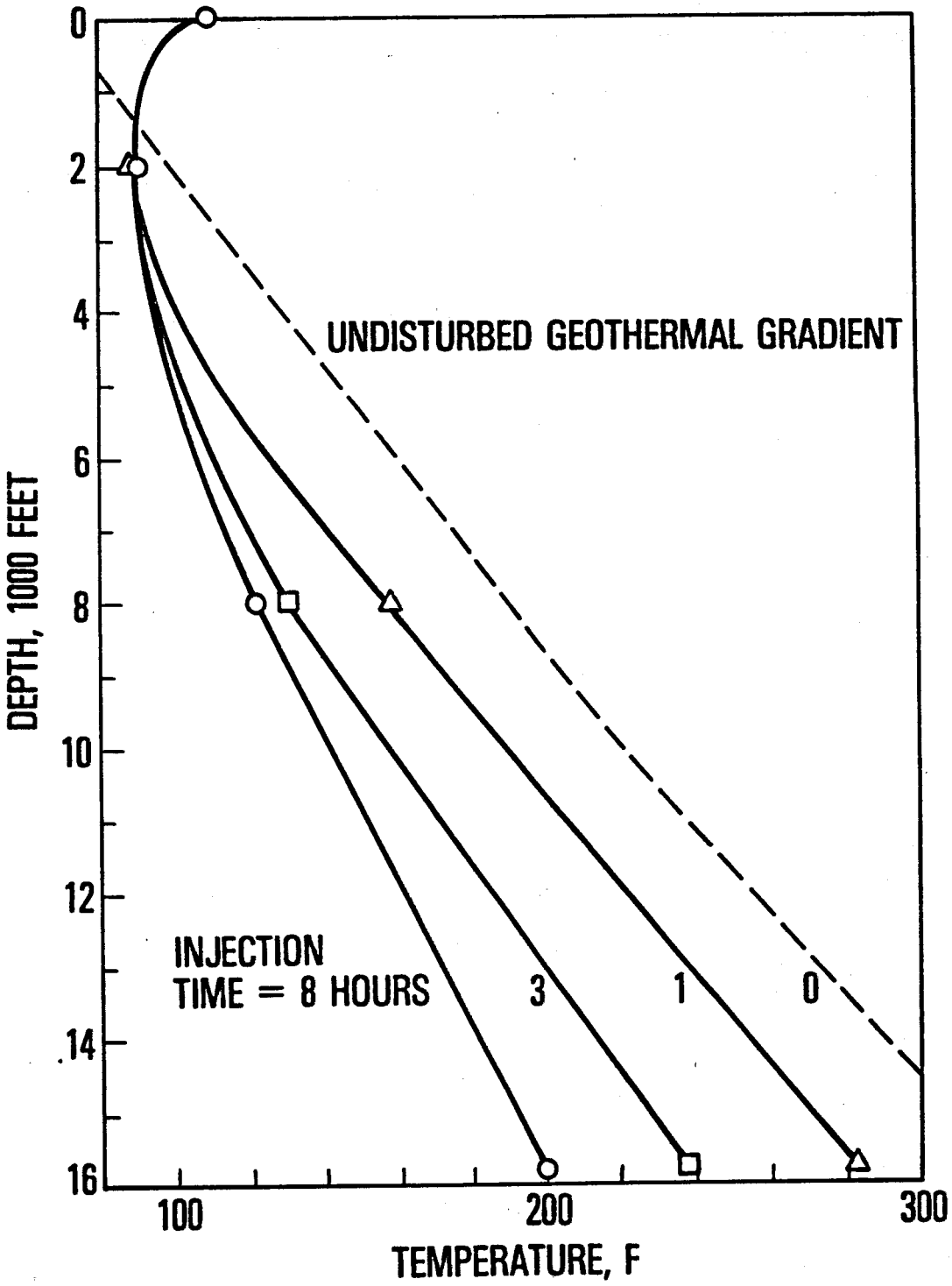

Figure 7

Transient Temperature Behavior

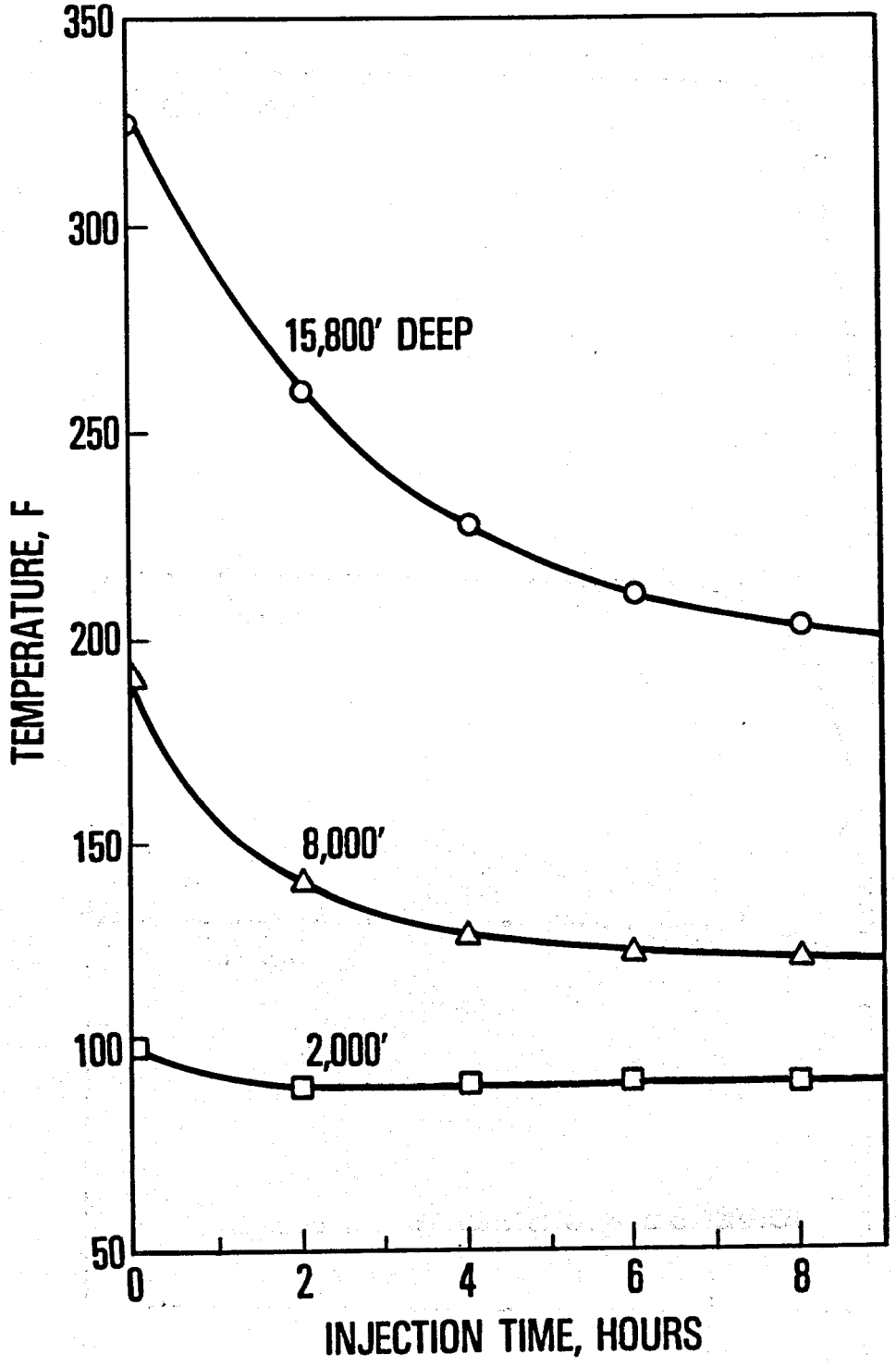

Figure 8

Soil Temperature Distributions After 8 Hours of Injection

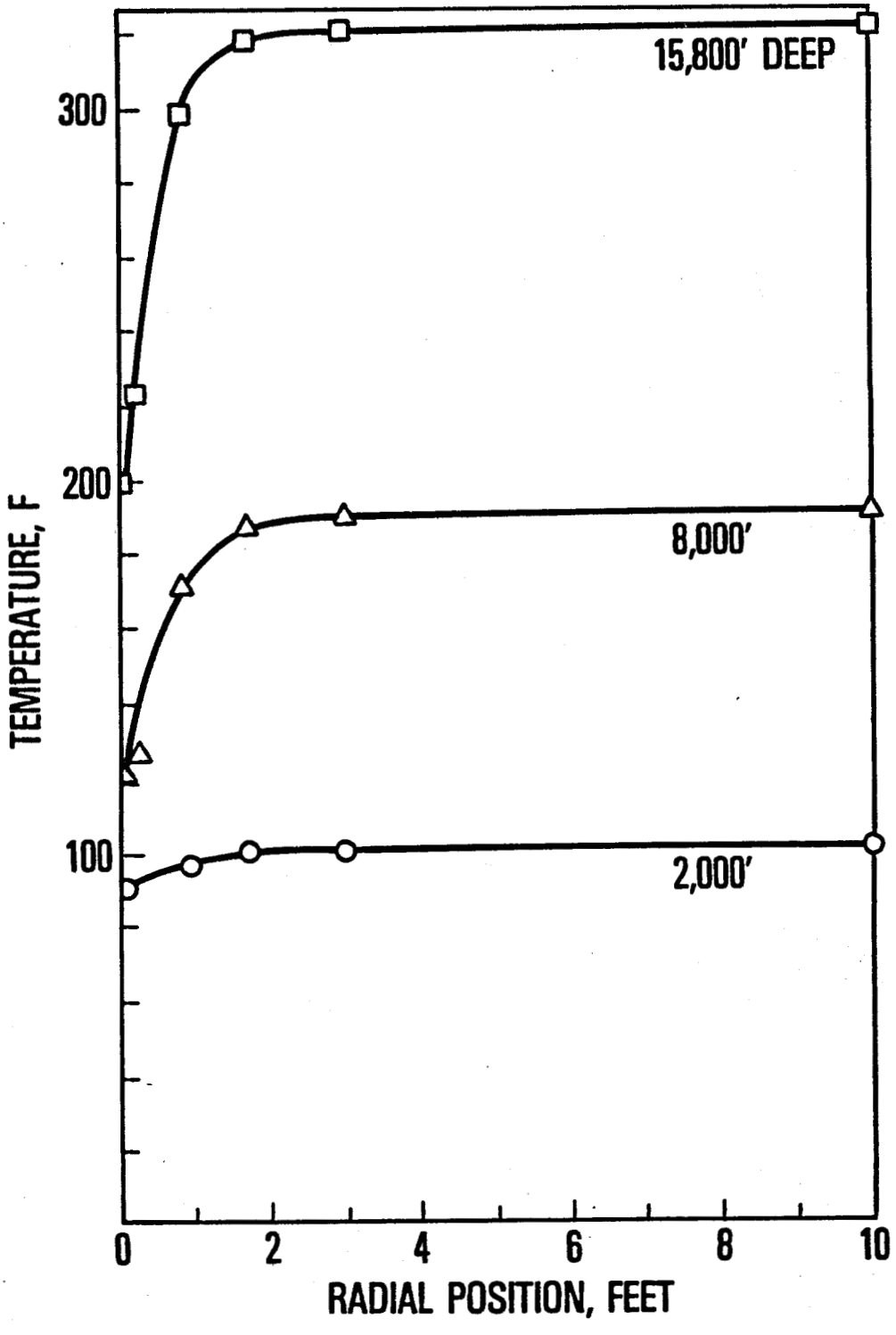

Figure 9

Convergence of Injection Fluid Temperature at 15,800 Feet

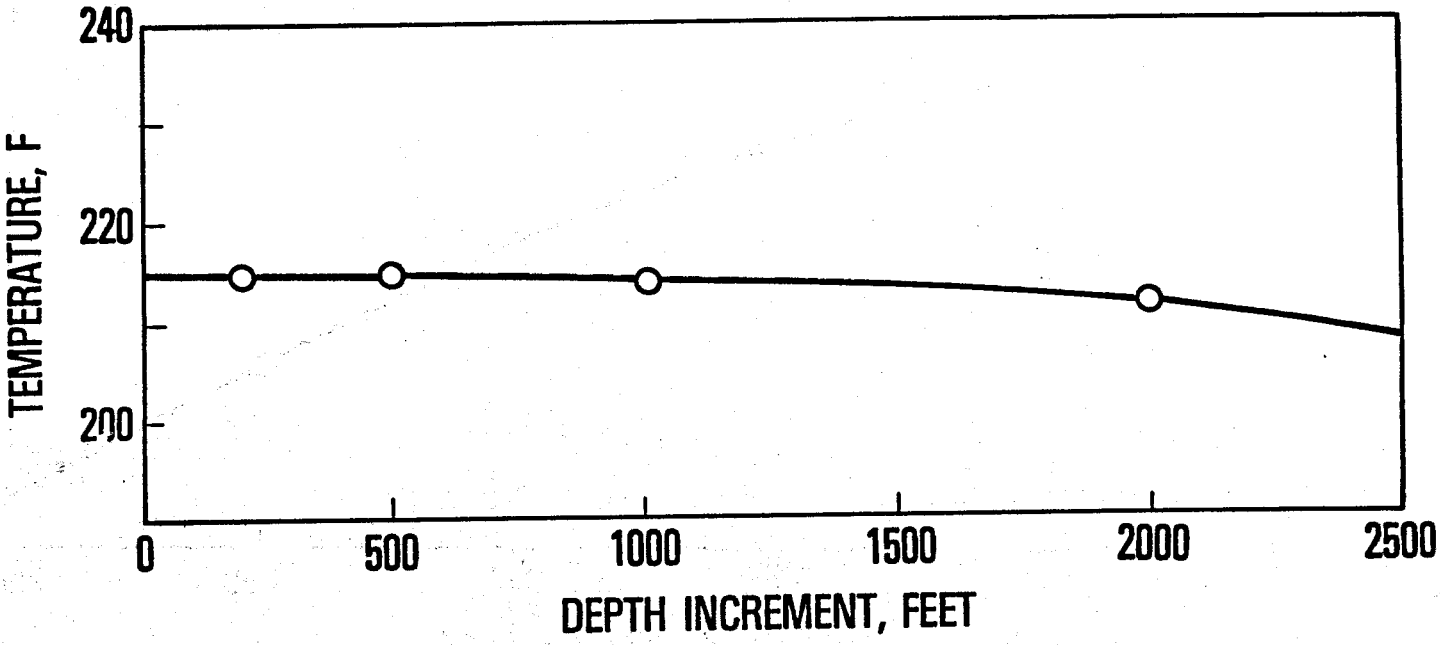

Figure 10

Convergence of Injection Fluid Temperature at 8000 Feet

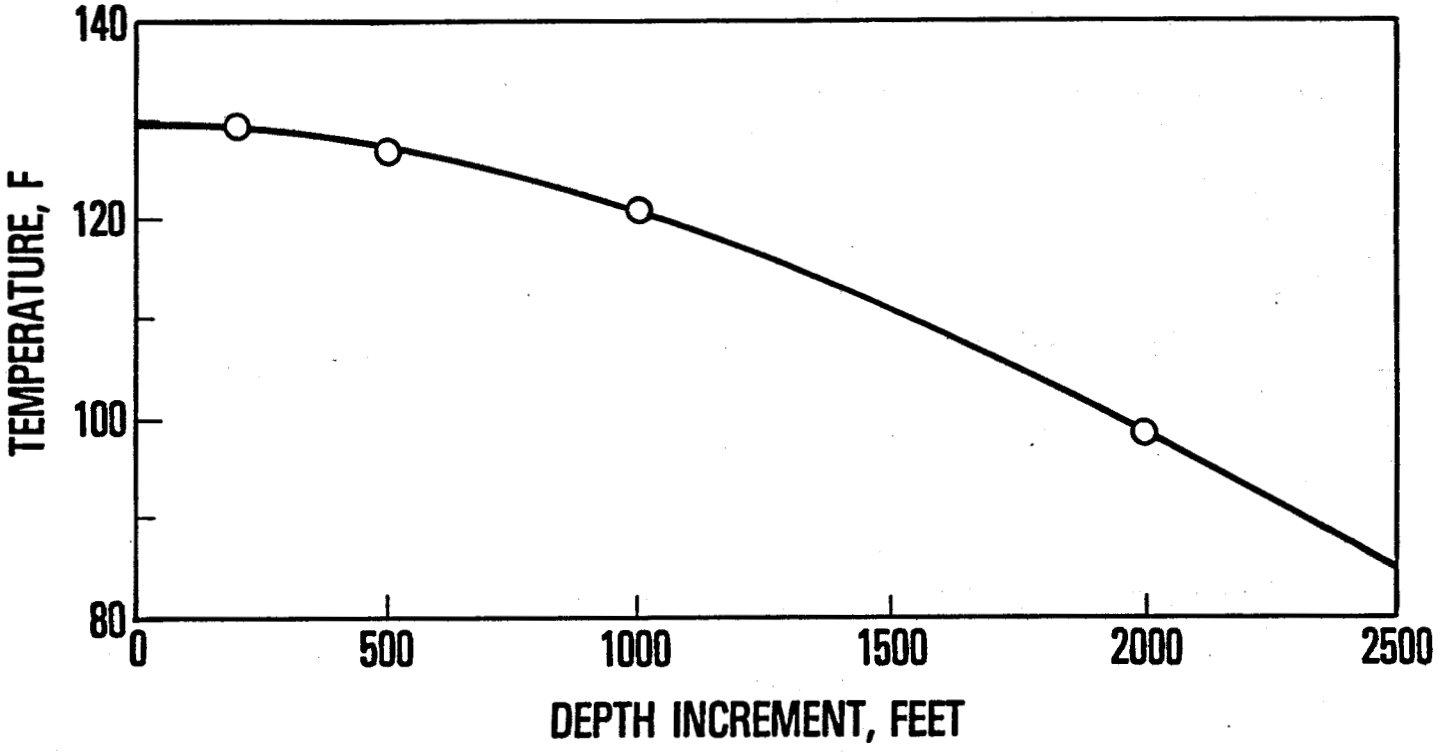

Figure 11

Convergence of Injection Fluid Temperature at 2000 Feet

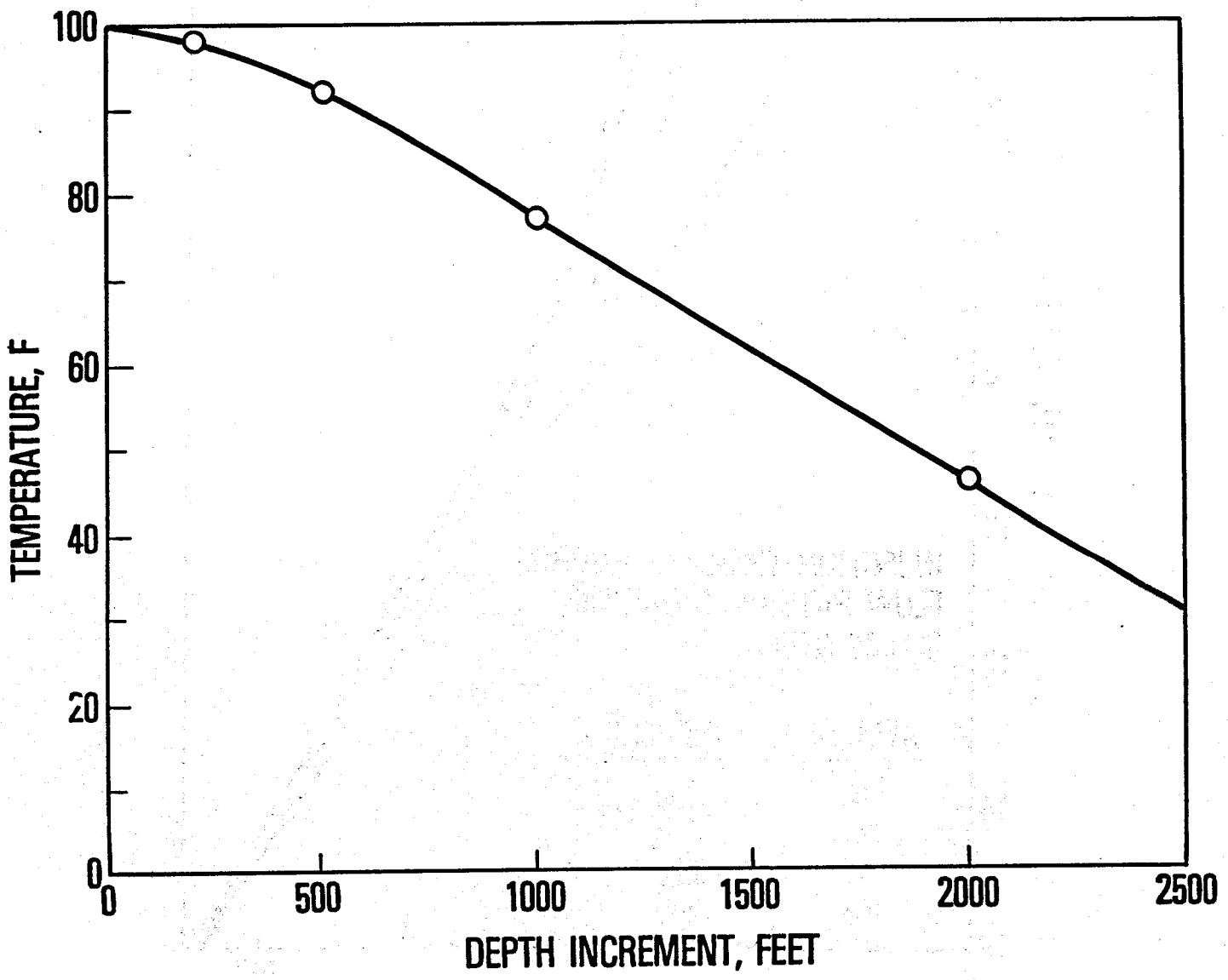

Figure 12

Effect of Depth Increment on Injection Fluid Temperature Profile

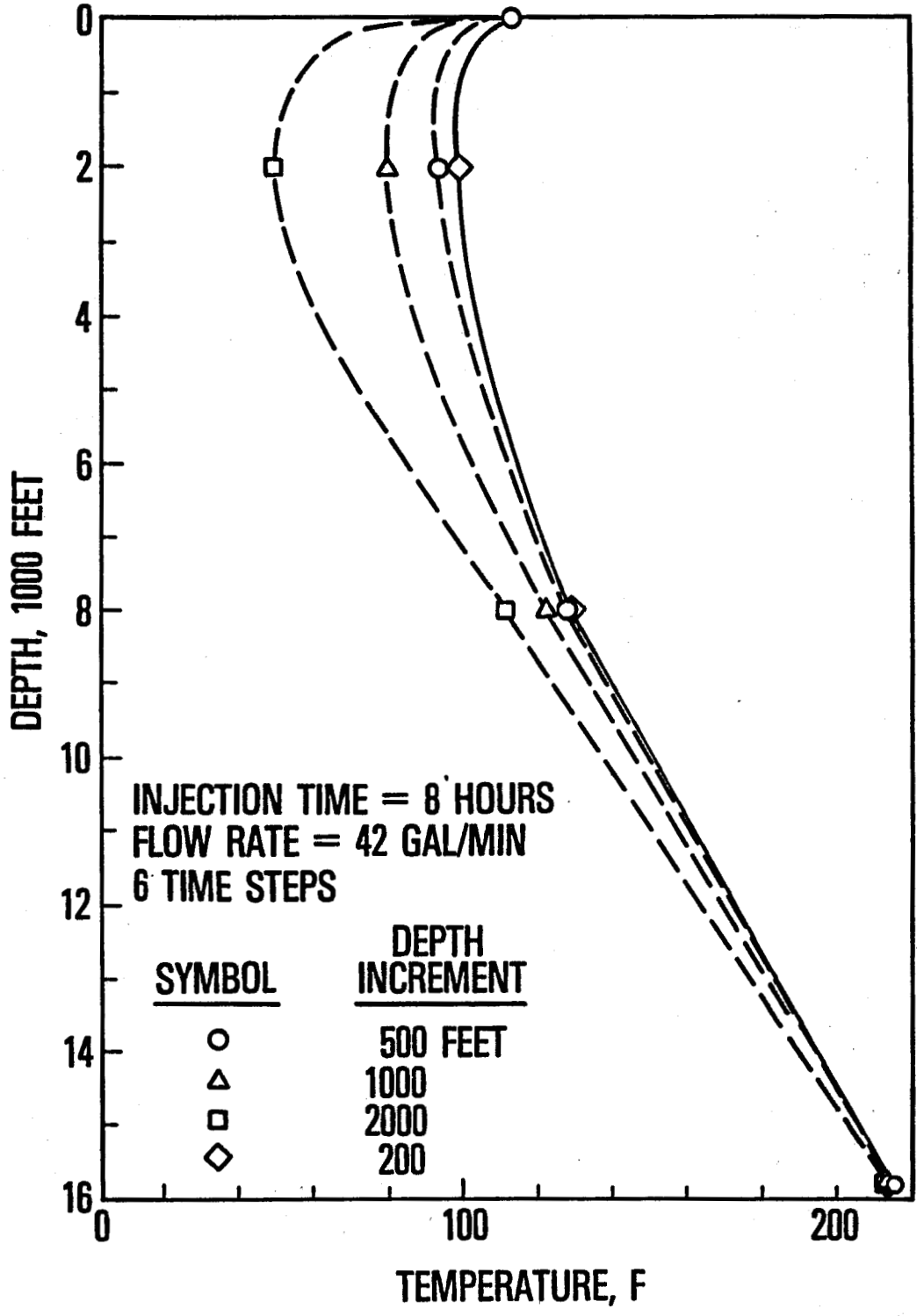

Figure 13

Effect of Time Increment on Injection Fluid Temperature

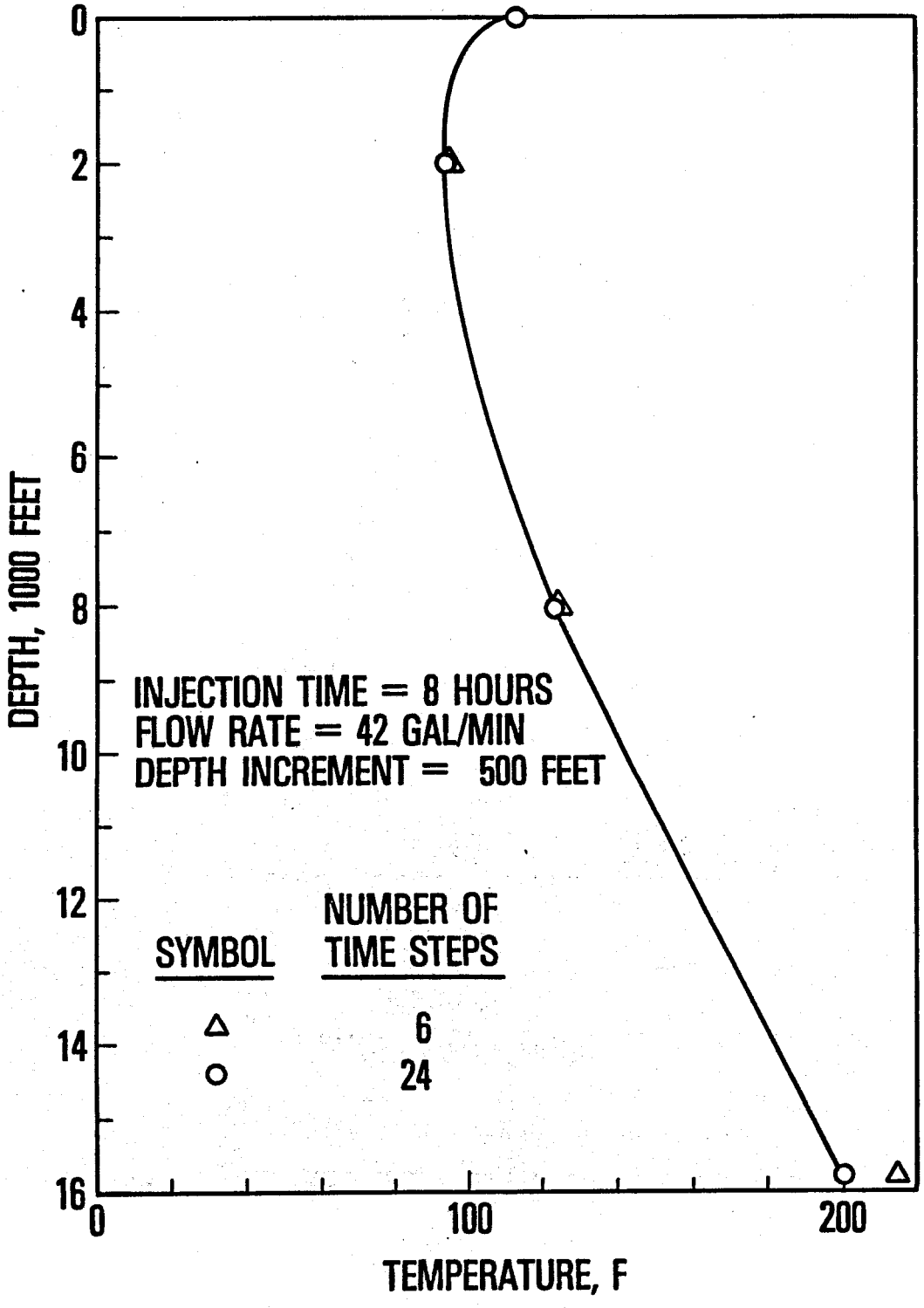

Figure 14

Undisturbed Temperature Distribution
Republic Geothermal Well #1

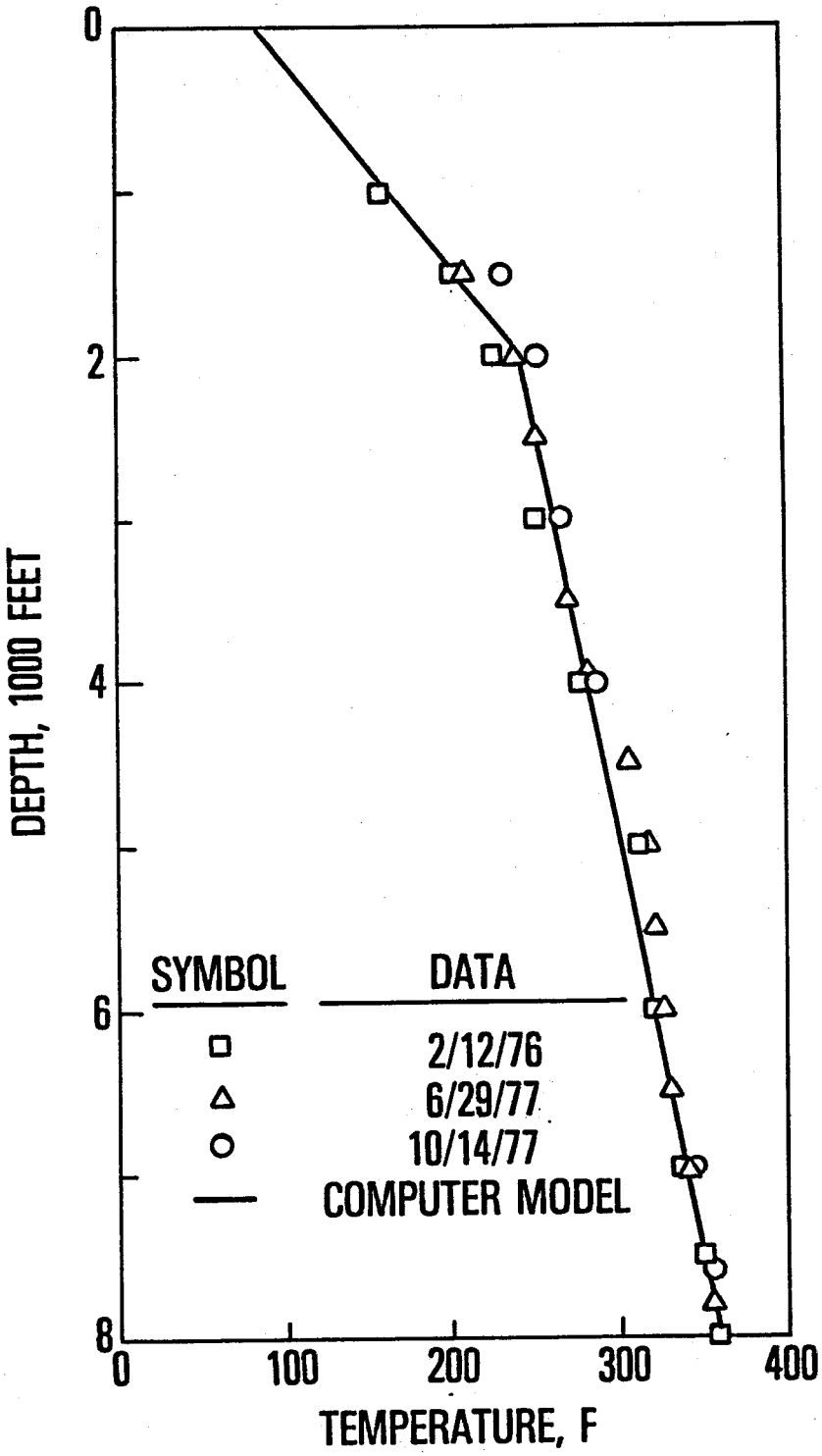

Figure 15

Steady-State Production Fluid Temperature Profile
Republic Geothermal Well #1

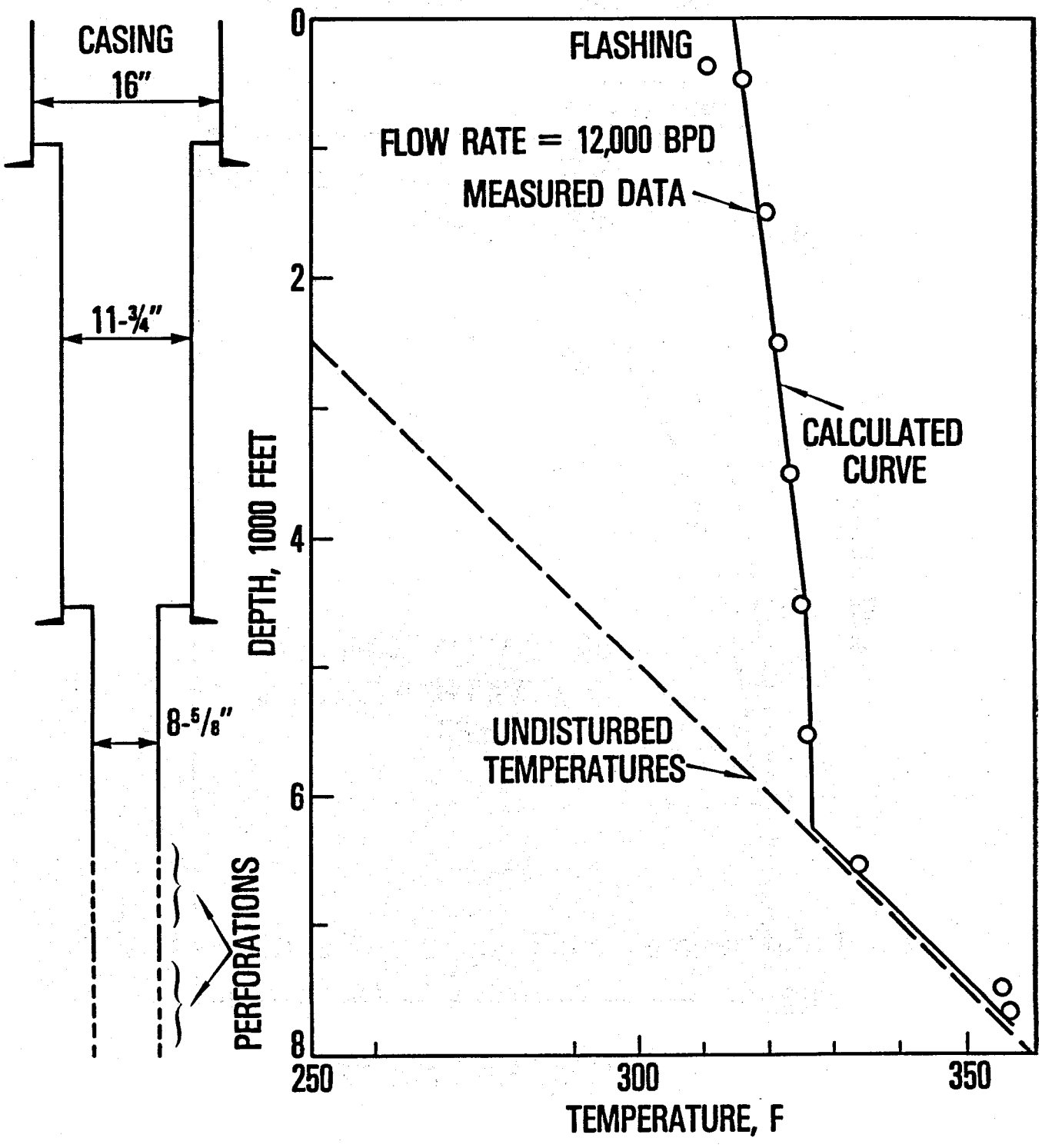

Figure 16

Transient Temperature Behavior at Various Depths Republic Geothermal Well #1

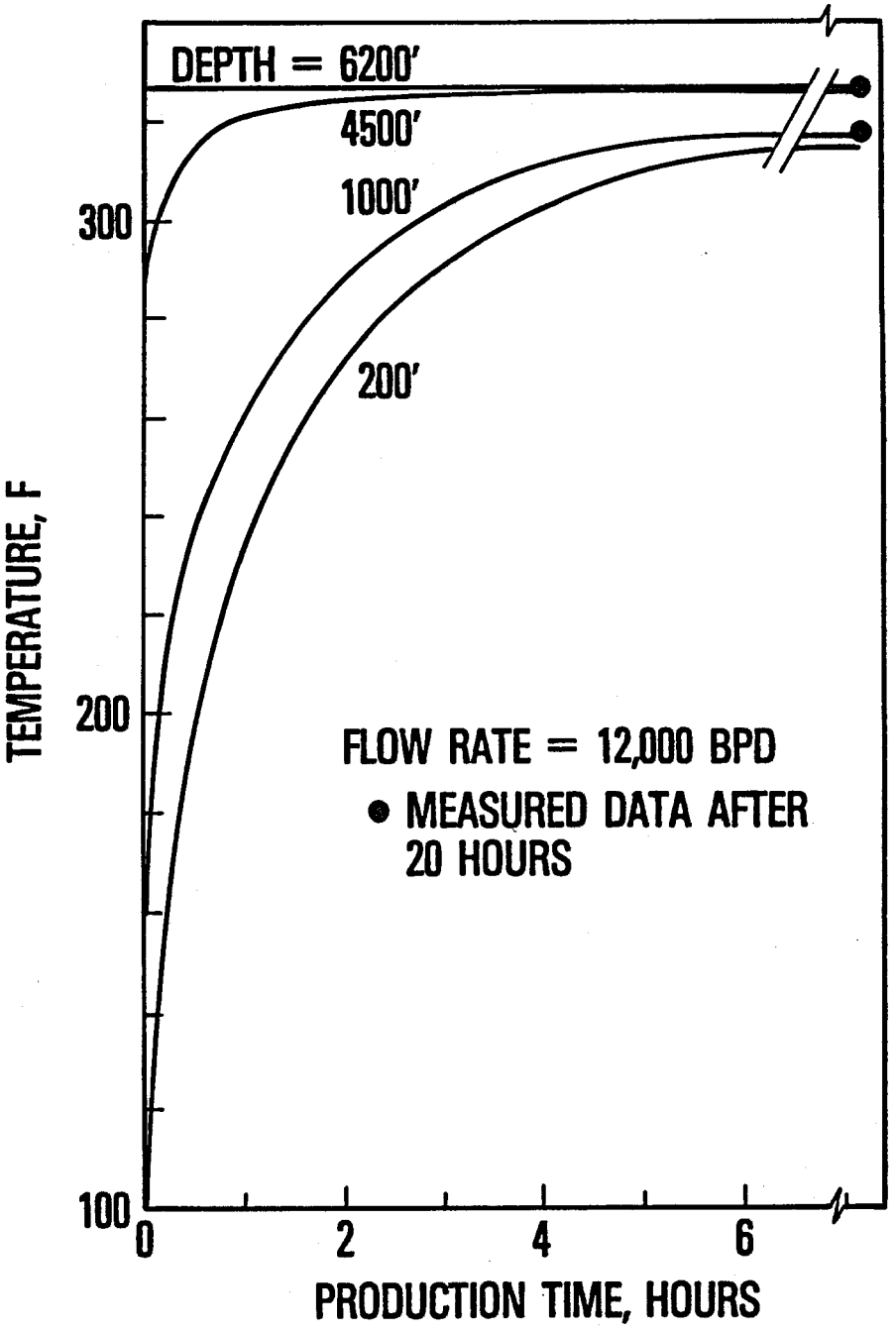

Figure 17

Undisturbed Temperature Distribution
Republic Geothermal Well #1

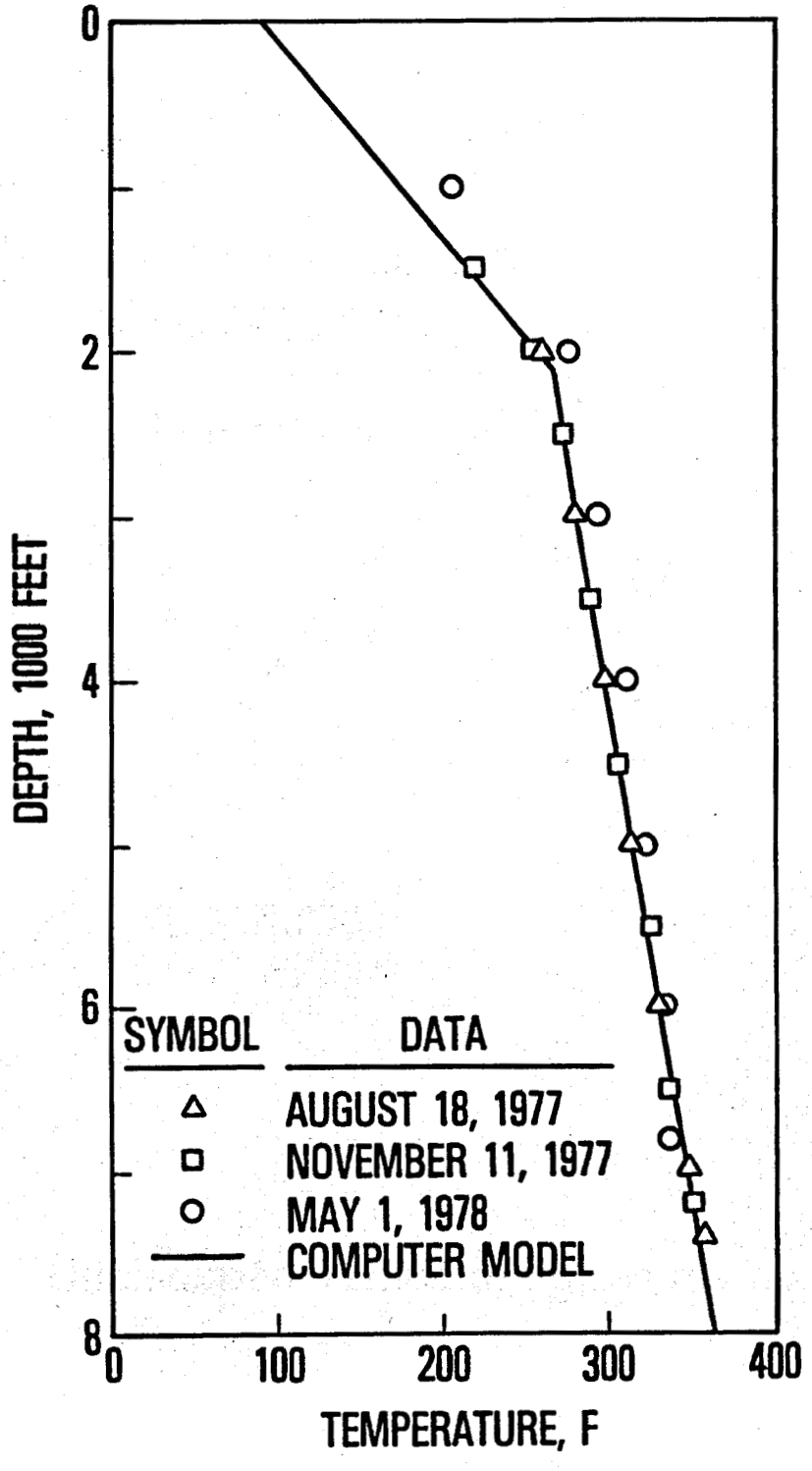

Figure 18

Steady-State Production Fluid Temperature Profile
Republic Geothermal Well #2

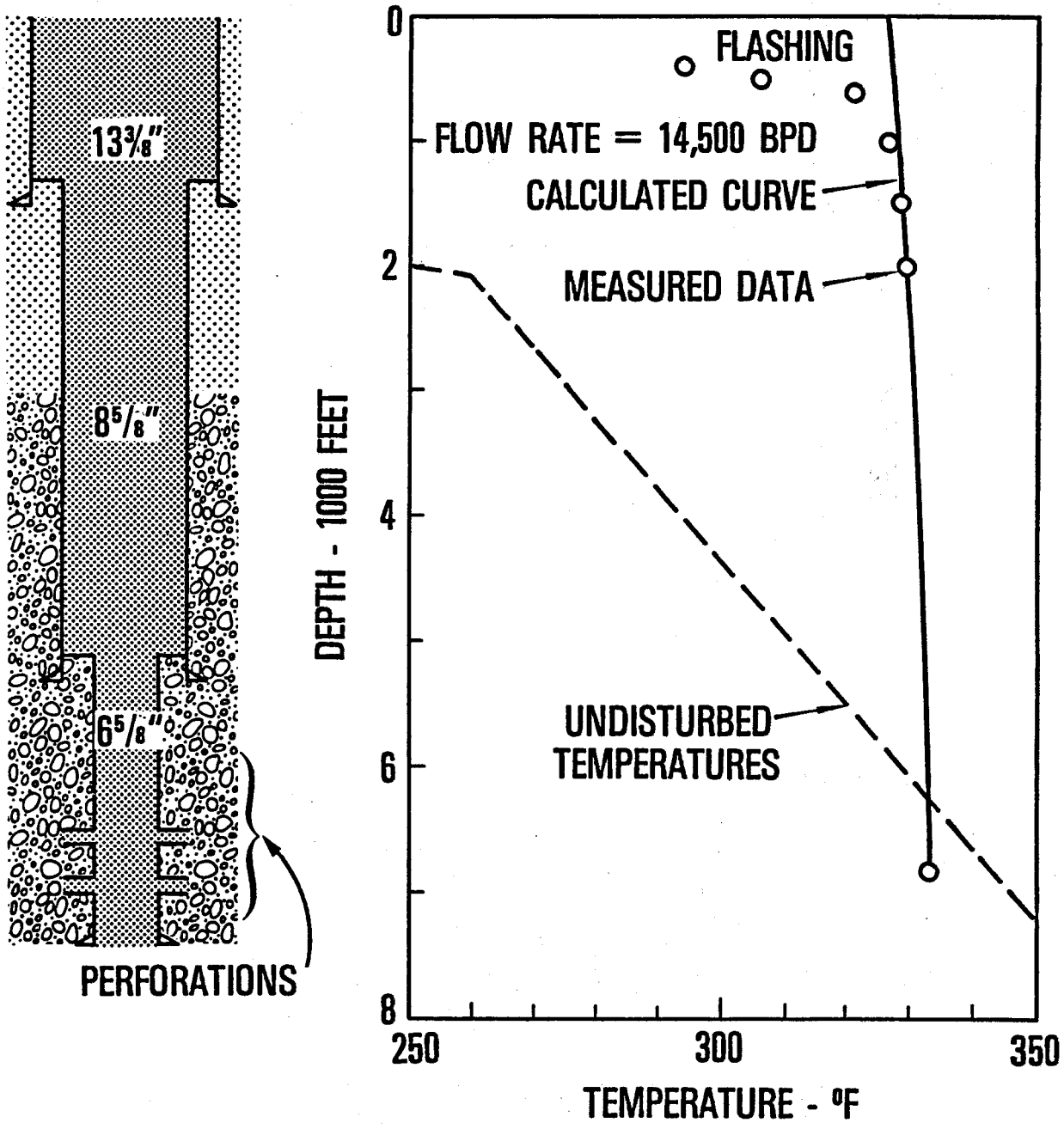

Figure 19

Transient Fluid Temperature Behavior
Republic Geothermal Well #2

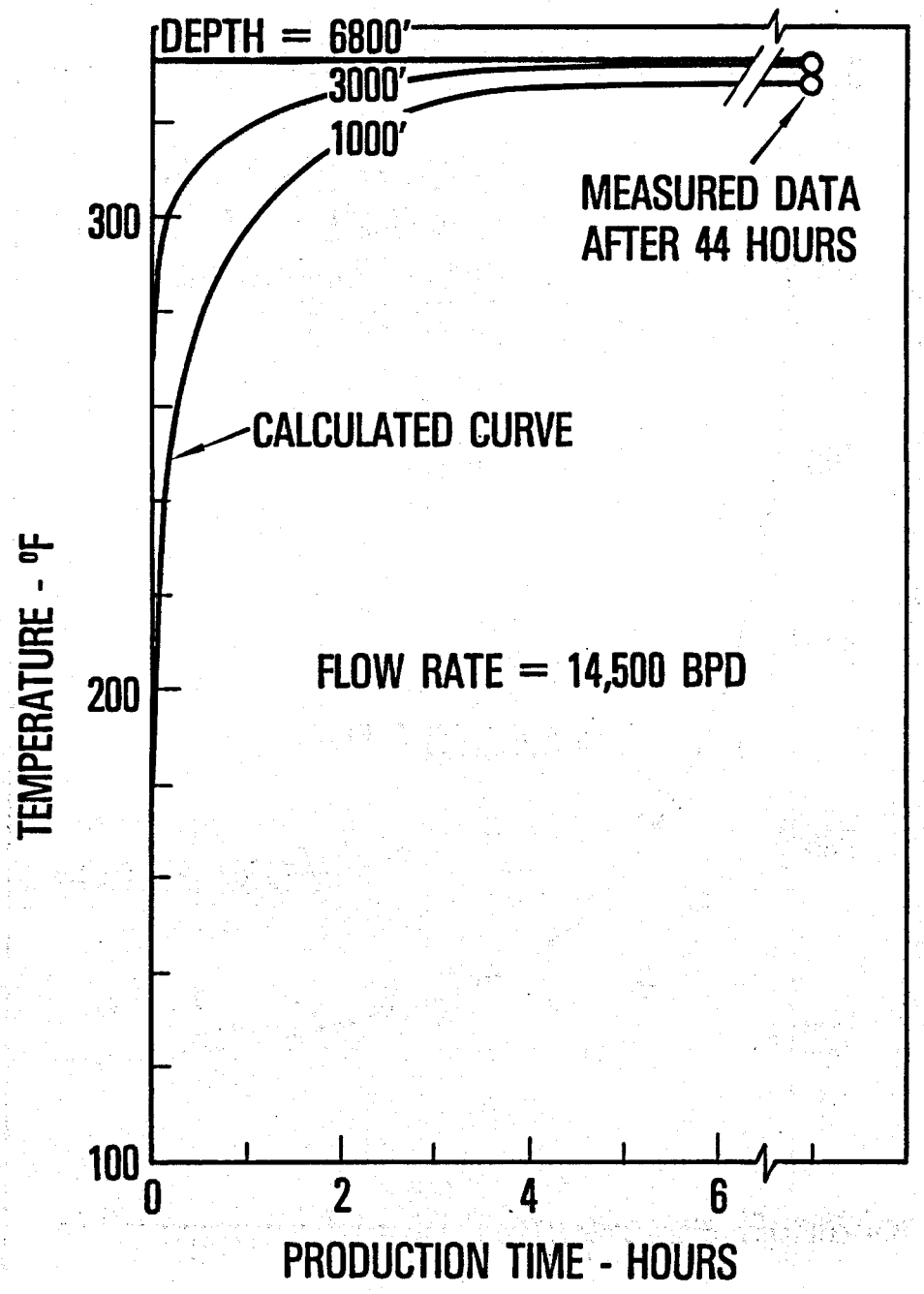

Figure 20

Comparison of Computed and Measured Bottom Hole Circulating Temperatures Gulf Well #1

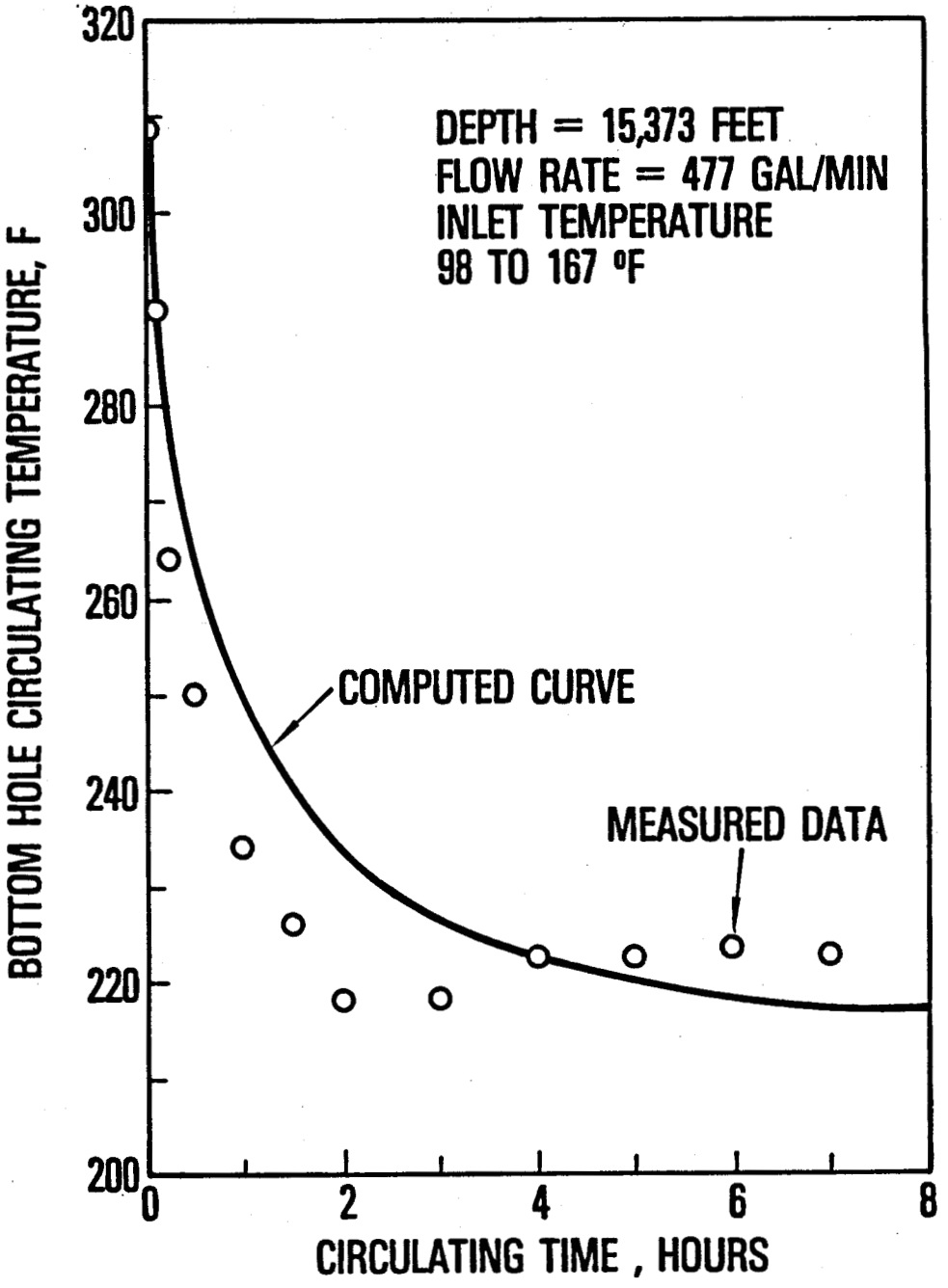

Figure 21

Circulating Fluid Temperature Profiles
Gulf Well #1

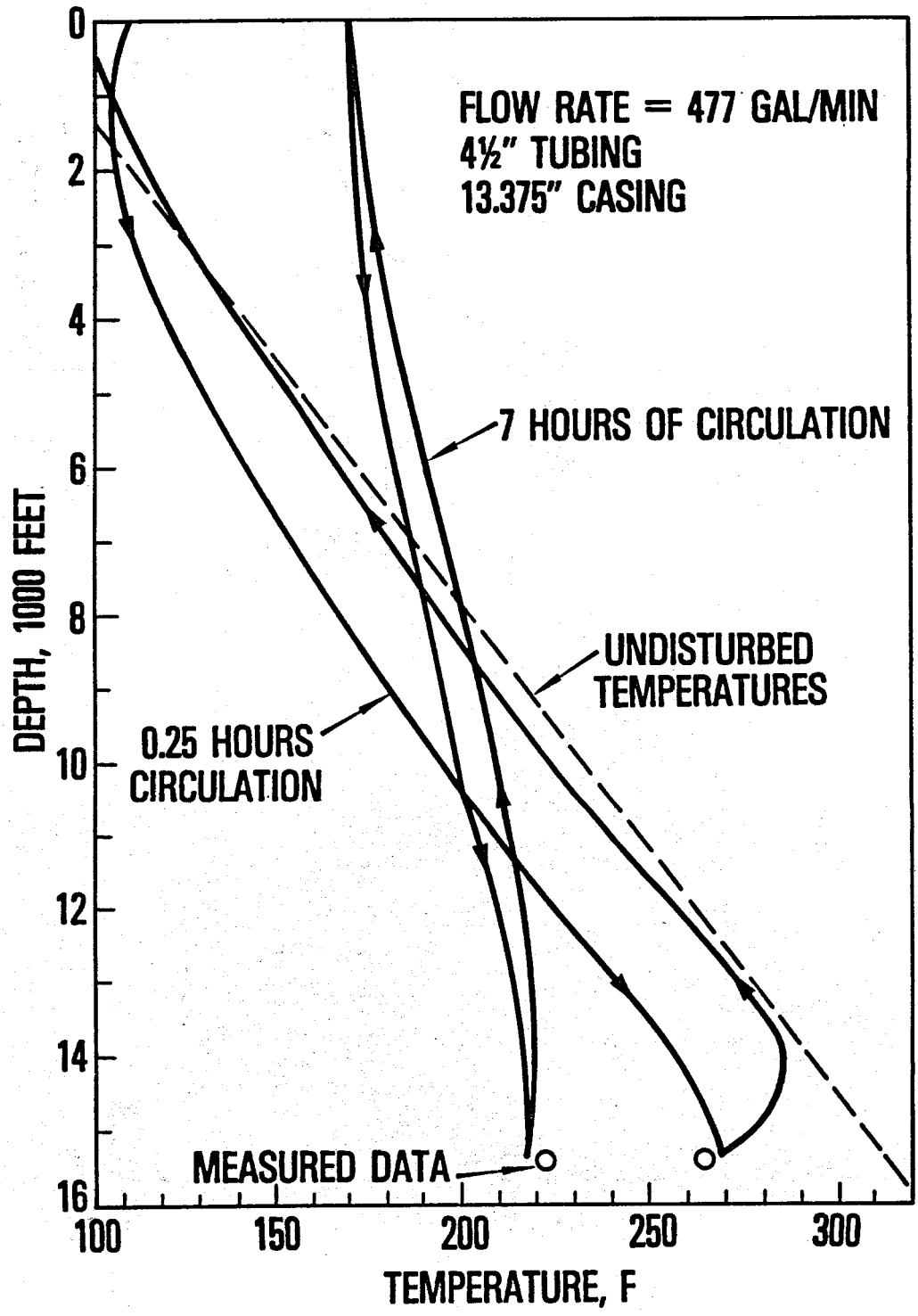

Figure 22

Computed and Measured Transient Temperature Response Gulf Well # 2

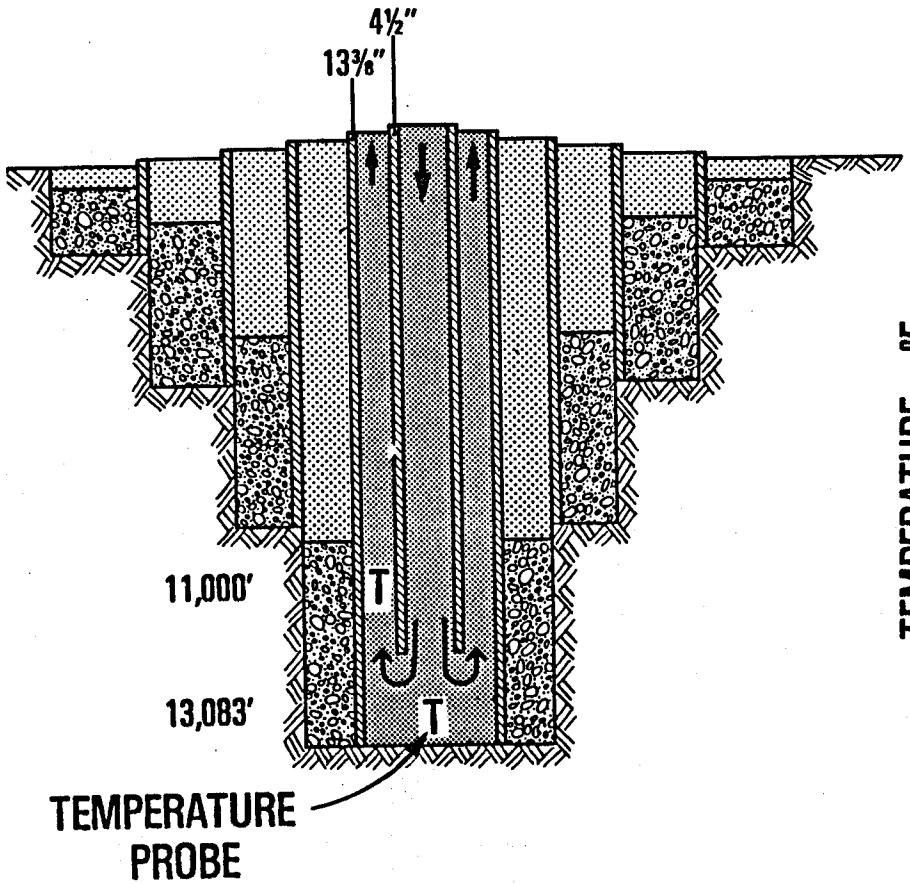

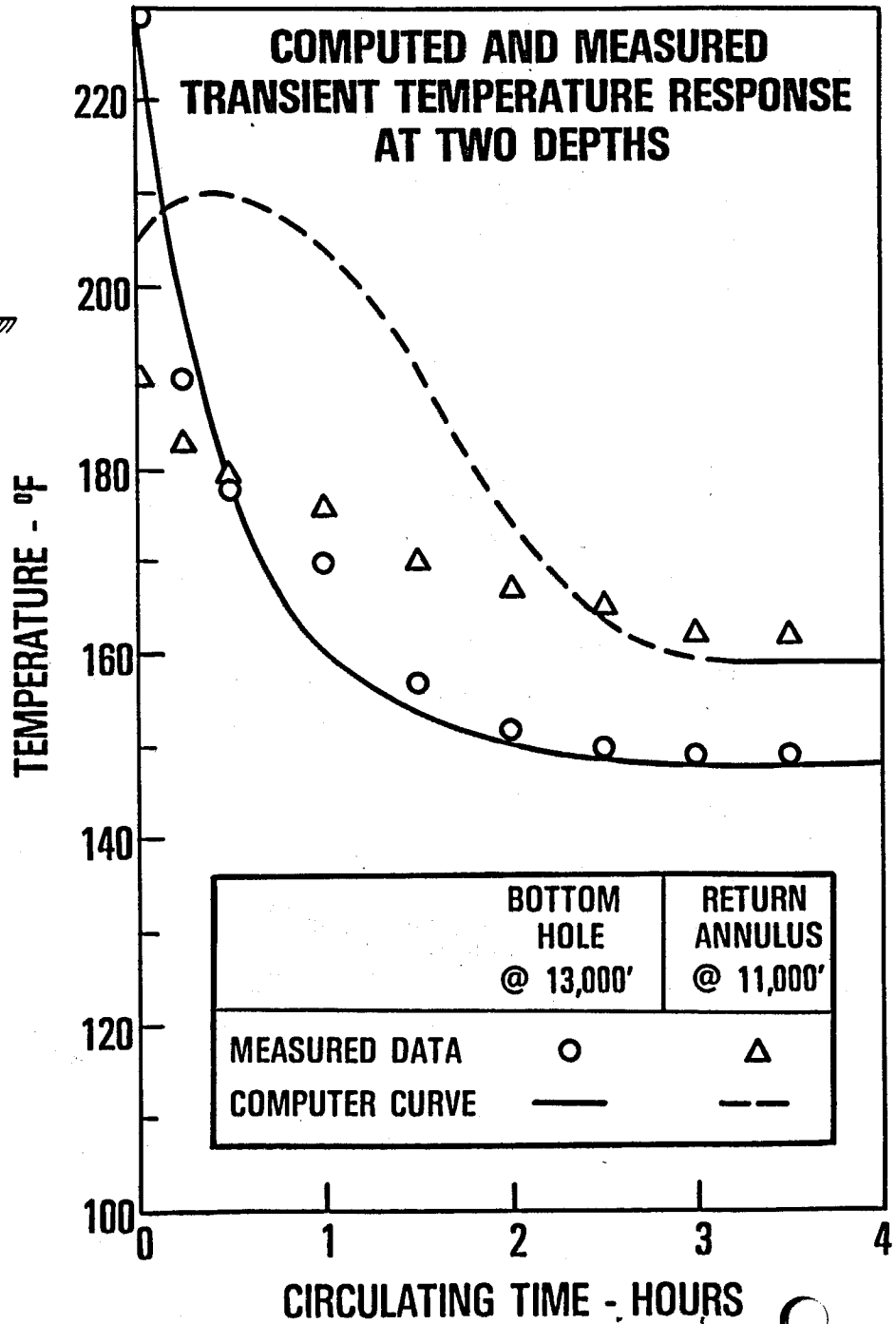

Figure 23

Fluid Temperature Profile After 30 Minutes of Circulation Gulf Well # 2

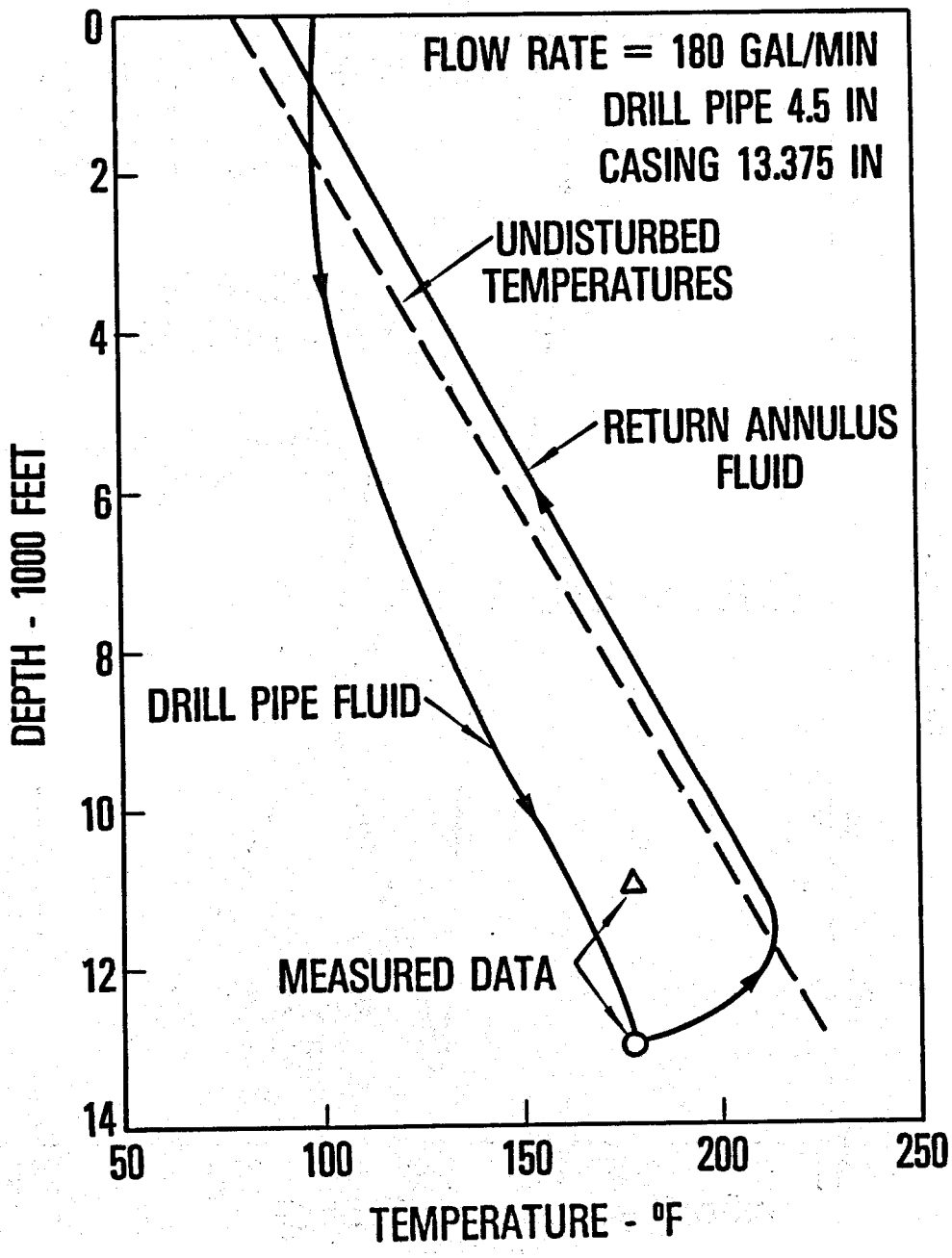

Figure 24

Fluid Temperature Profile
After 3 hours of Circulation
Gulf Well #2

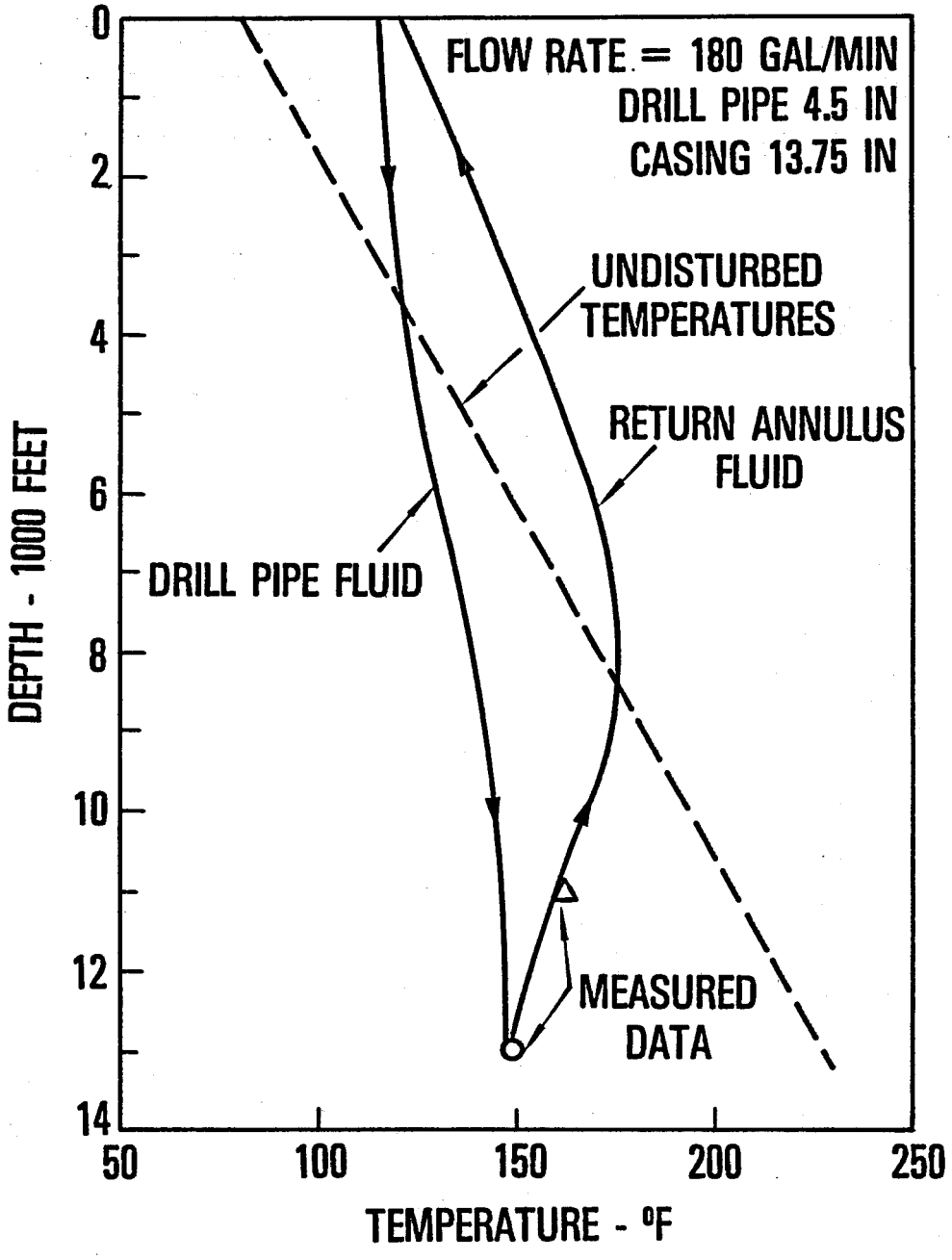

Figure 25

Sensitivity of Bottom Hole Temperature To Flow Rate

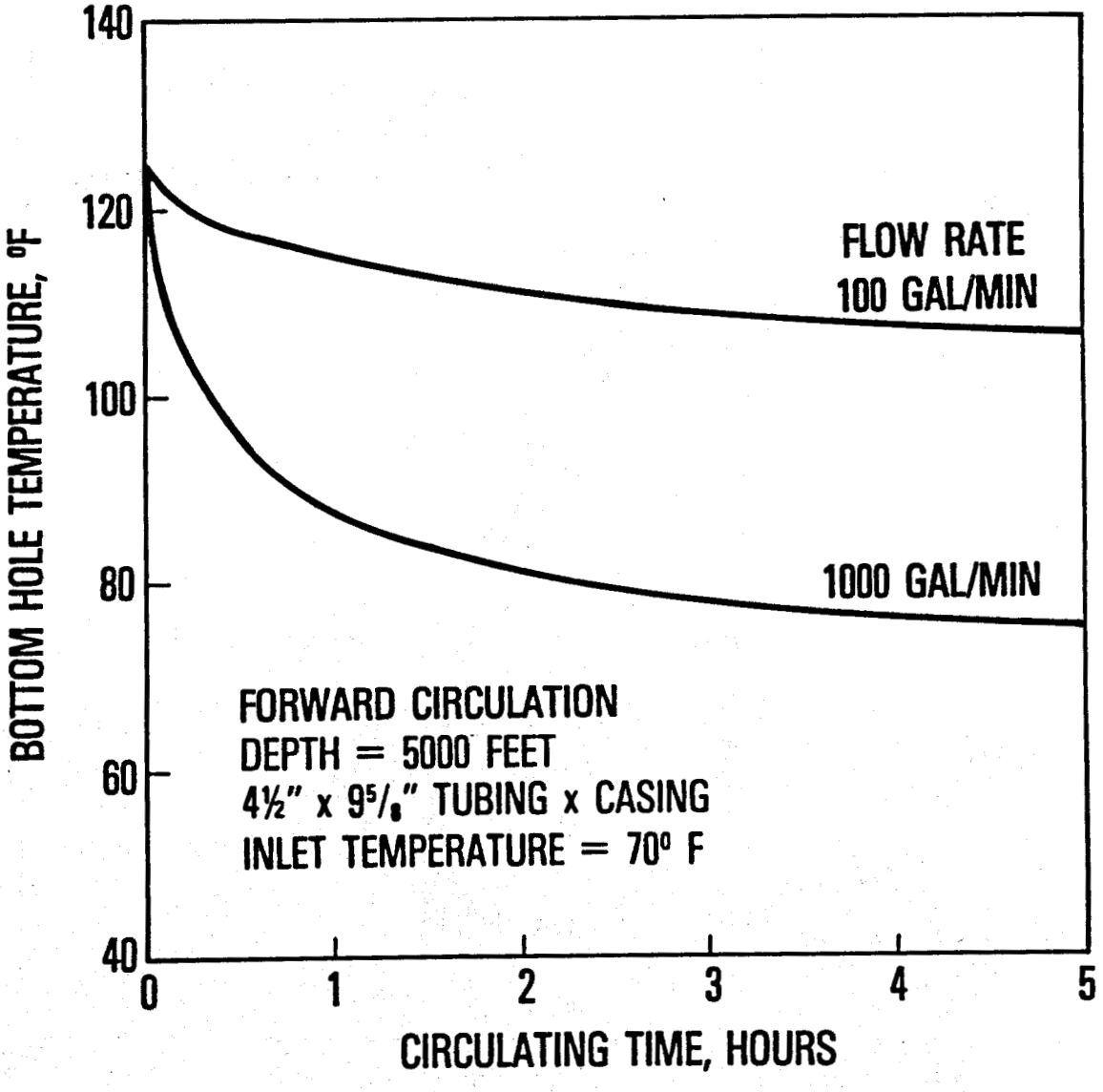

Figure 26

Sensitivity of Fluid Temperature Profile To Flow Rate

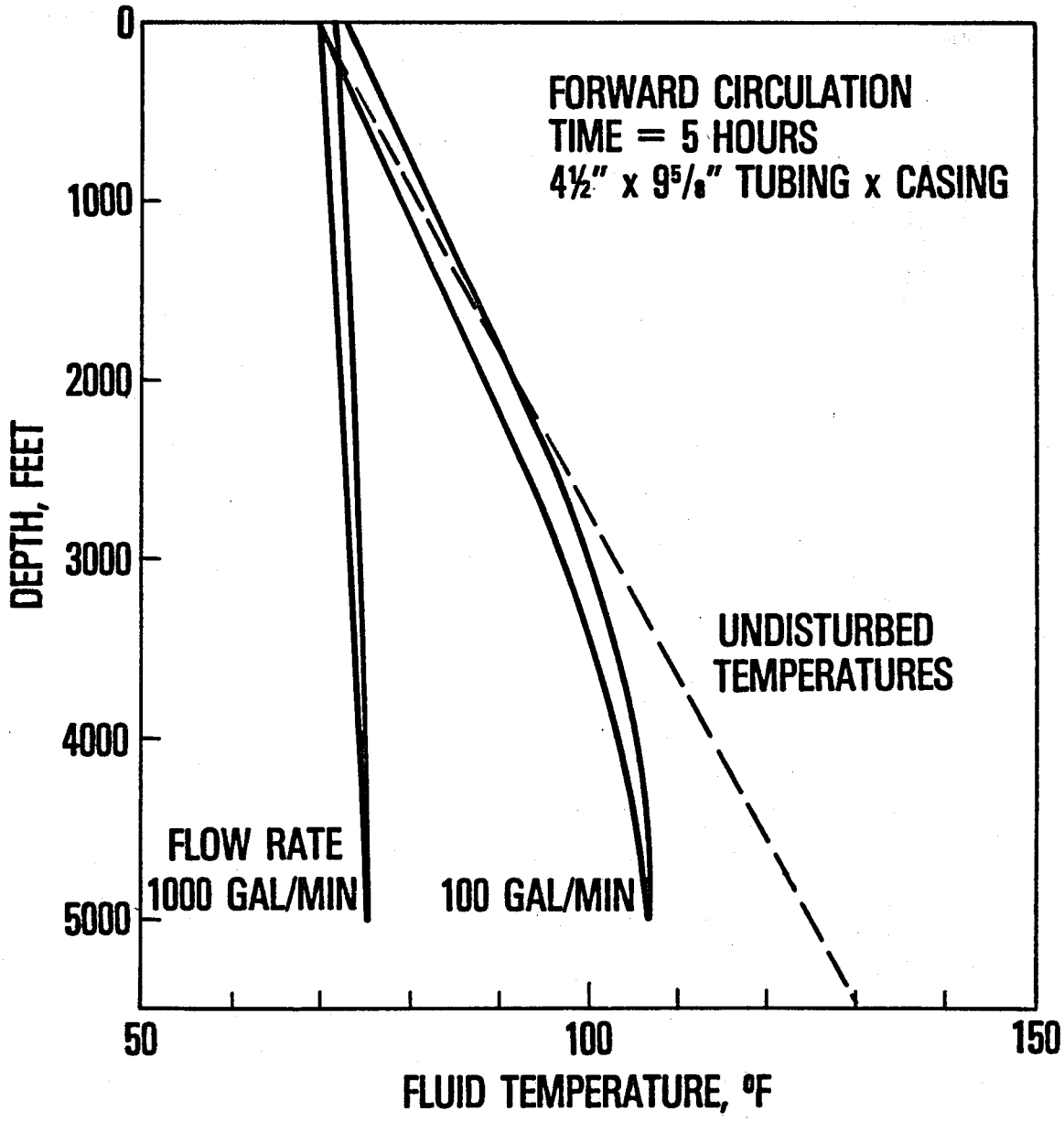

Figure 27

Sensitivity of Bottom Hole Temperature To Inlet Temperature

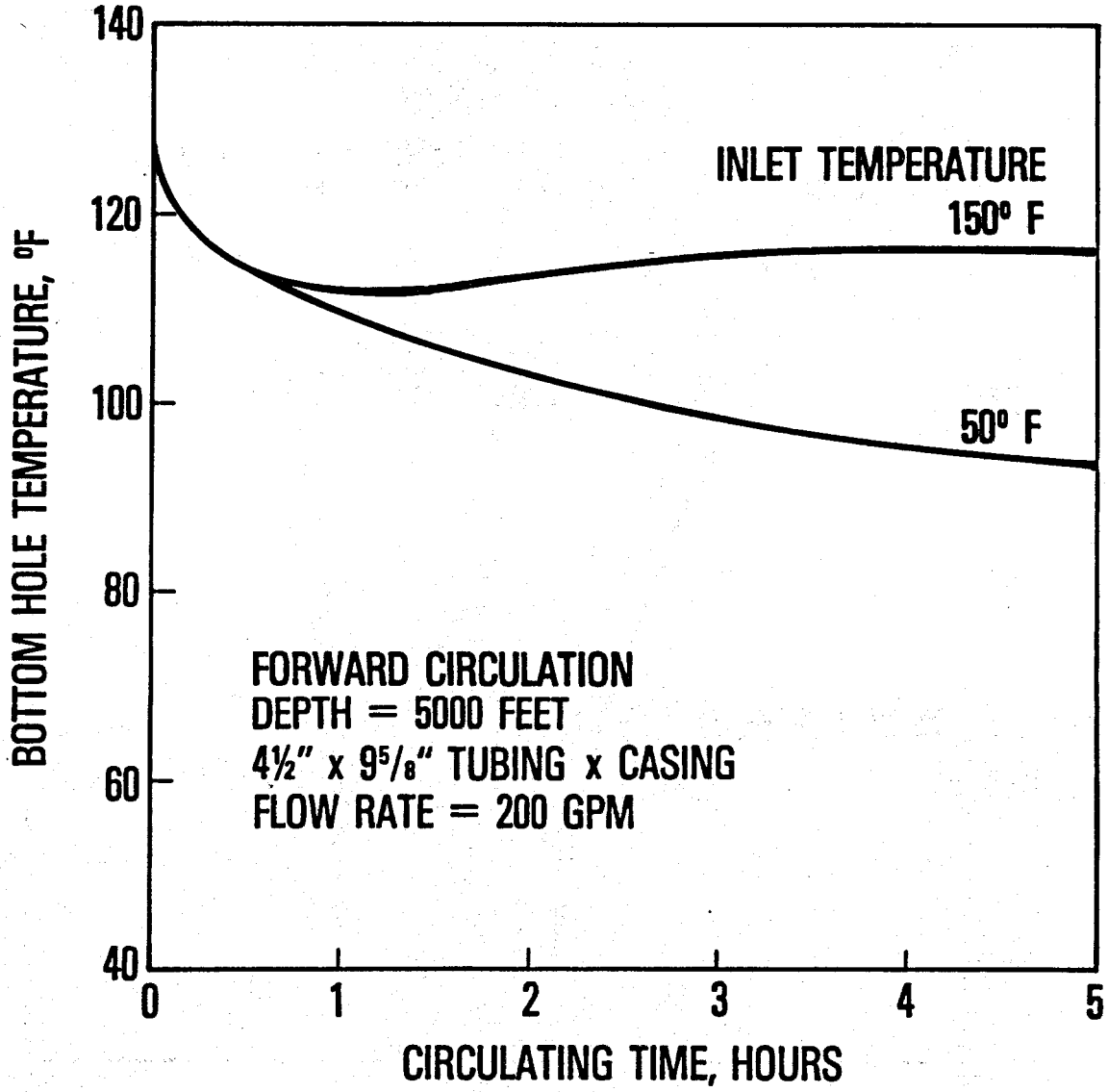

Figure 28

Sensitivity of Fluid Temperature Profile To Inlet Temperature

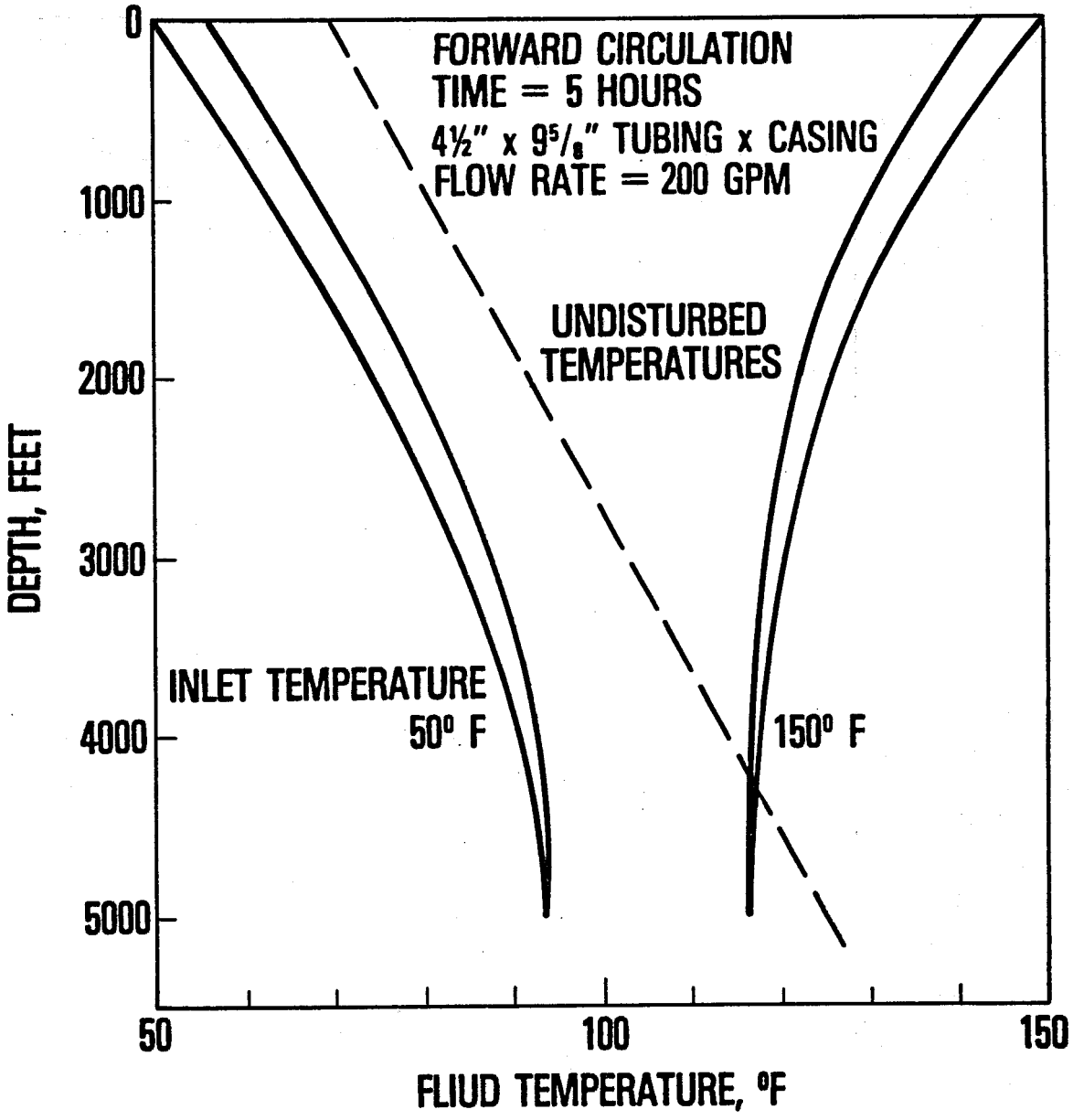

Figure 29

Sensitivity of Bottom Hole Temperature To Fluid Density

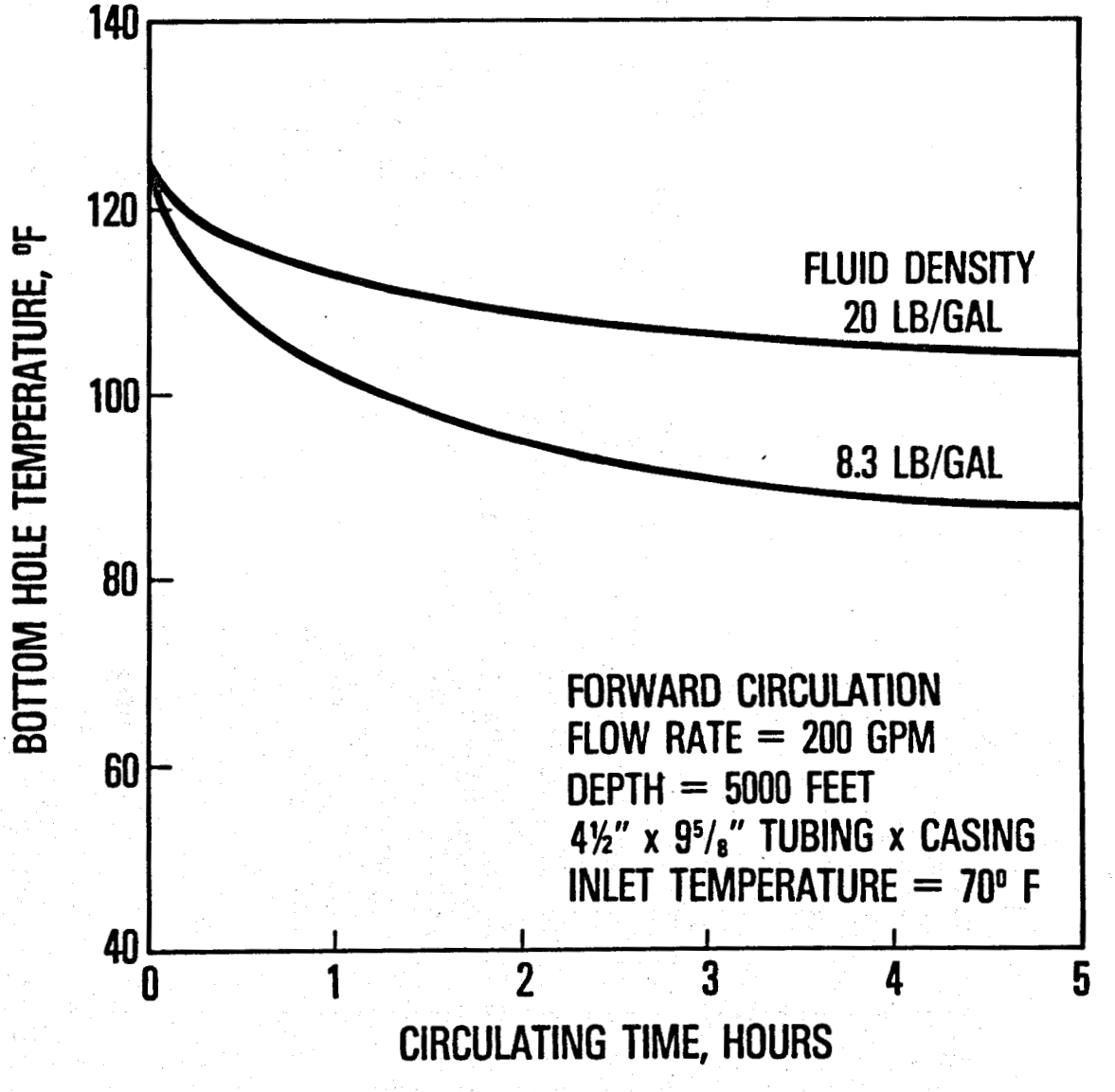

Figure 30

Sensitivity of Fluid Temperature Profile To Fluid Density

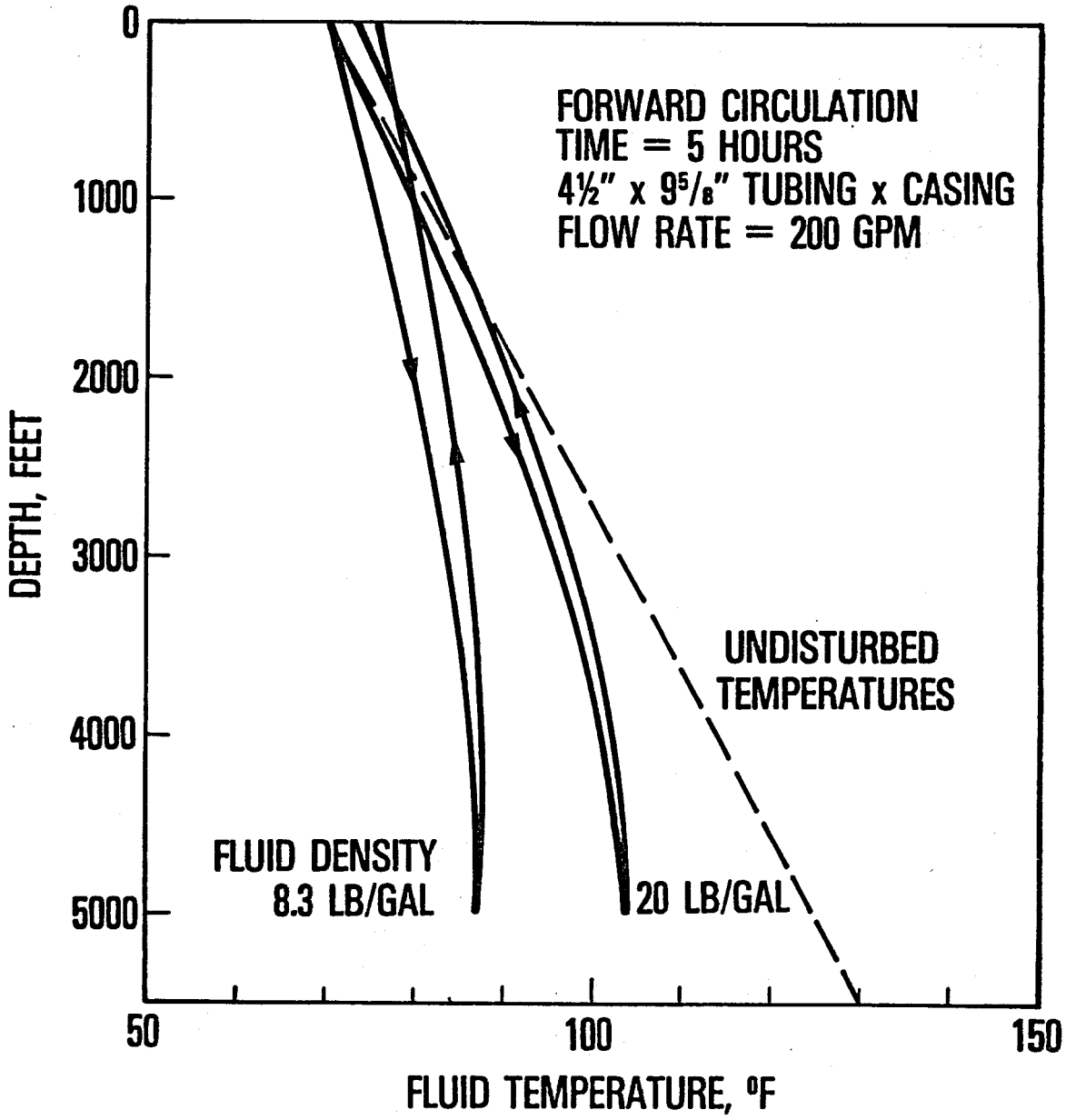

Figure 31

Sensitivity of Bottom Hole Temperature To Fluid Plastic Viscosity

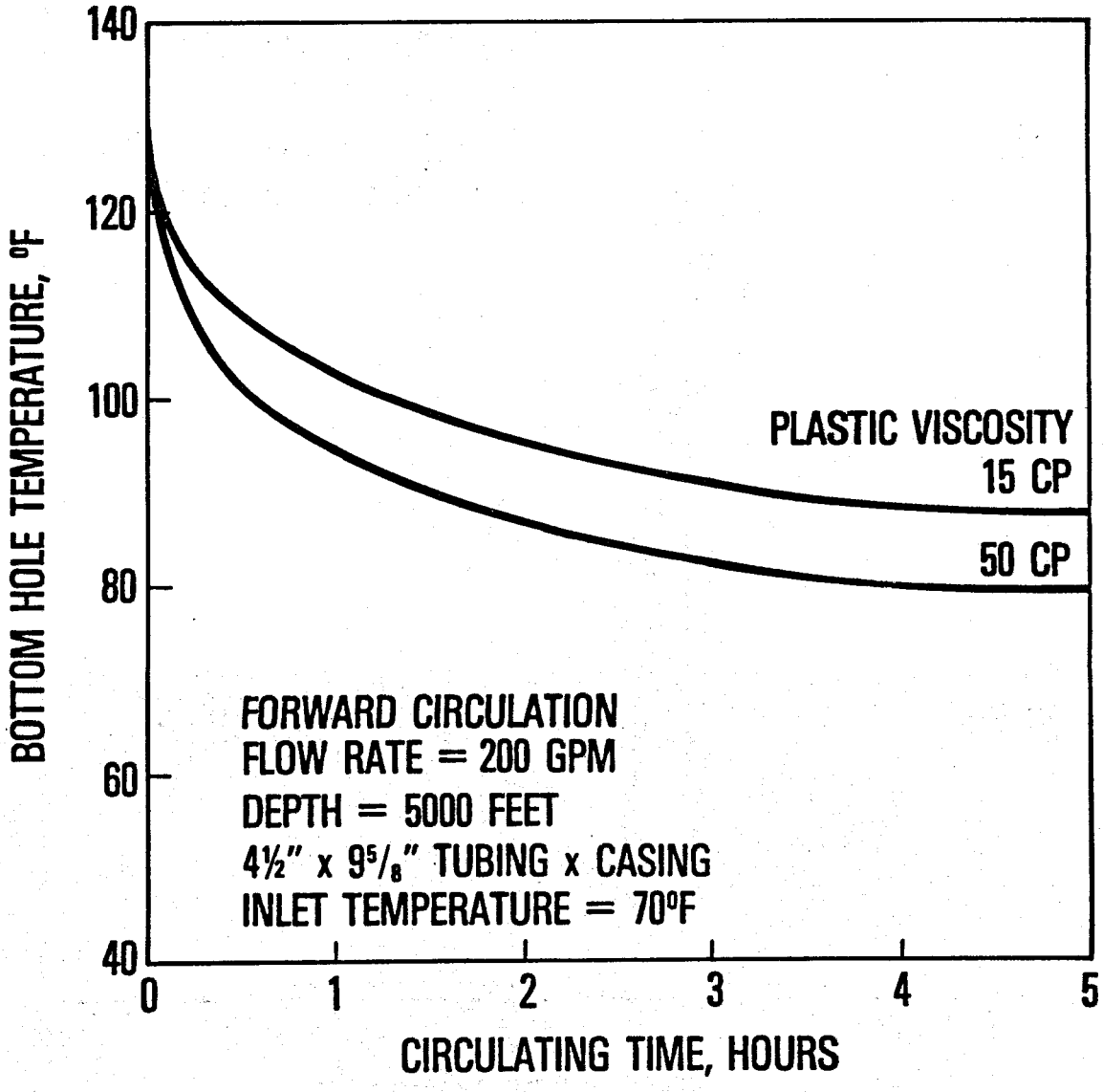

Figure 32

Sensitivity of Fluid Temperature Profile To Fluid Plastic Viscosity

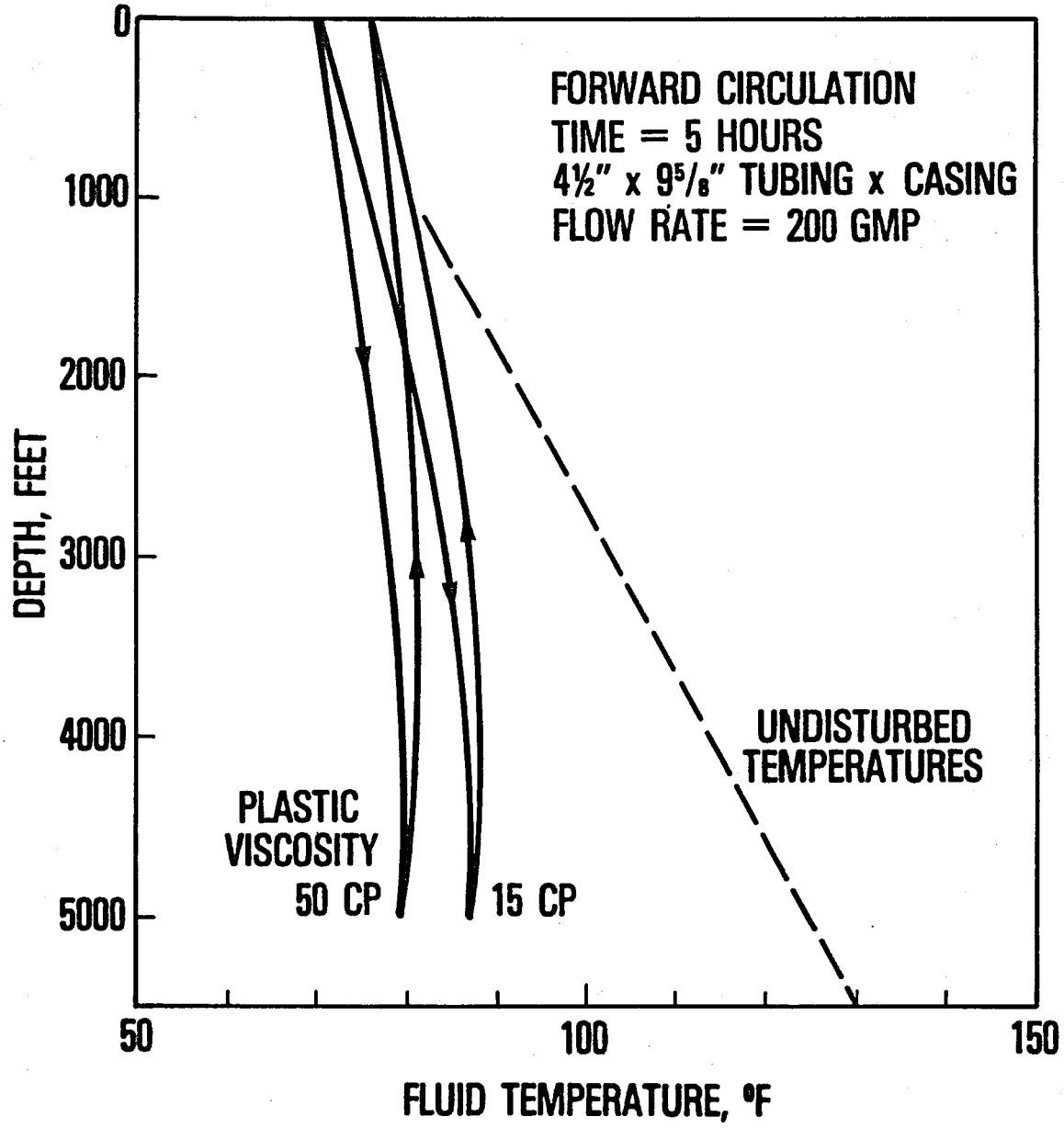

Figure 33

Sensitivity of Bottom Hole Temperature To Undisturbed Temperature Gradient

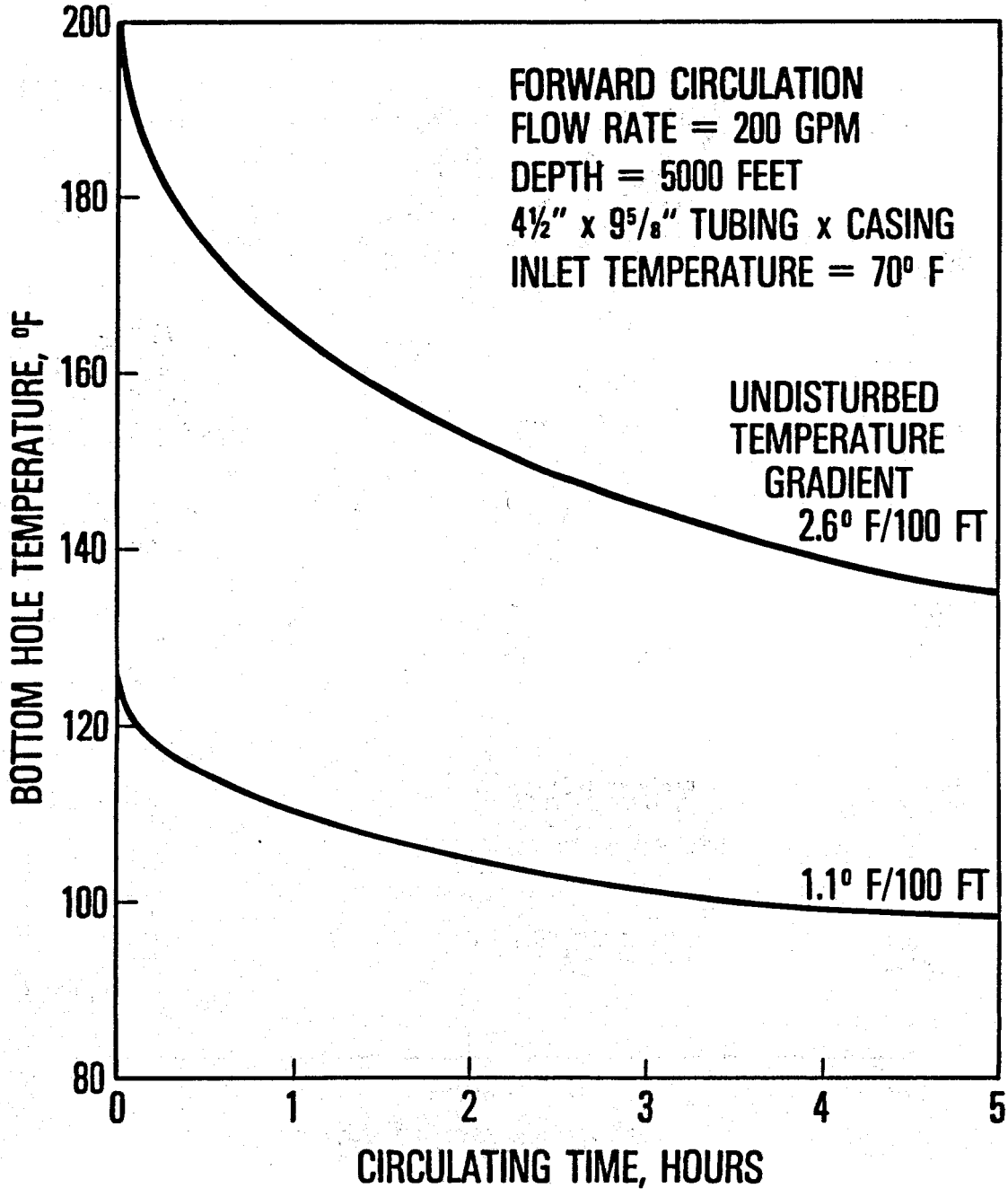

Figure 34

Sensitivity of Fluid Temperature Profile To Undisturbed Temperature Gradient

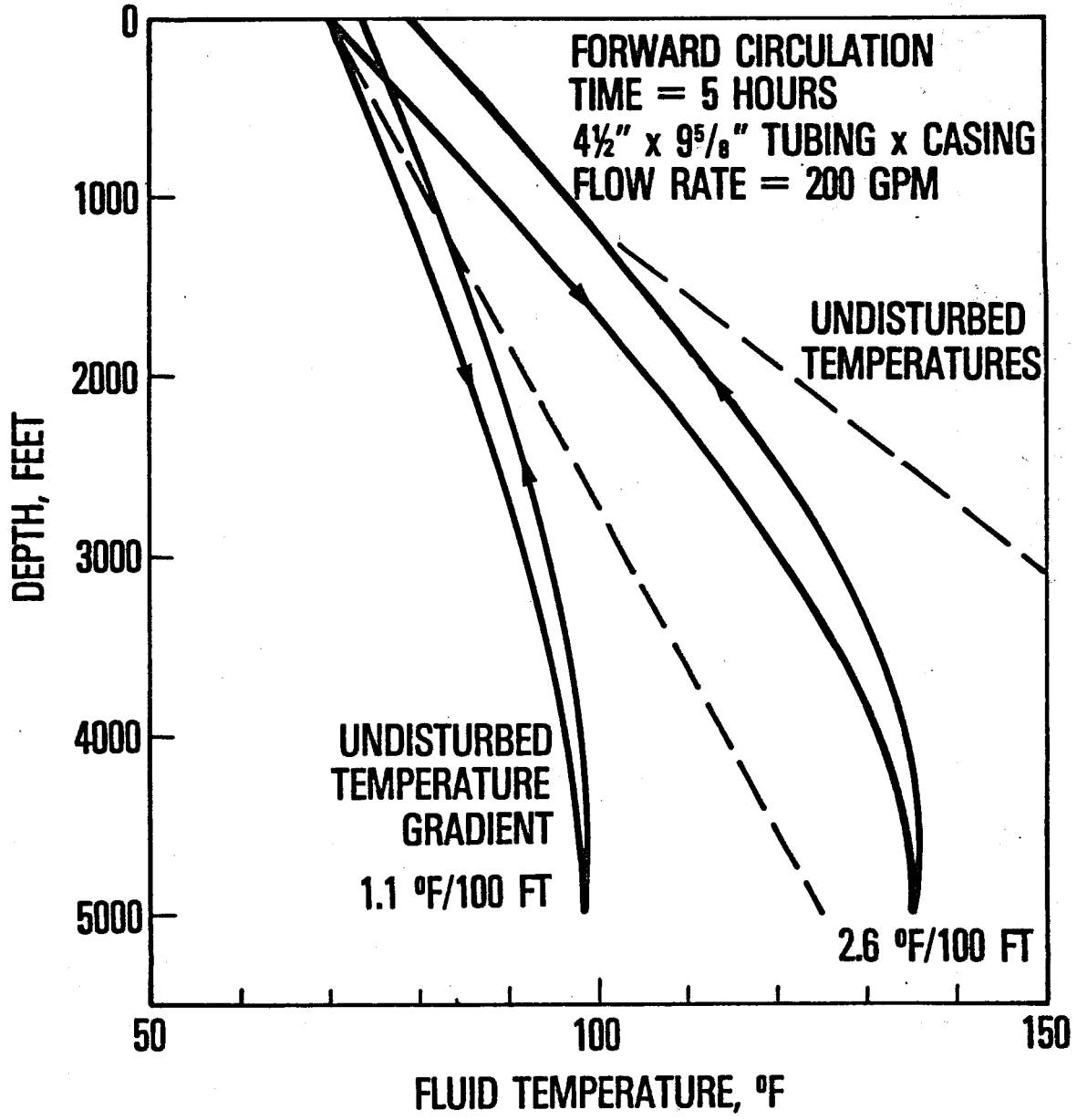

Figure 35

Sensitivity of Bottom Hole Temperature To Soil Thermal Conductivity

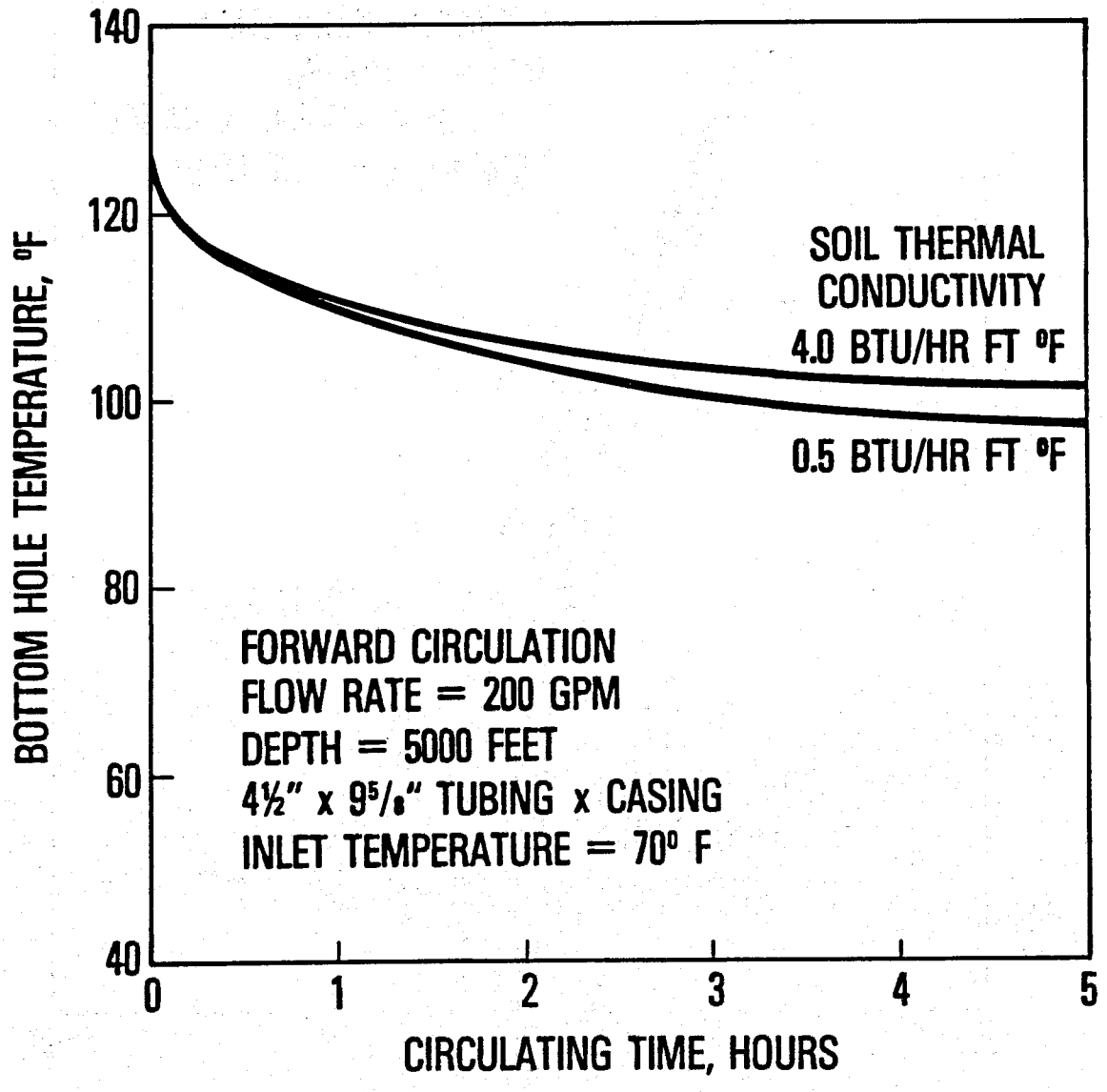

Figure 36

Sensitivity of Fluid Temperature Profile To Soil Thermal Conductivity

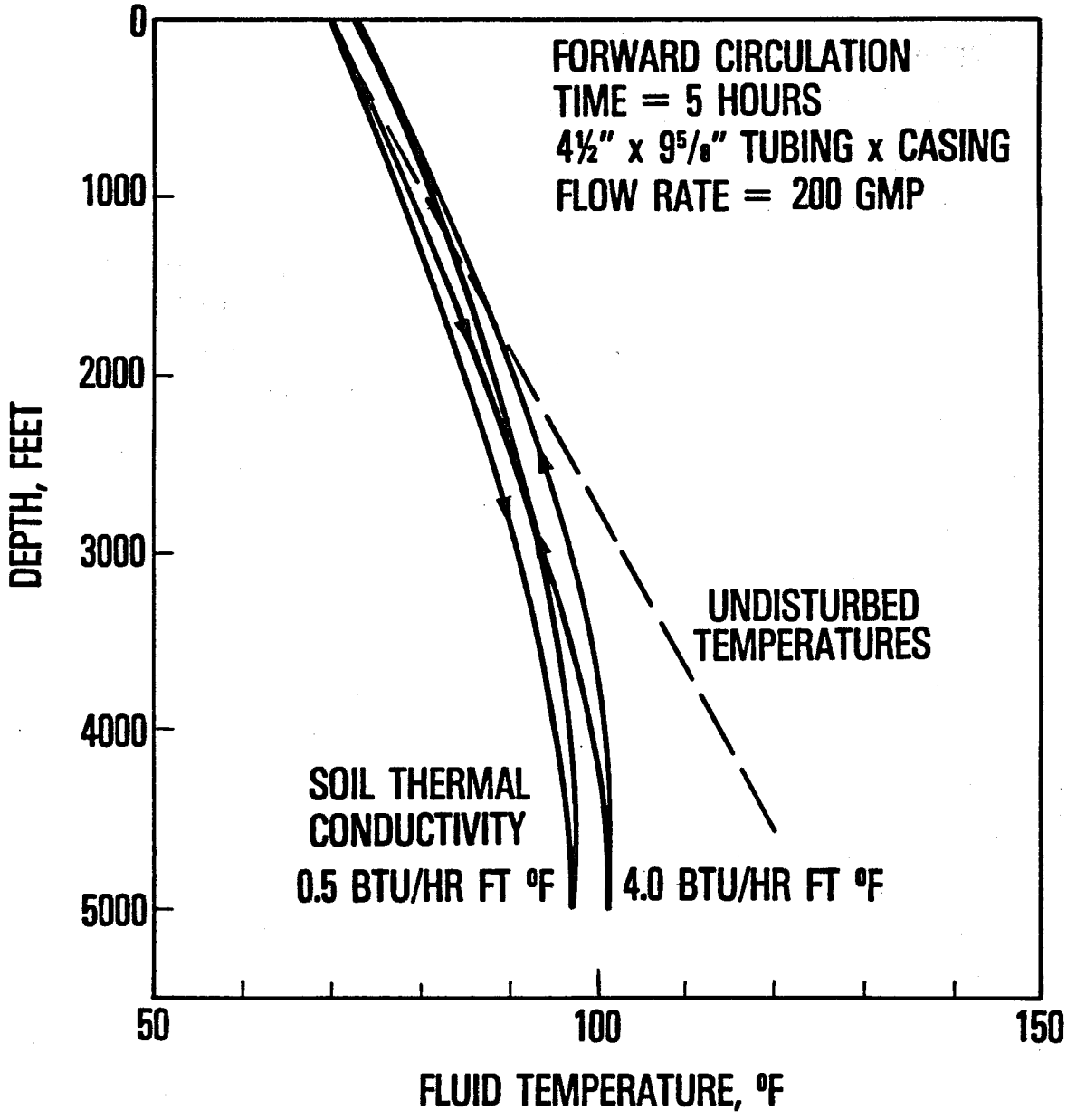

Figure 37

Sensitivity of Bottom Hole Temperature To Well Depth

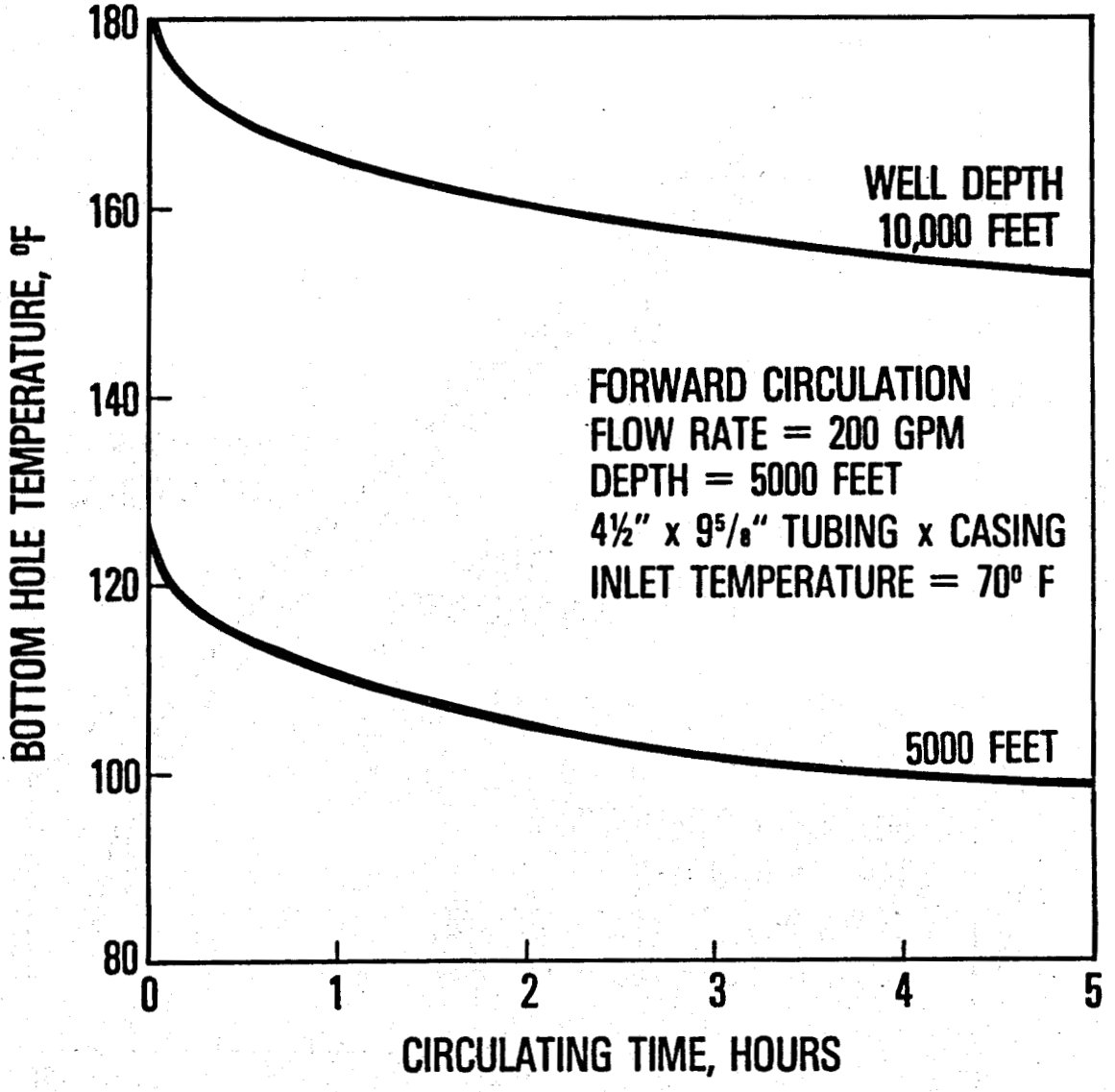

Figure 38

Sensitivity of Fluid Temperature Profile To Well Depth

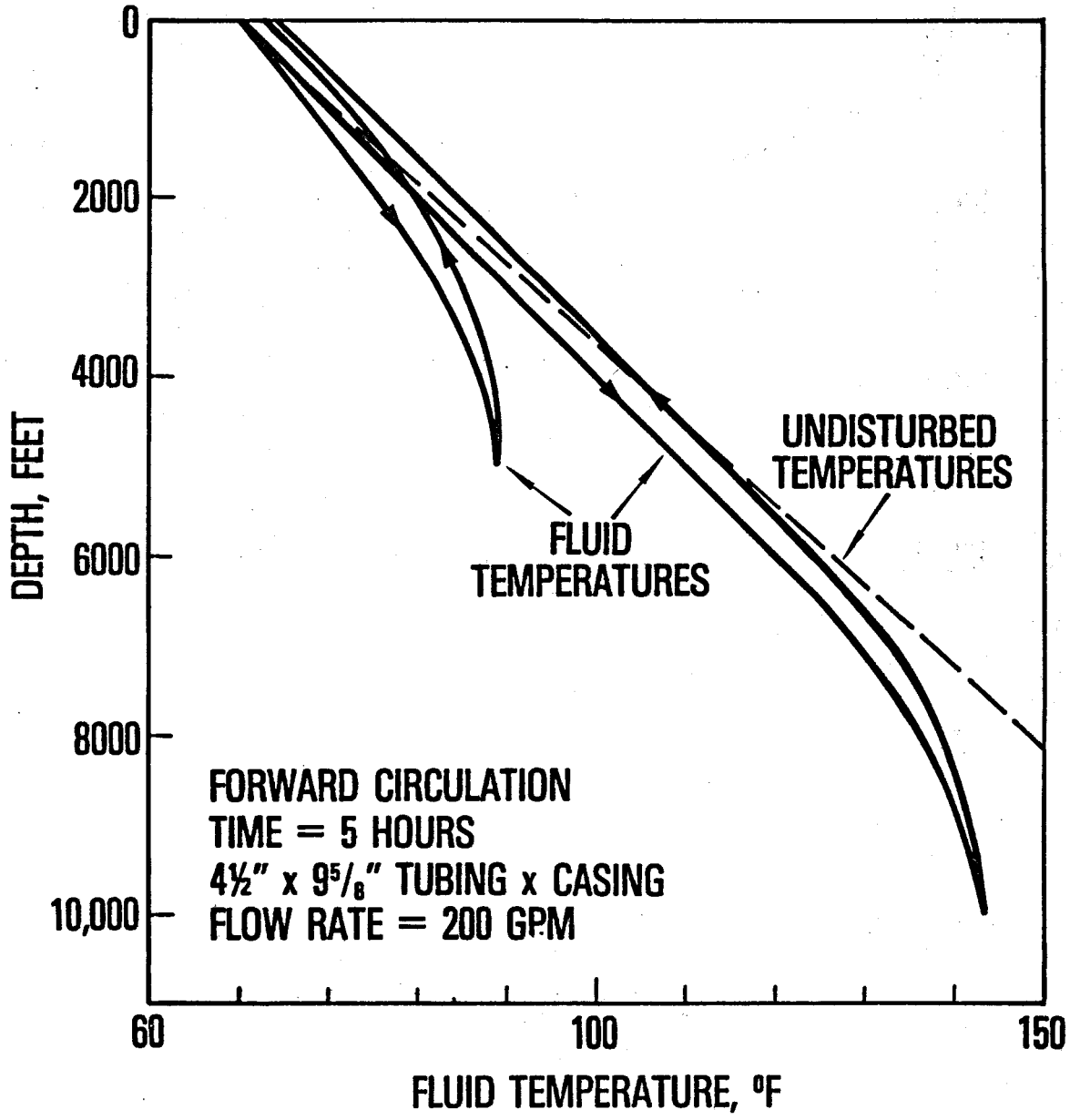

Figure 39

Sensitivity of Bottom Hole Temperature To Flow Rate

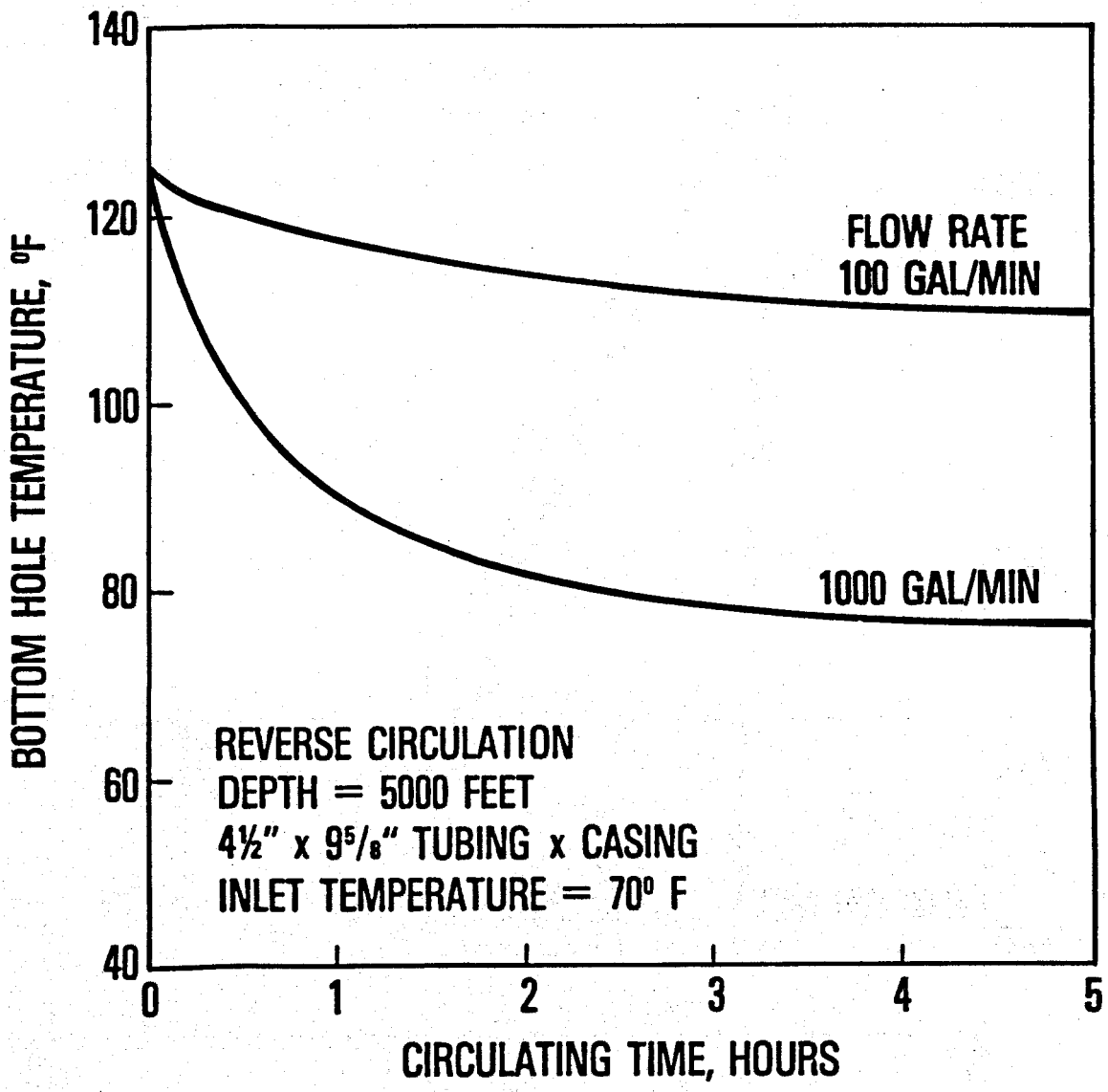

Figure 40

Sensitivity of Fluid Temperature Profile To Flow Rate

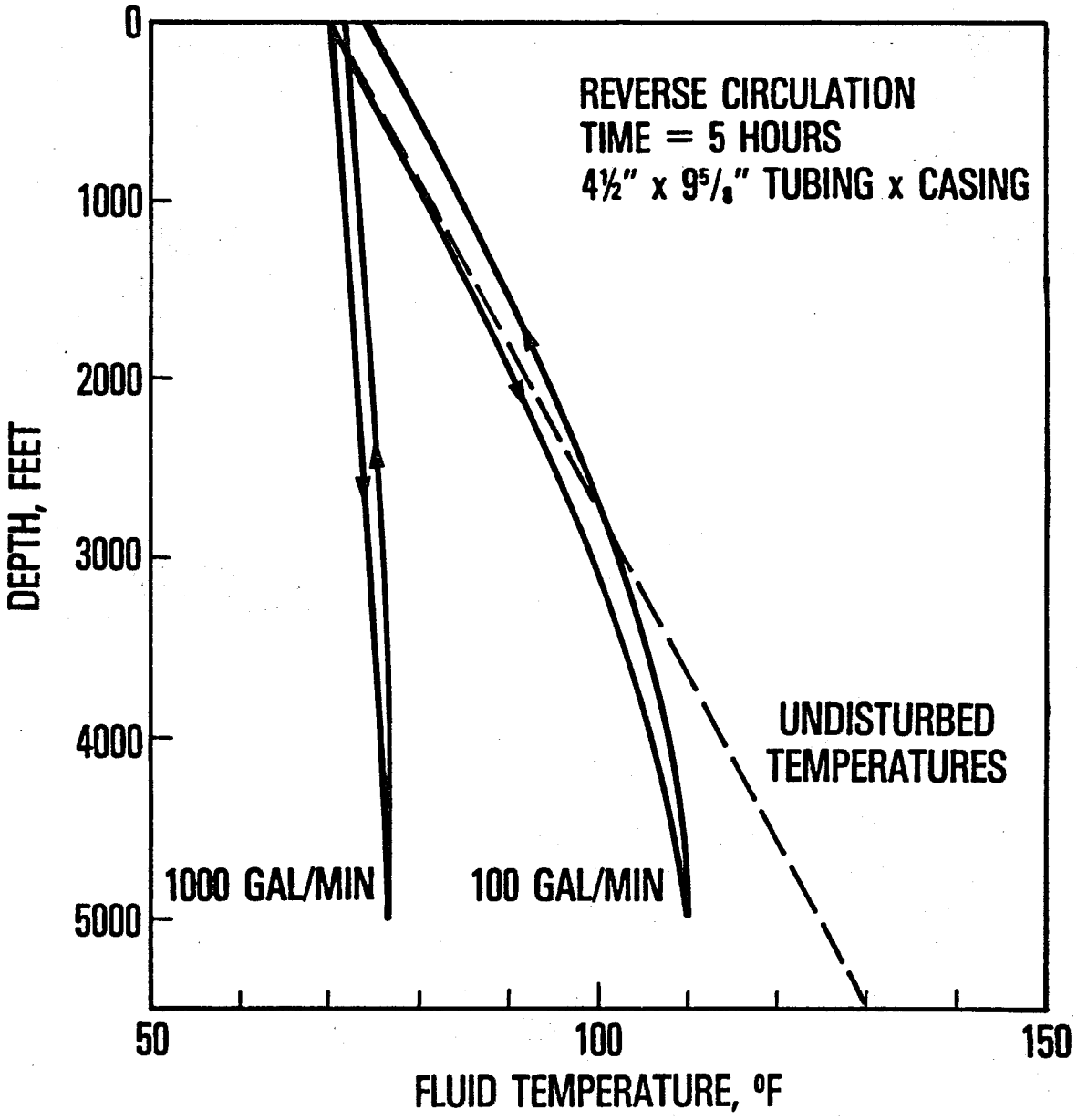

Figure 41

Sensitivity of Bottom Hole Temperature To Inlet Temperature

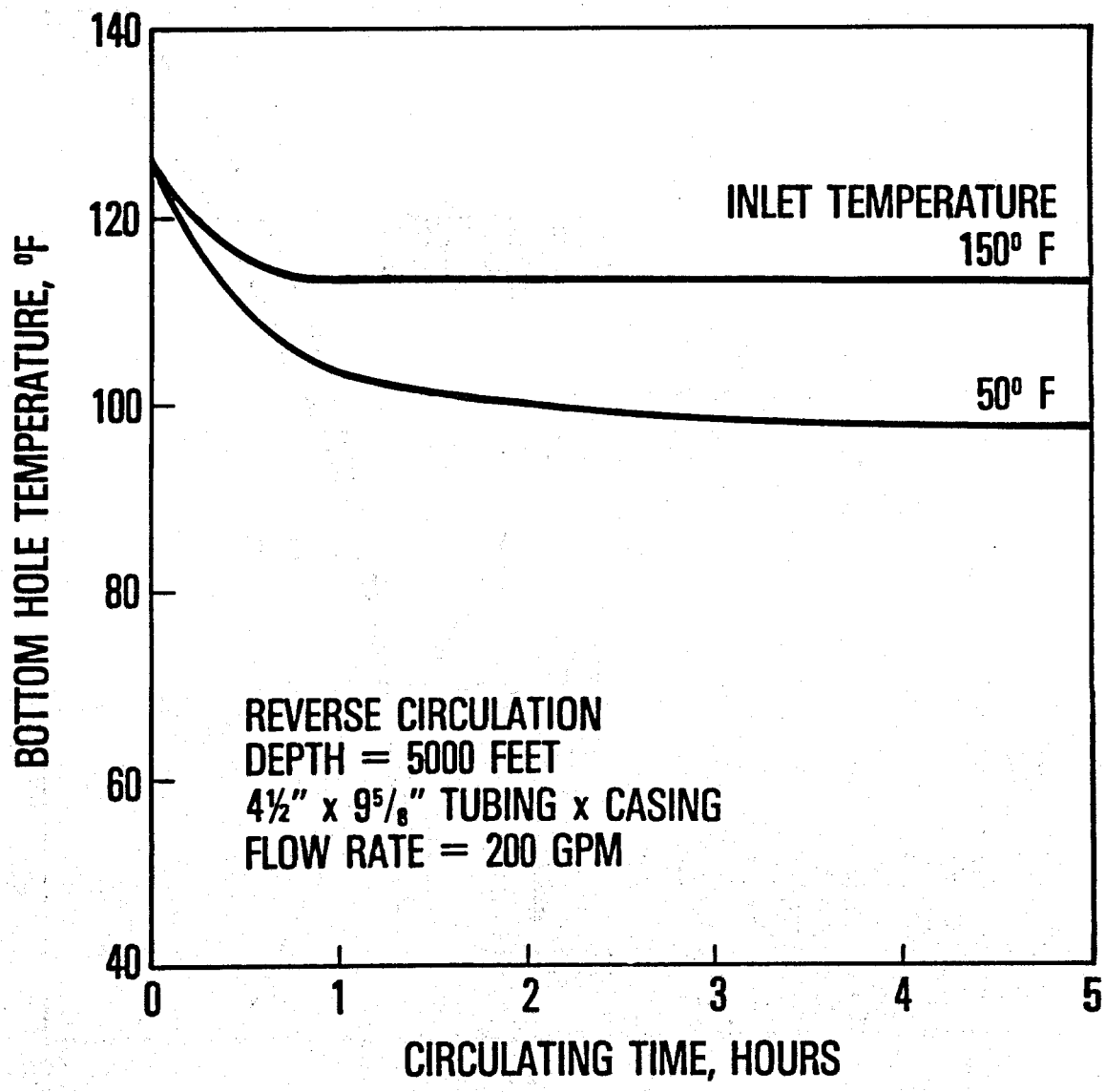

Figure 42

Sensitivity of Fluid Temperature Profile To Inlet Temperature

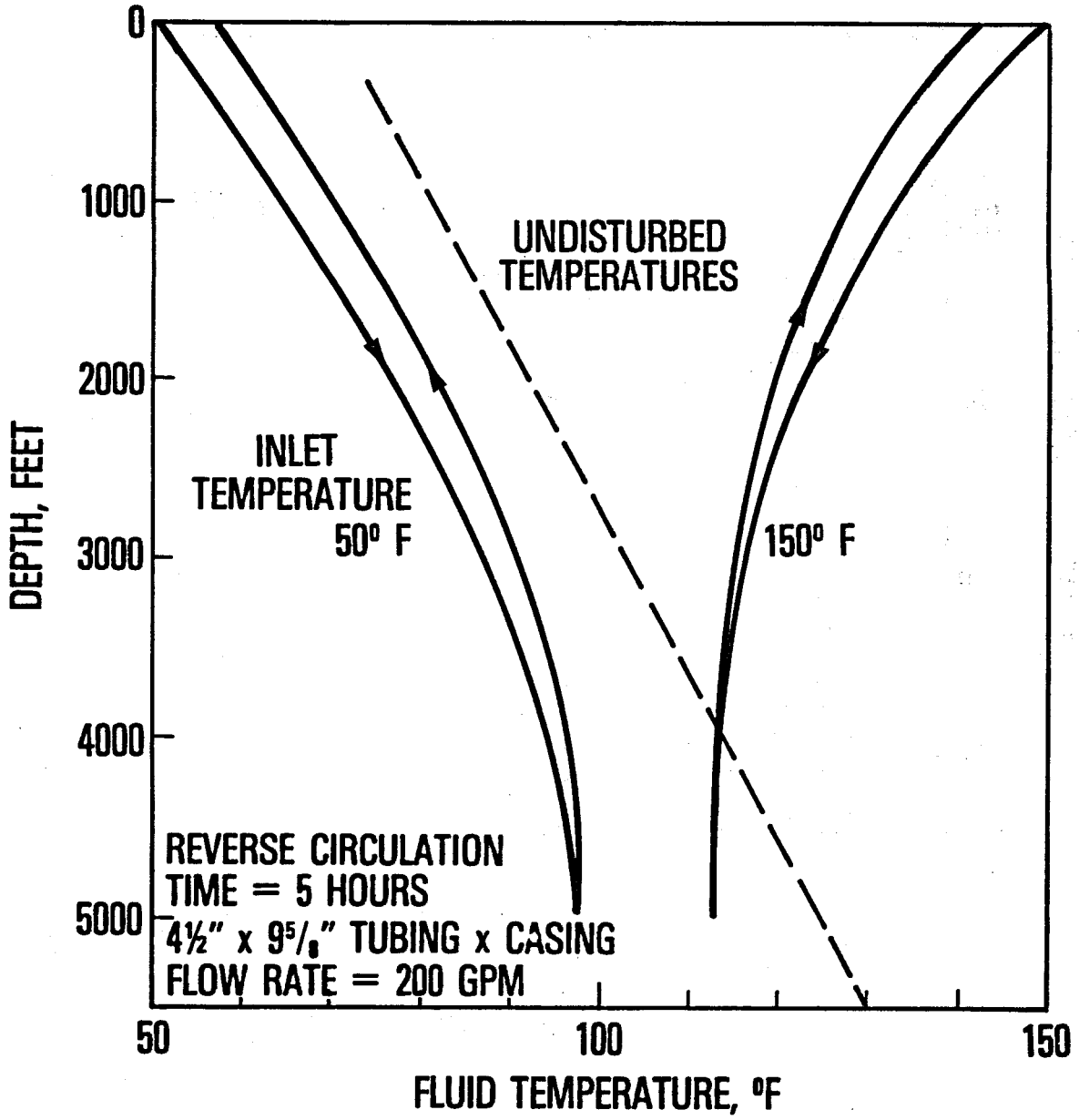

Figure 43

Sensitivity of Bottom Hole Temperature To Fluid Density

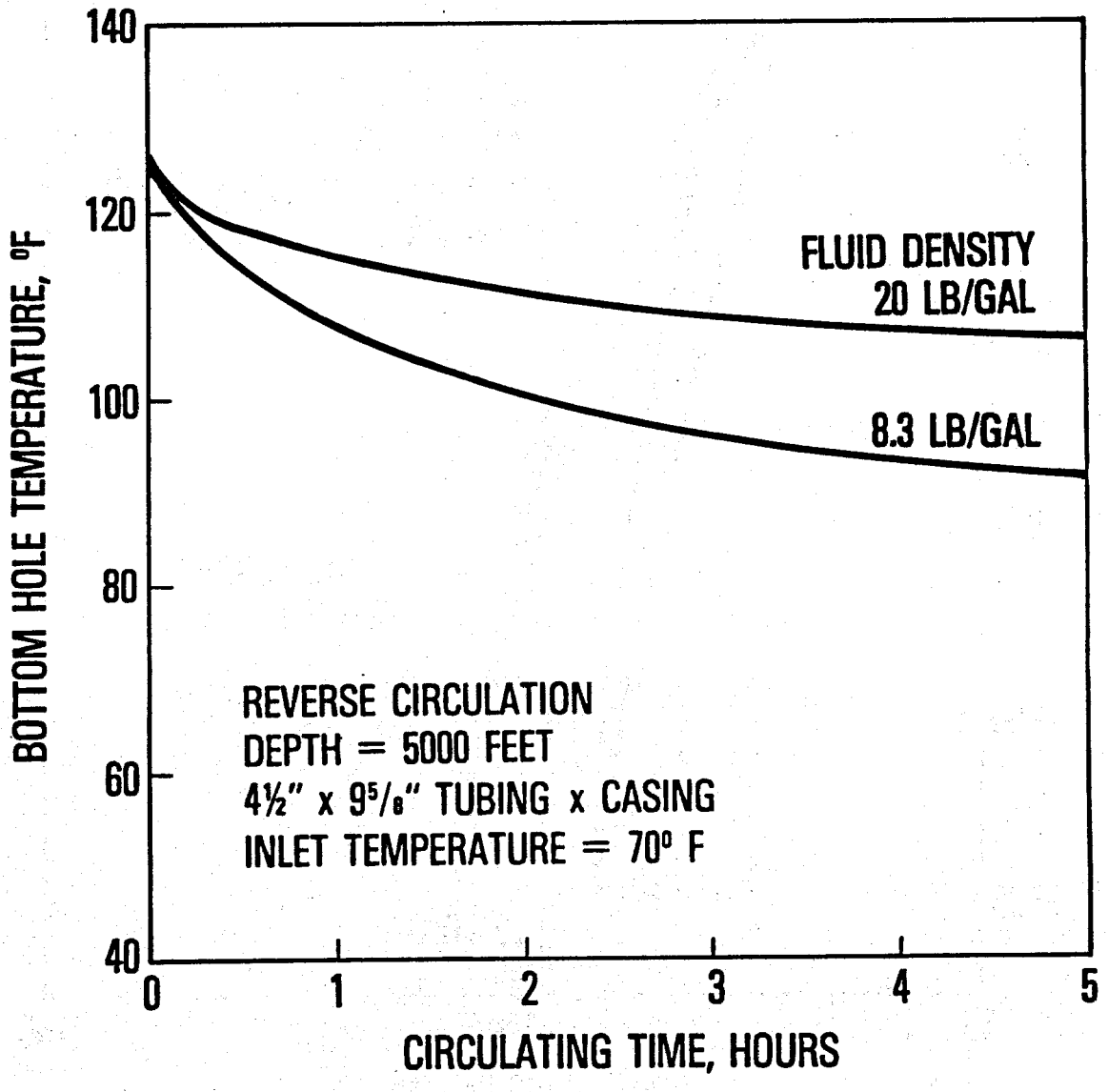

Figure 44

Sensitivity of Fluid Temperature Profile To Fluid Density

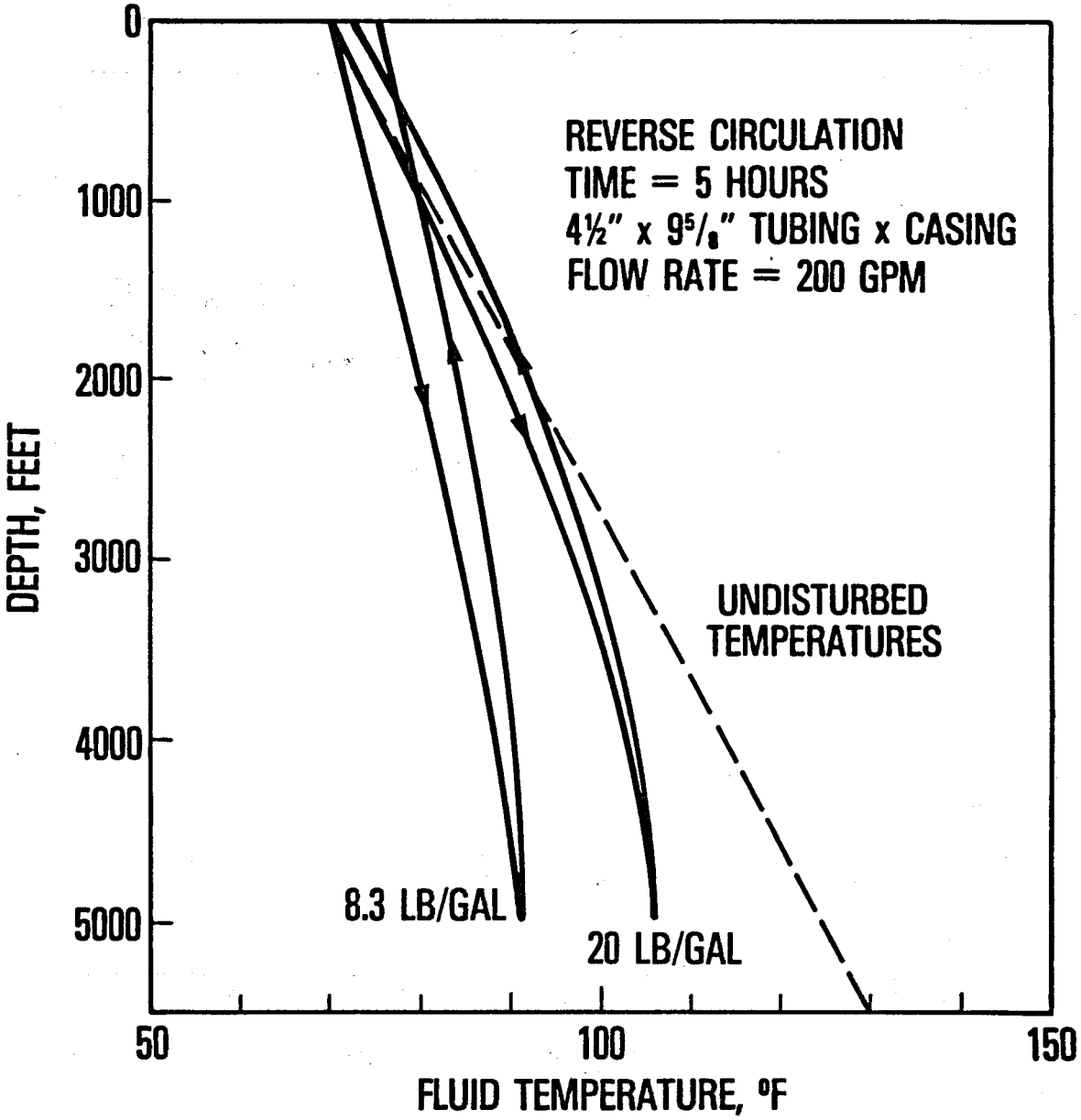

Figure 45

Sensitivity of Bottom Hole Temperature To Fluid Plastic Viscosity

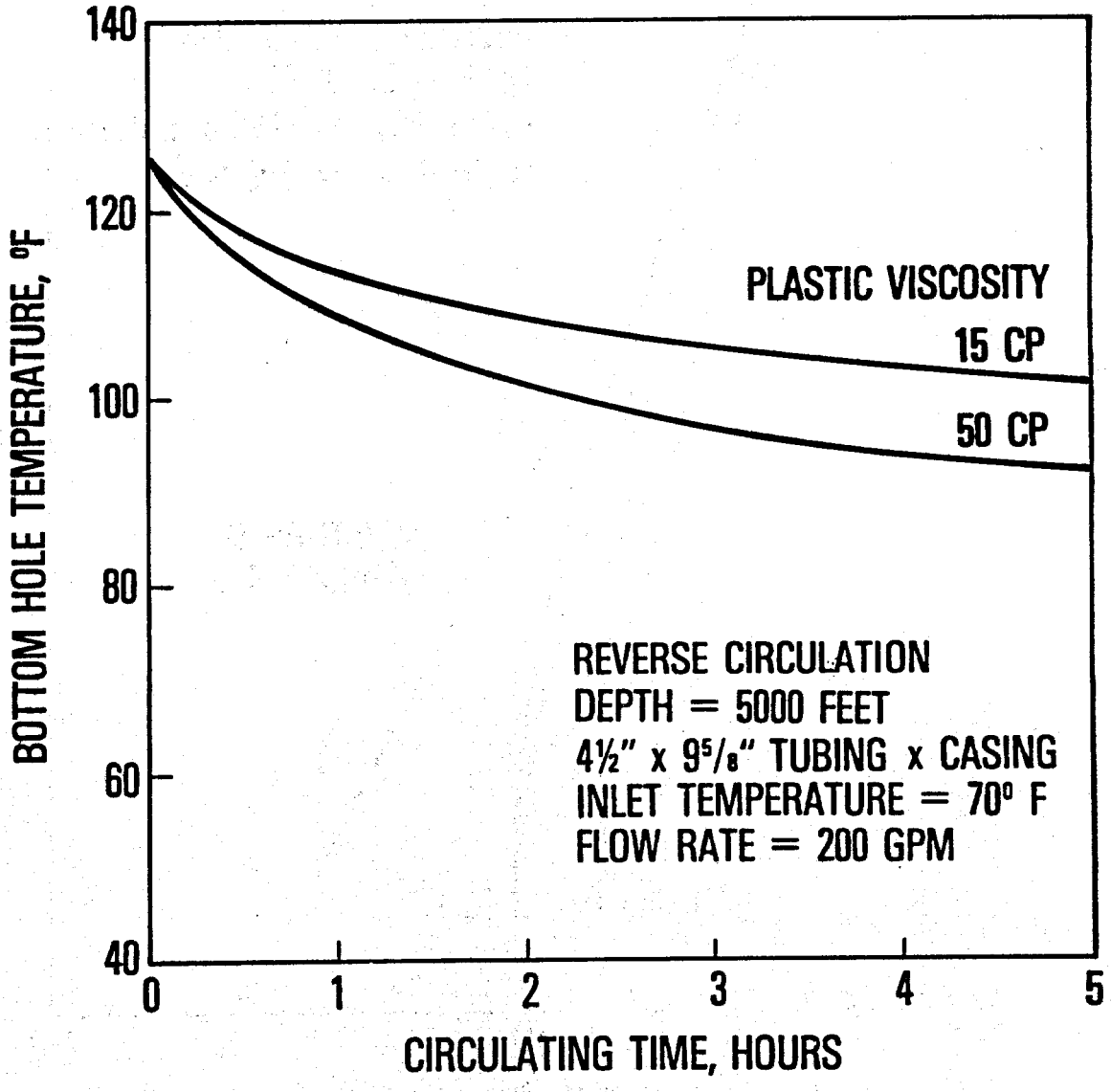

Figure 46

Sensitivity of Fluid Temperature Profile To Fluid Plastic Viscosity

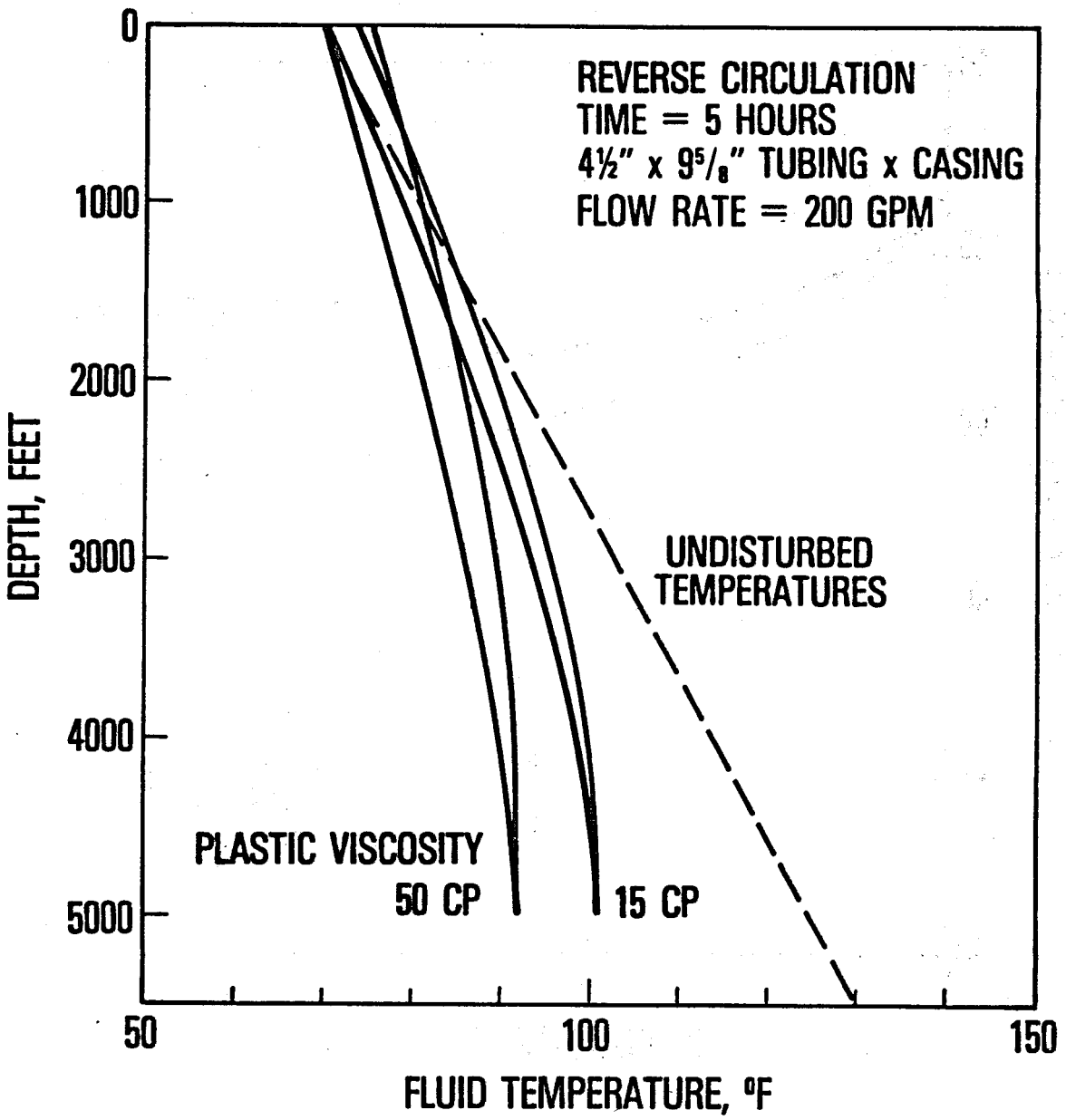

Figure 47

Sensitivity of Bottom Hole Temperature To Undisturbed Temperature Gradient

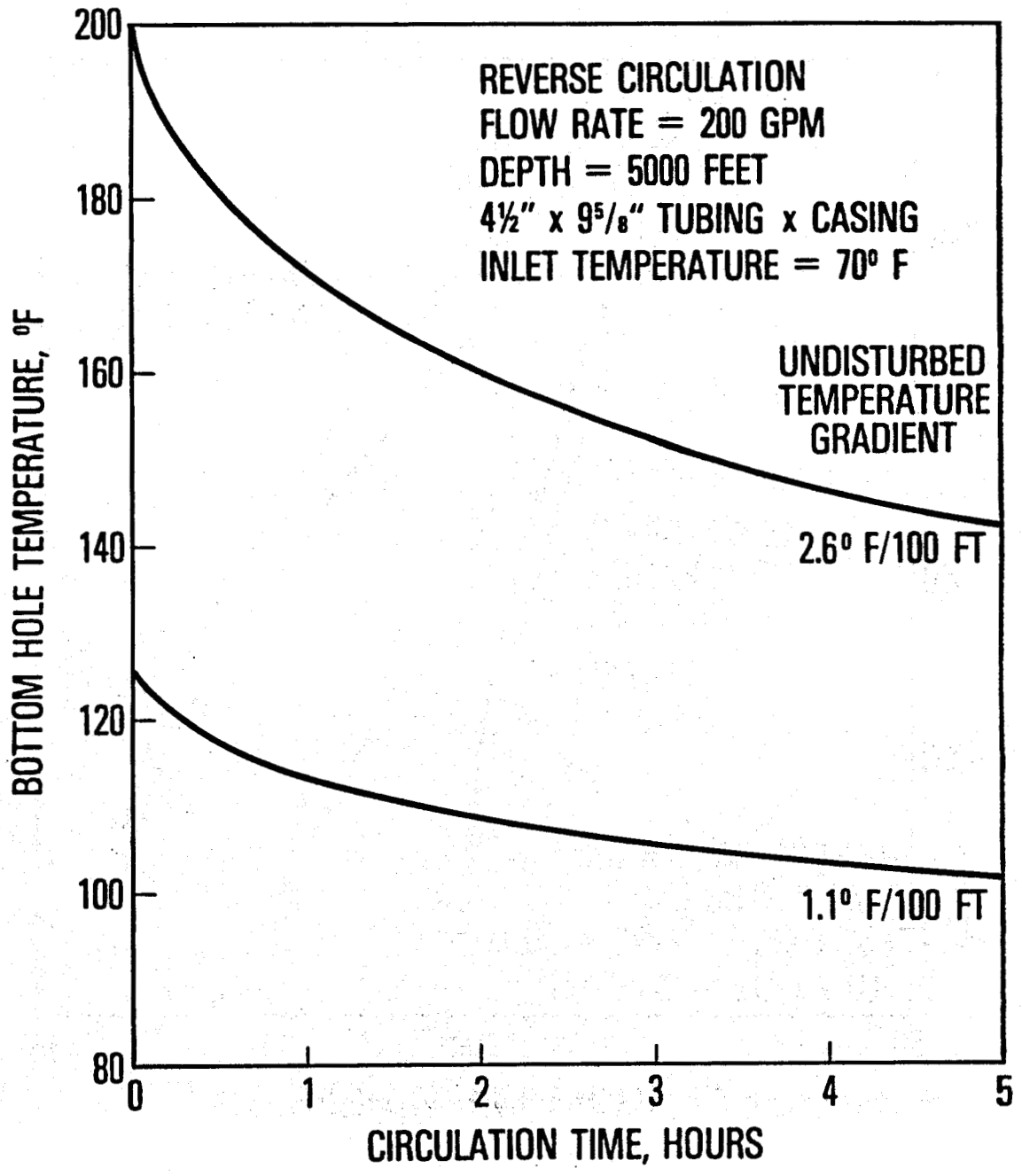

Figure 48

Sensitivity of Fluid Temperature Profile To Undistrurbed Temperature Gradient

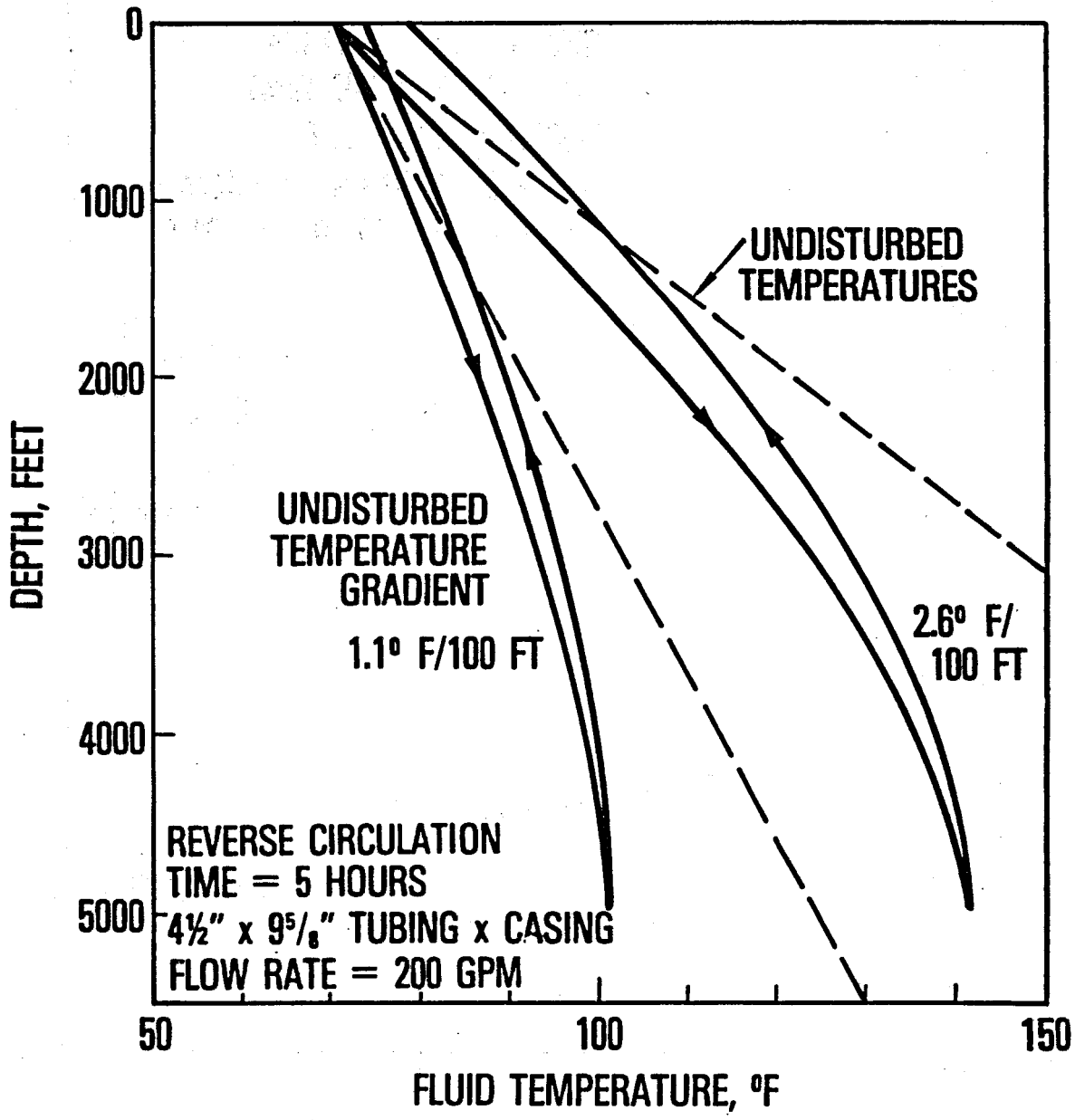

Figure 49

Sensitivity of Bottom Hole Temperature To Soil Thermal Conductivity

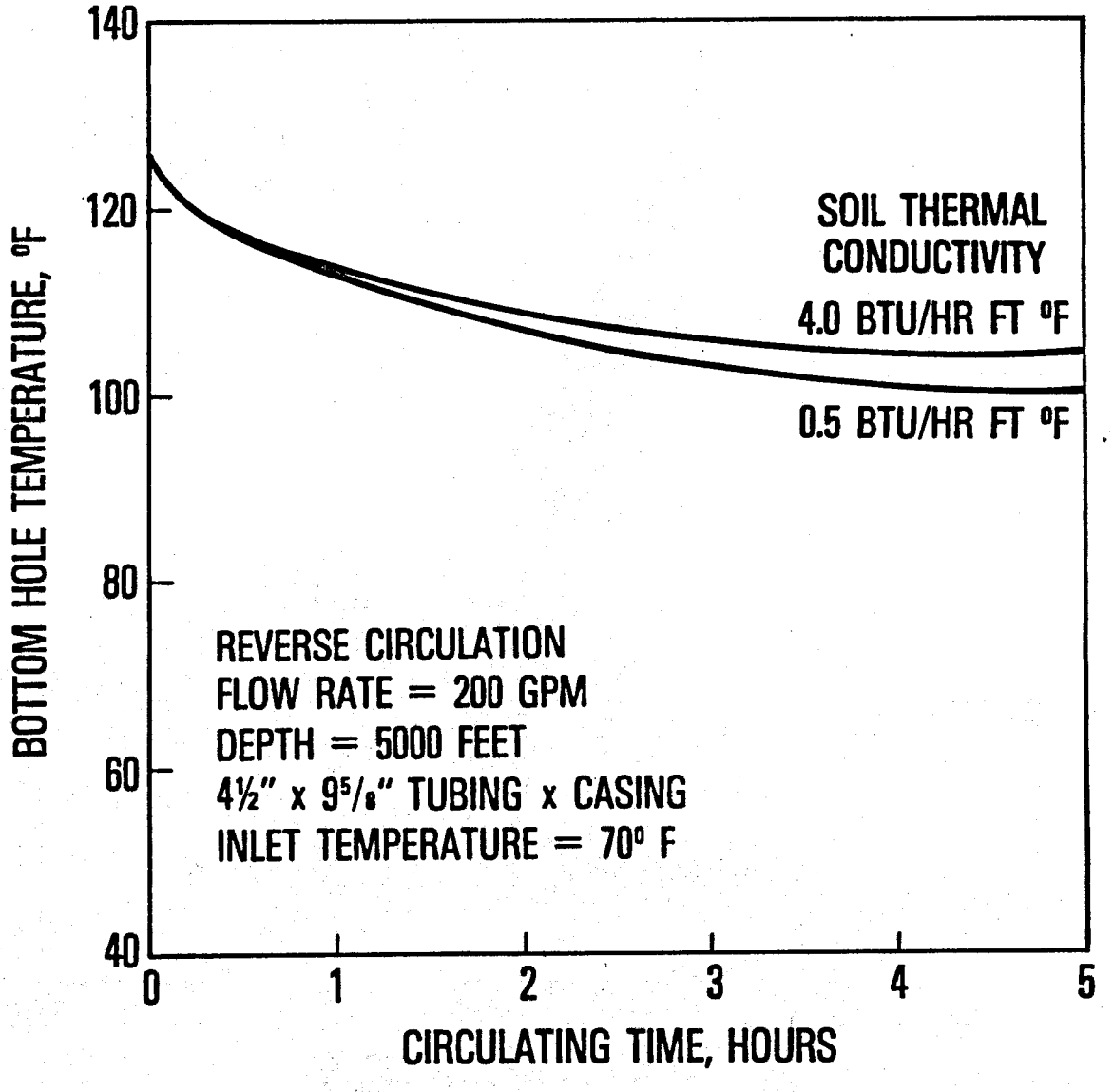

Figure 50

Sensitivity of Bottom Hole Temperature To Soil Thermal Conductivity

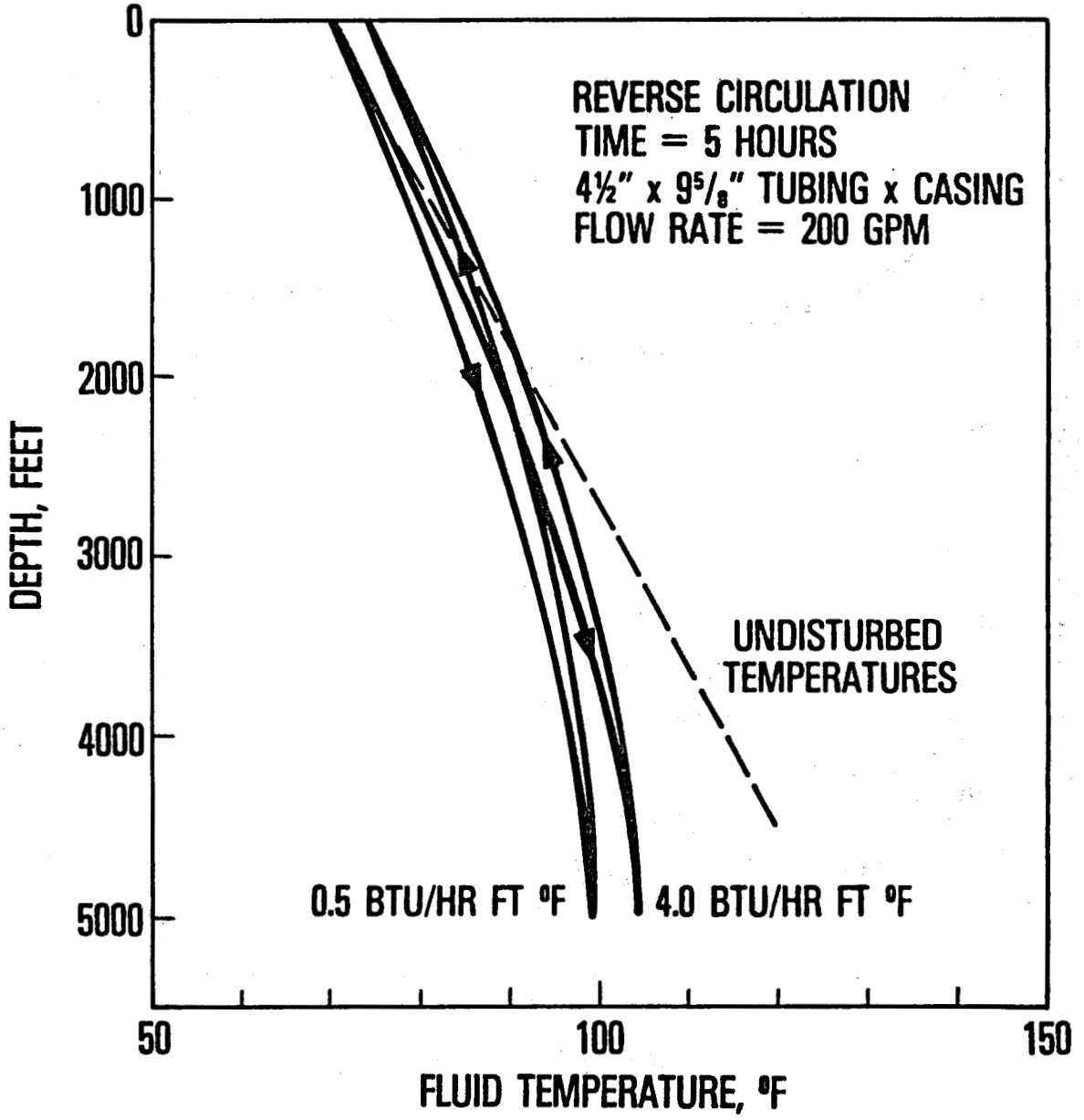

Figure 51

Sensitivity of Bottom Hole Temperature To Well Depth

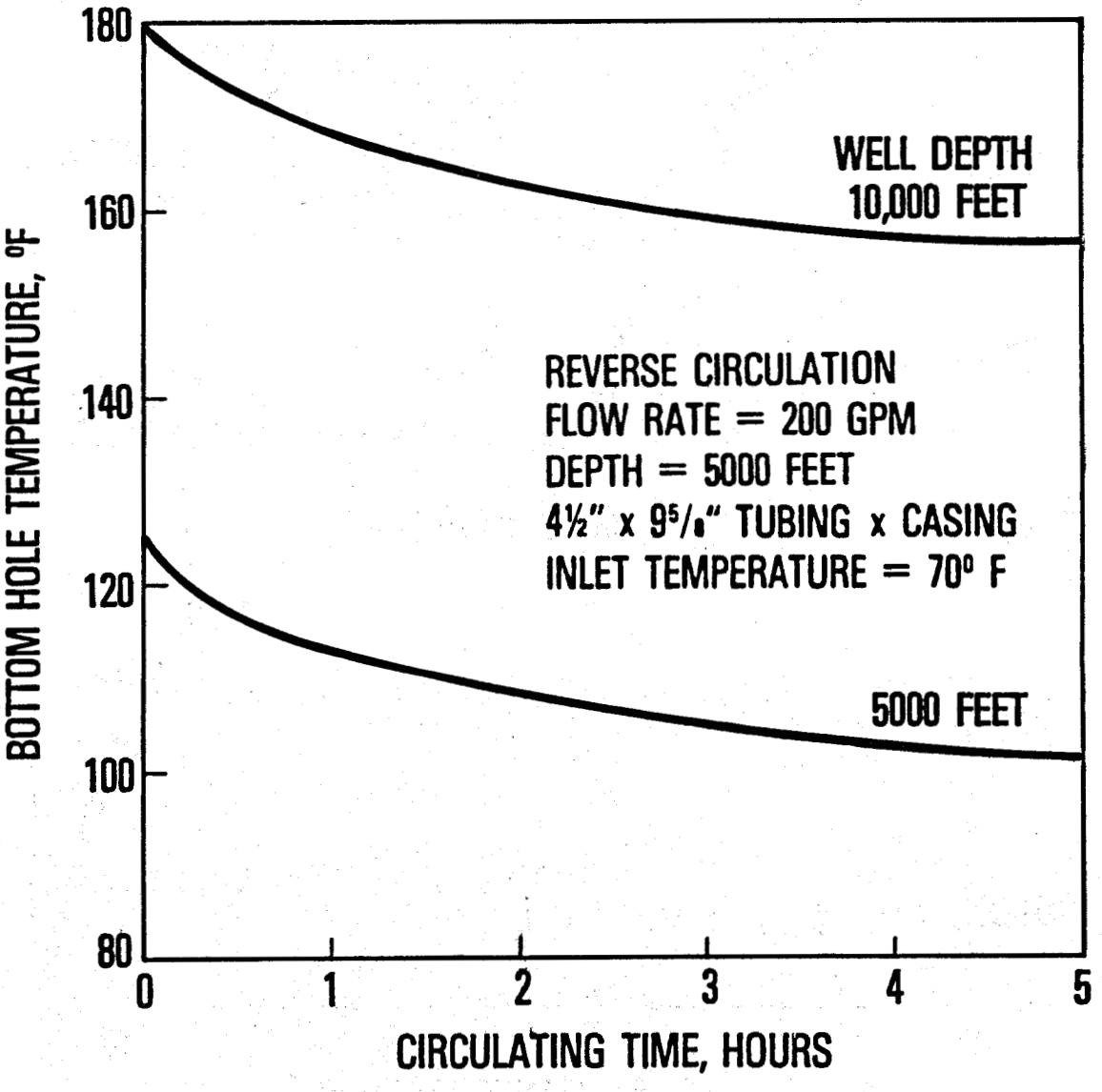

Figure 52

Sensitivity of Fluid Temperature Profile To Well Depth

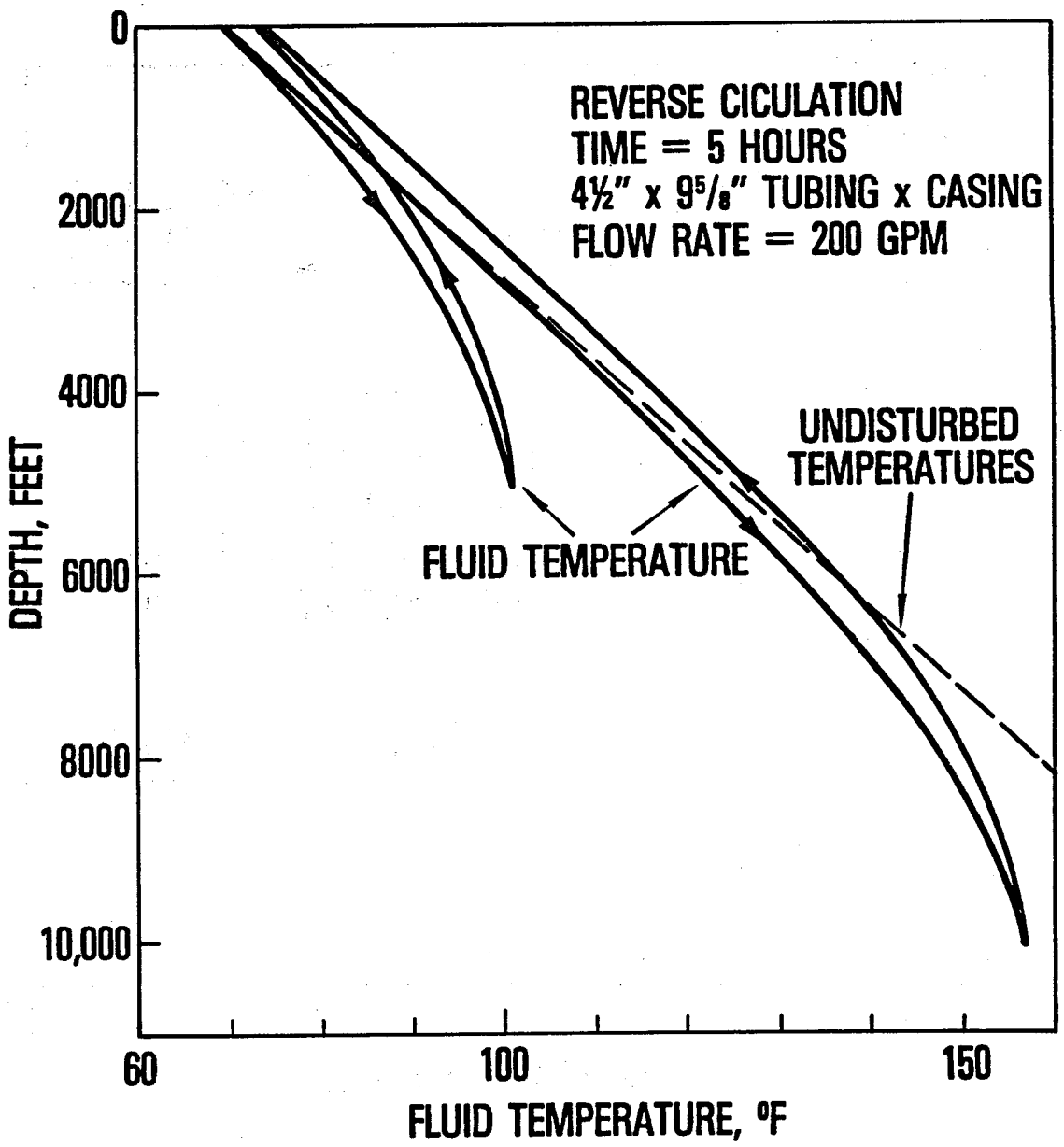

Figure 53

Sensitivity of Bottom Hole Temperature To Flow Rate

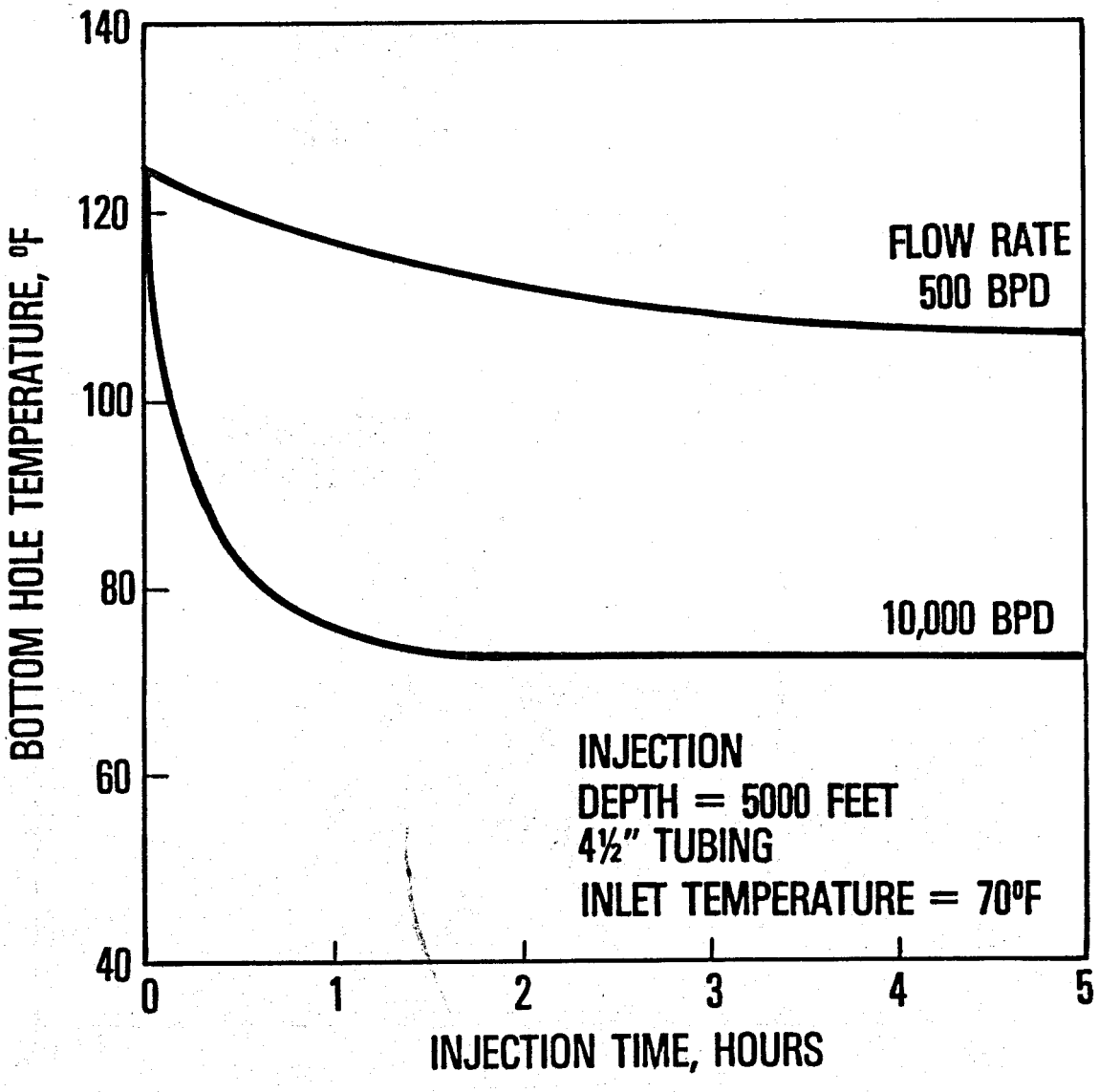

Figure 54

Sensitivity of Fluid Temperature Profile To Flow Rate

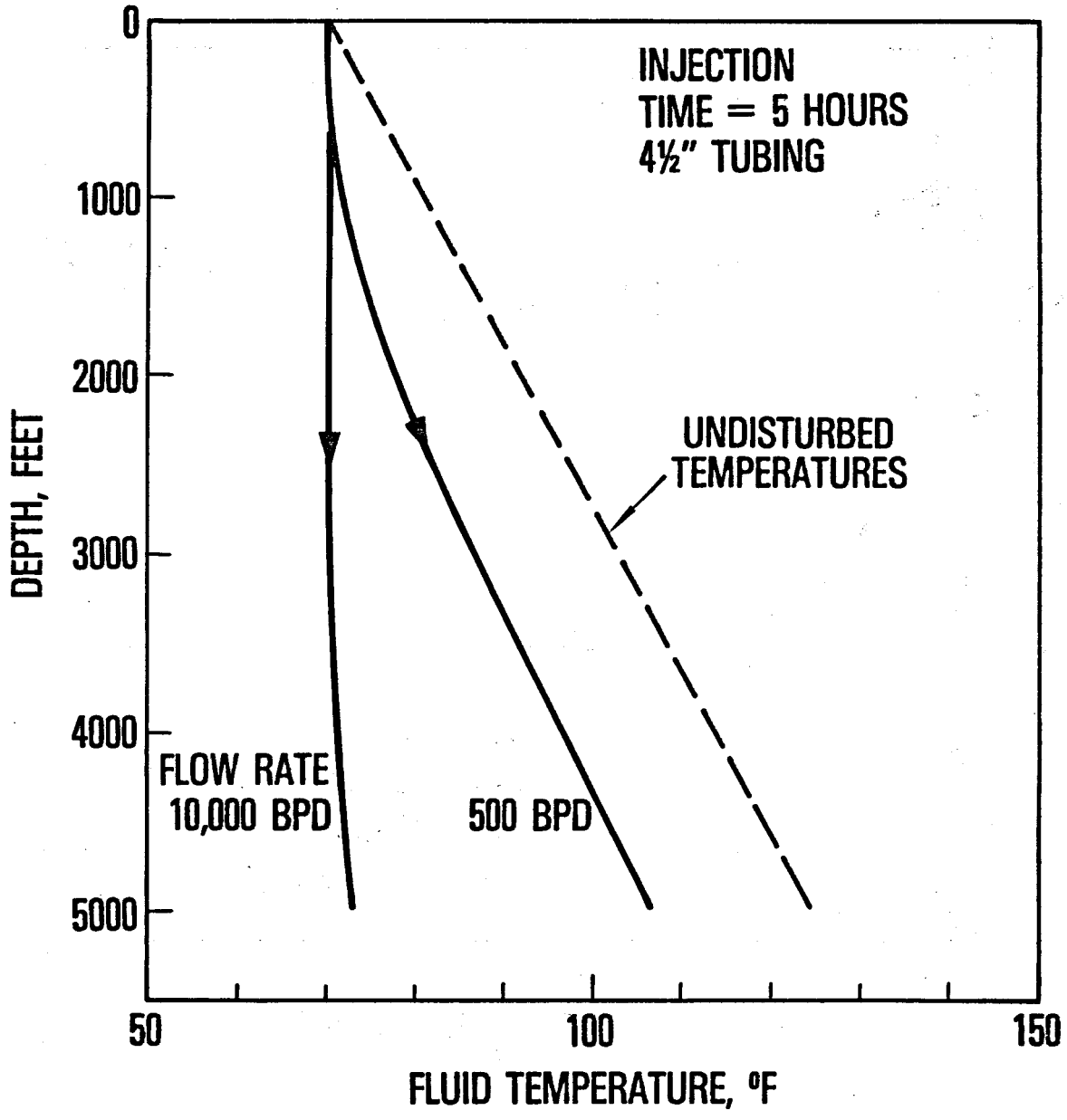

Figure 55

Sensitivity of Bottom Hole Temperature To Inlet Temperature

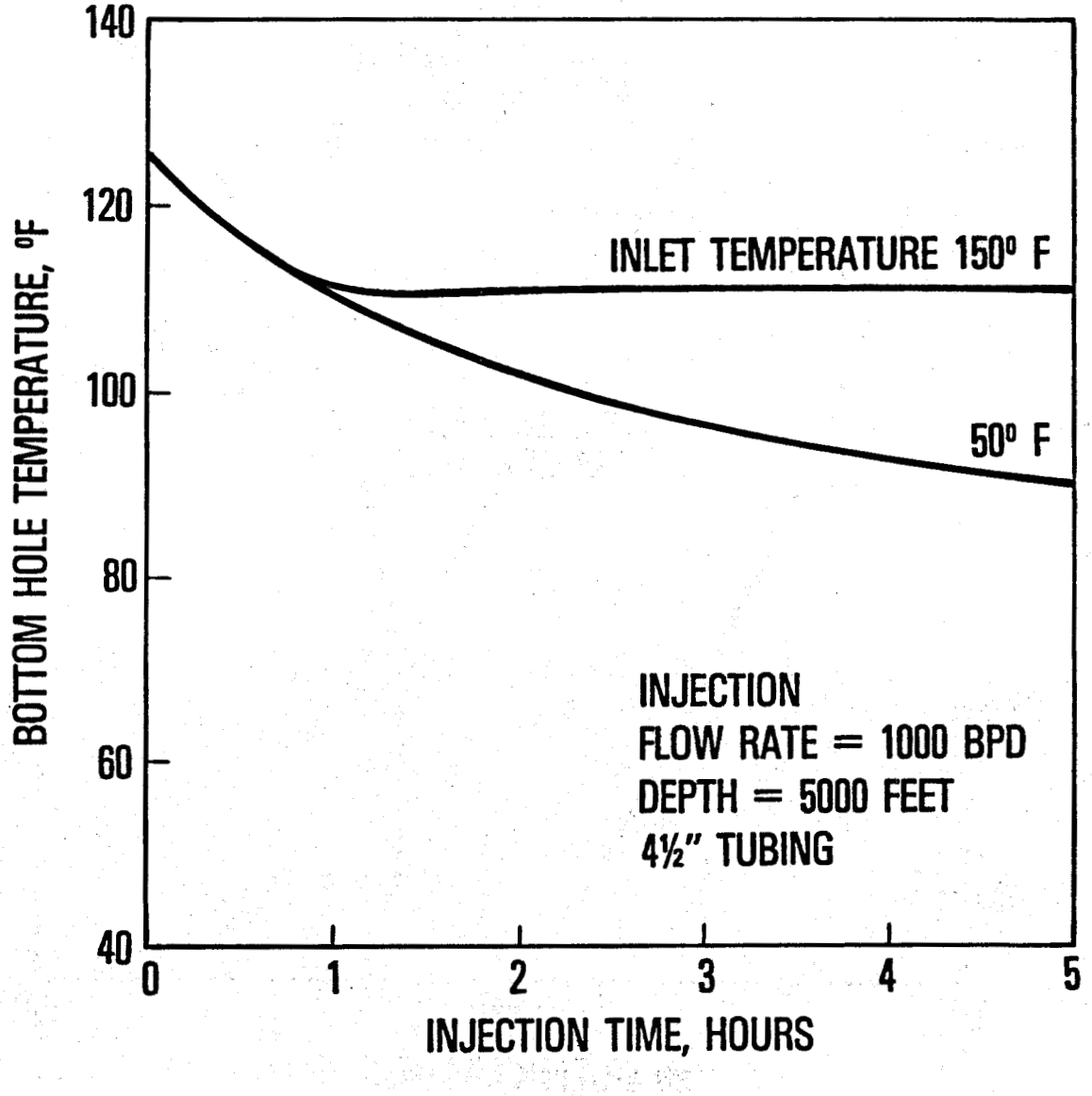

Figure 56

Sensitivity of Fluid Temperature Profile To Inlet Temperature

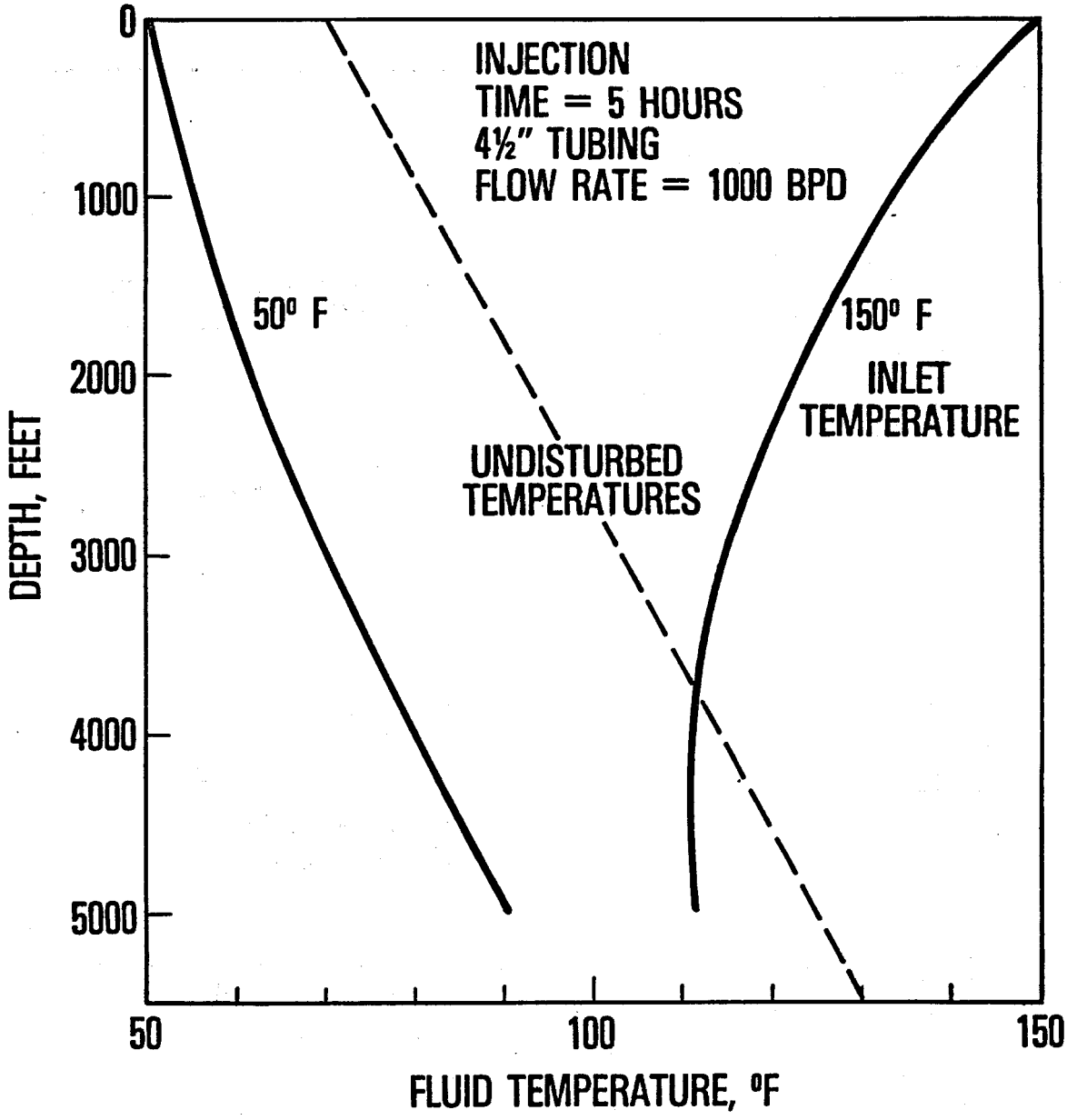

Figure 57

Sensitivity of Bottom Hole Temperature To Fluid Density

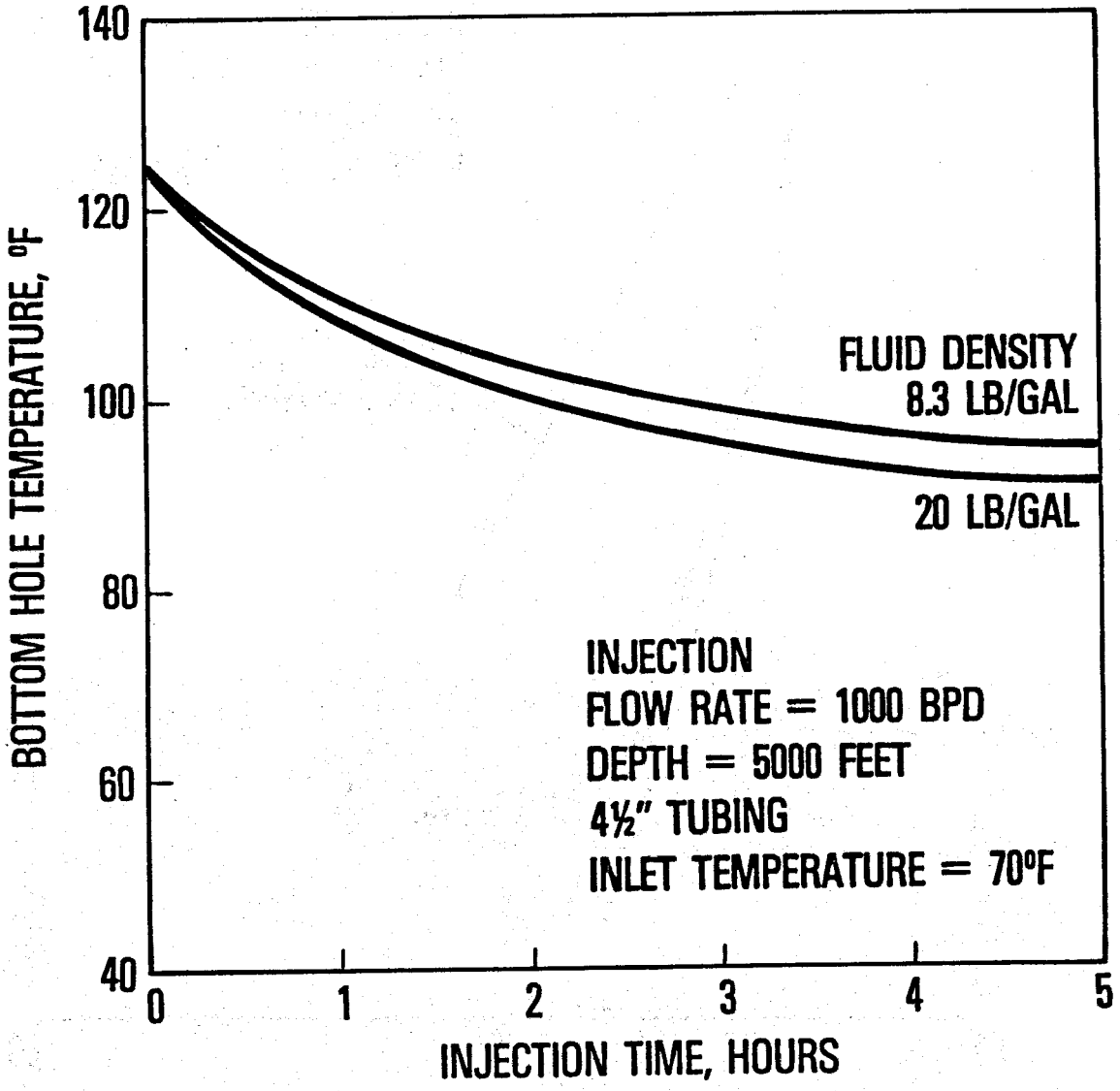

Figure 58

Sensitivity of Fluid Temperature Profile To Fluid Density

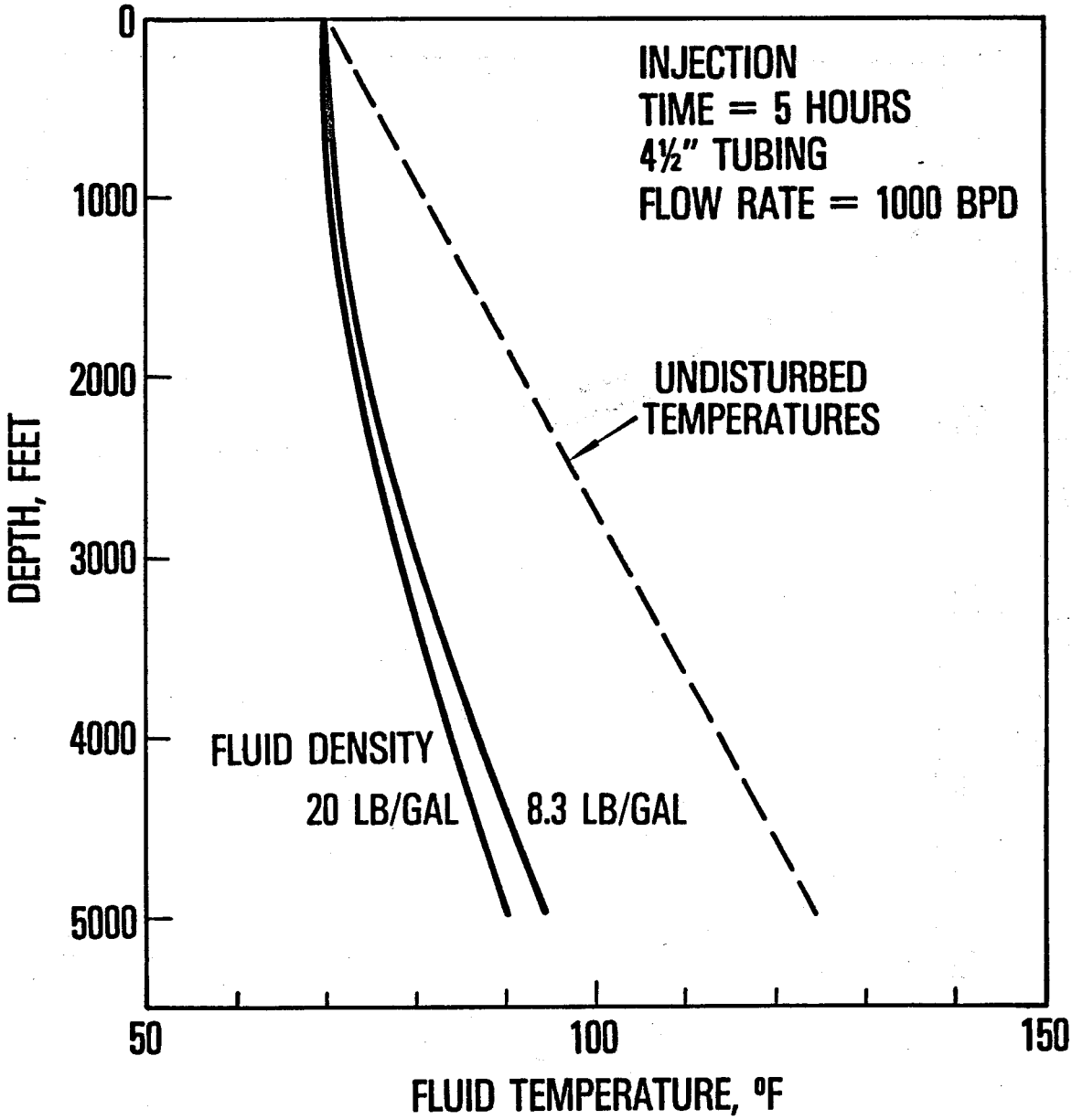

Figure 59

Sensitivity of Bottom Hole Temperature To Undisturbed Temperature Gradient

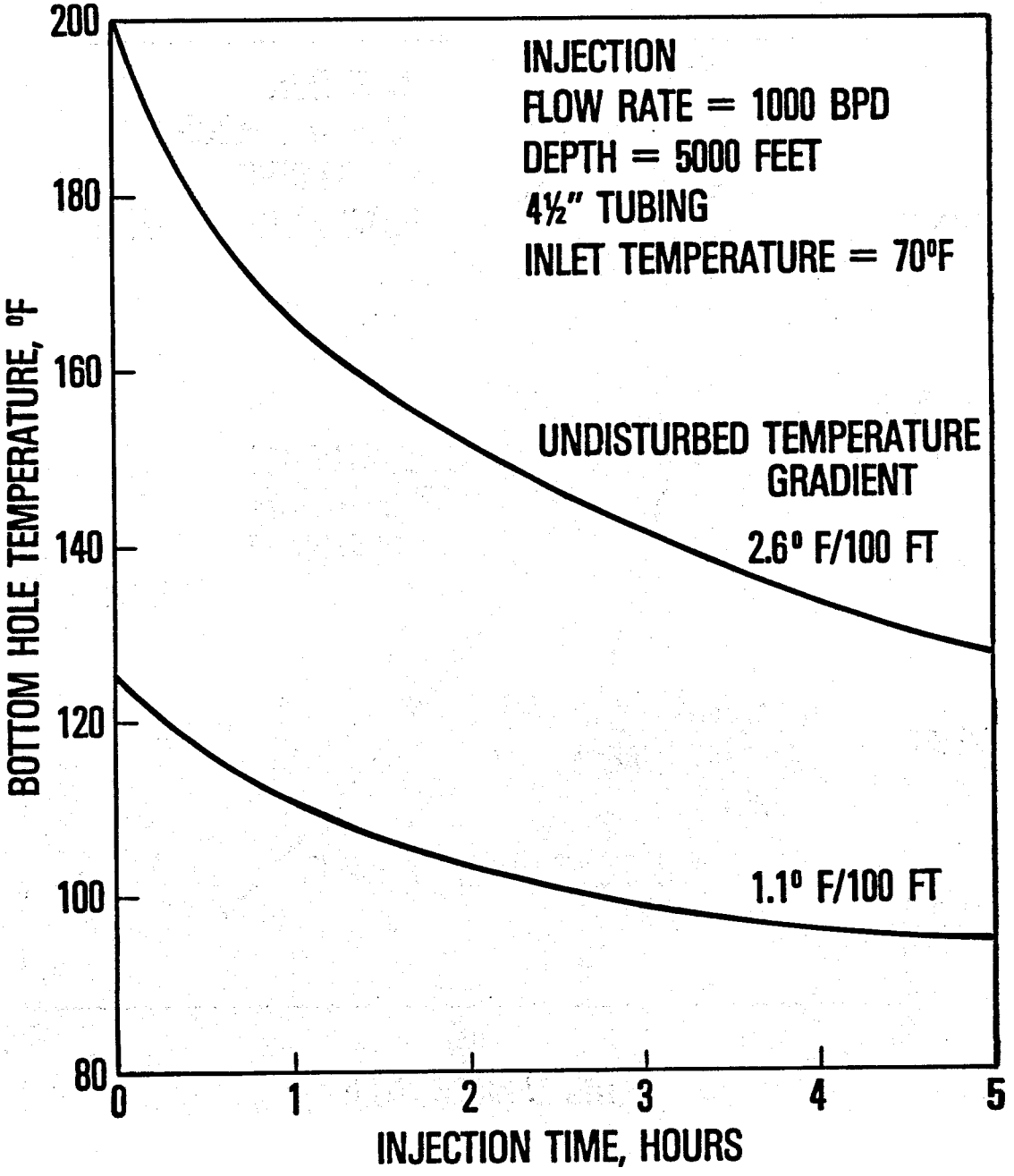

Figure 60

Sensitivity of Fluid Temperature Profile To Undistrurbed Temperature Gradient

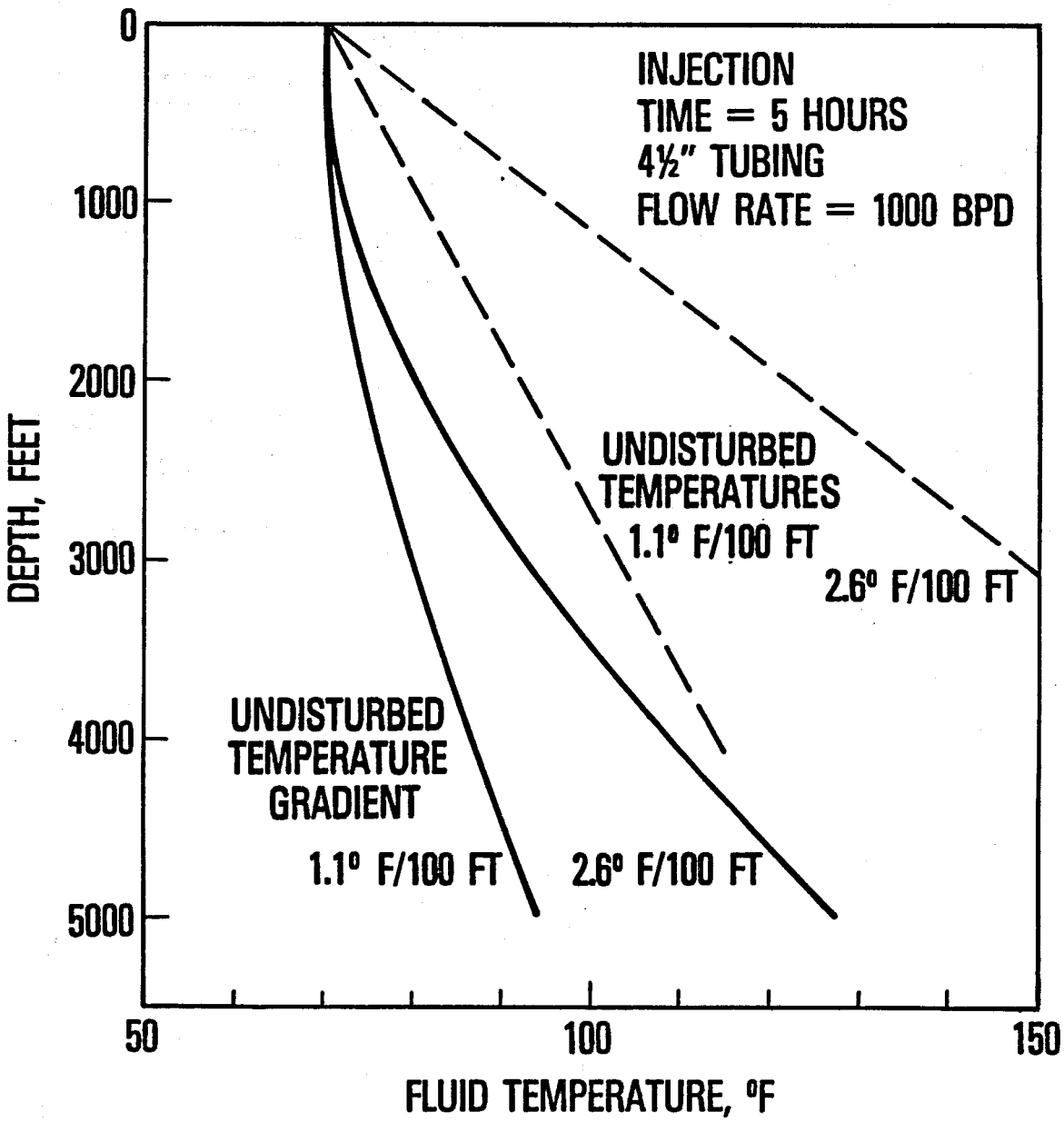

Figure 61

Sensitivity of Bottom Hole Temperature To Injection Depth

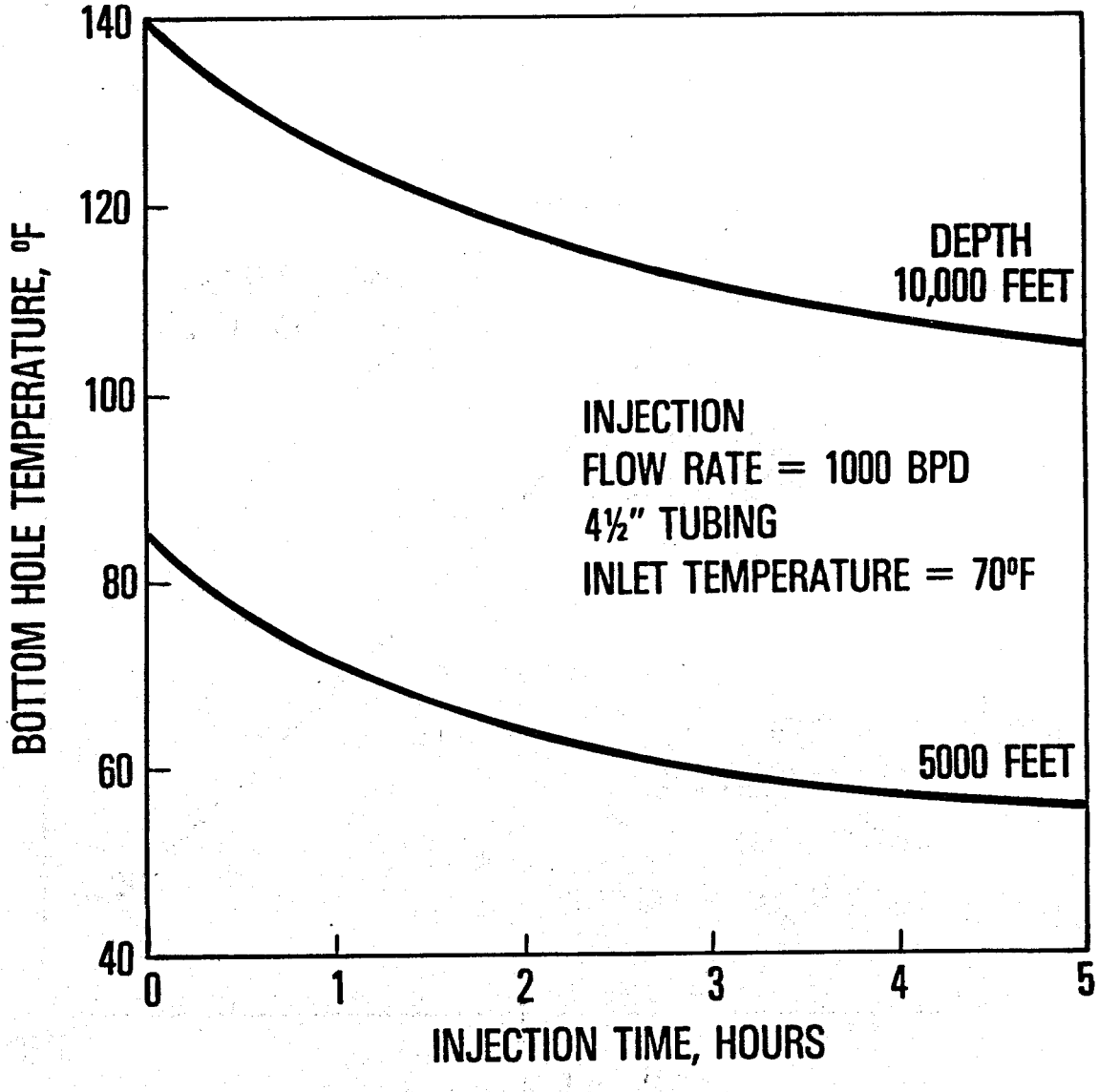

Figure 62

Sensitivity of Fluid Temperature Profile To Injection Depth

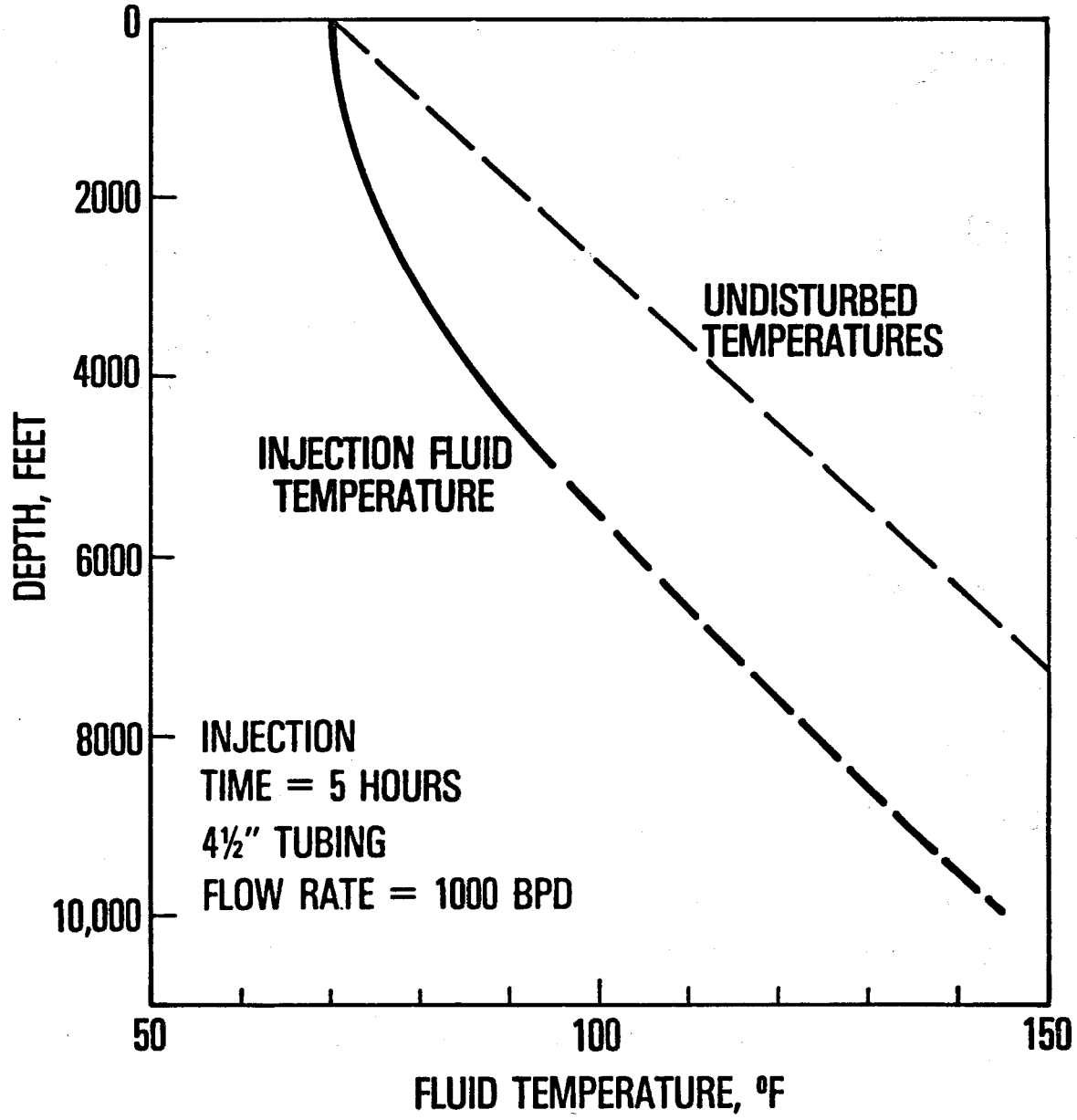

Figure 63

Sensitivity of Surface Temperature To Flow Rate

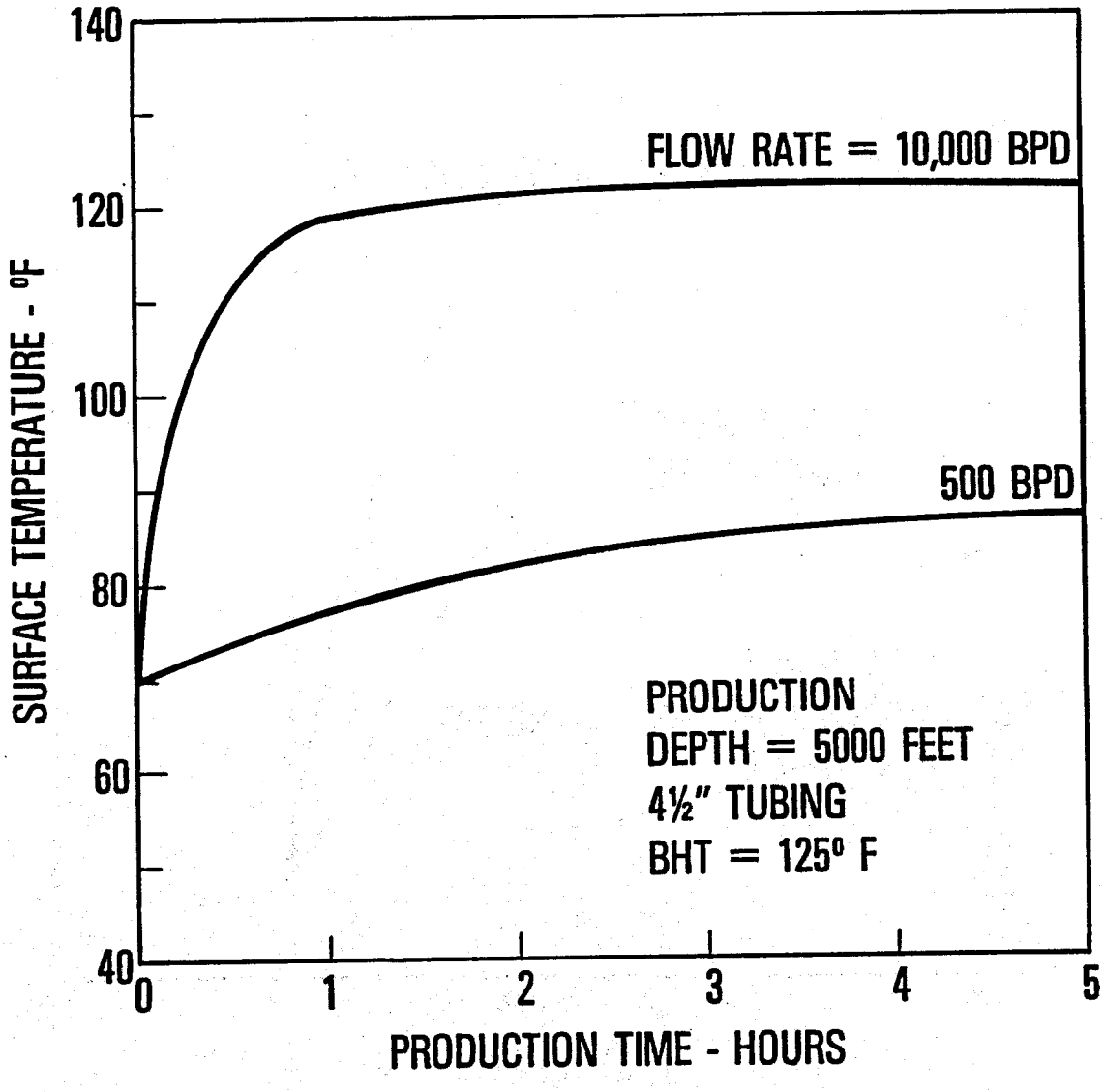

Figure 64

Sensitivity of Fluid Temperature Profile To Flow Rate

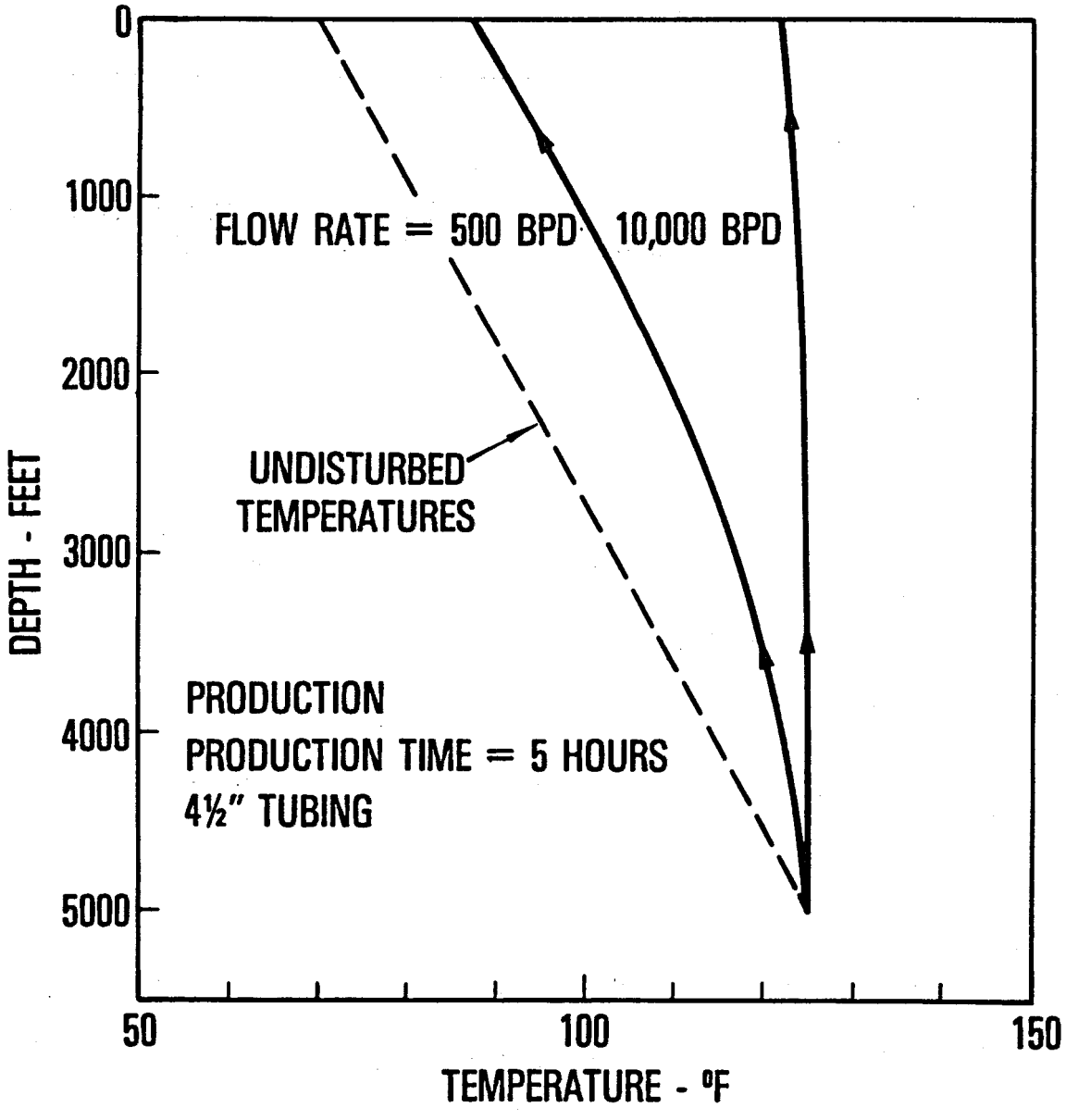

Figure 65

Sensitivity of Surface Temperature To Production Fluid Density

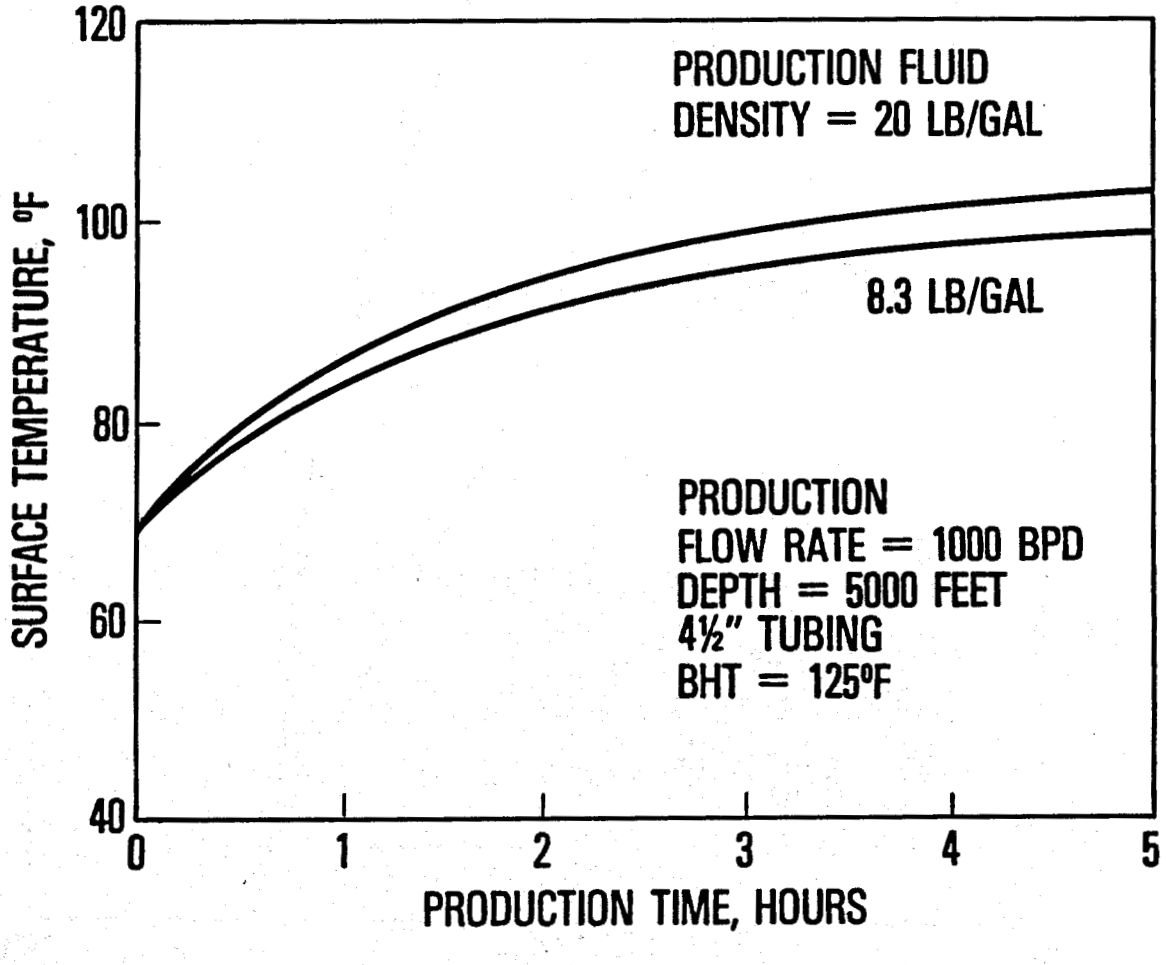

Figure 66

Sensitivity of Fluid Temperature Profile To Production Fluid Density

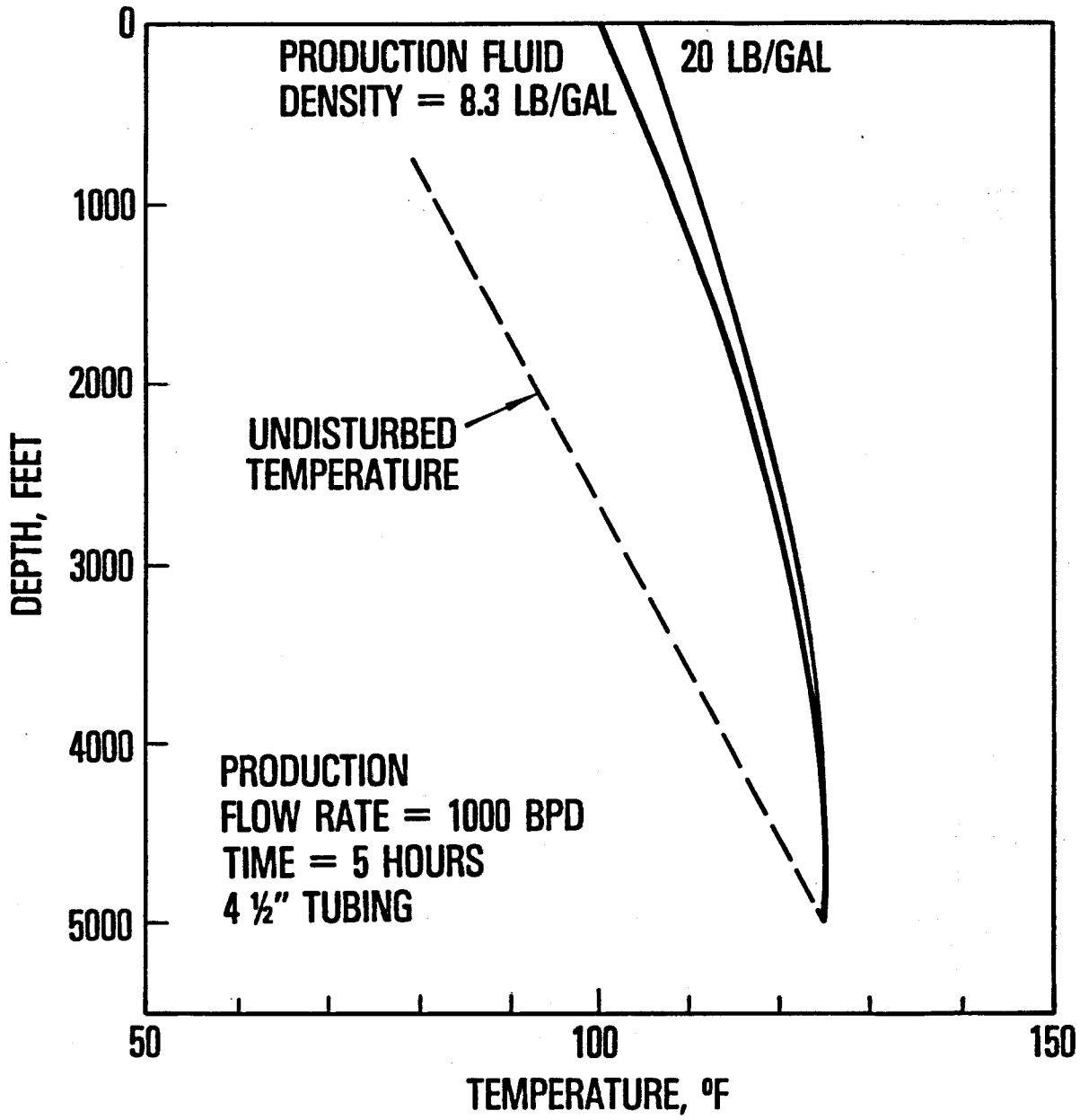

Figure 67

Sensitivity of Surface Temperature To Undisturbed Geothermal Gradient

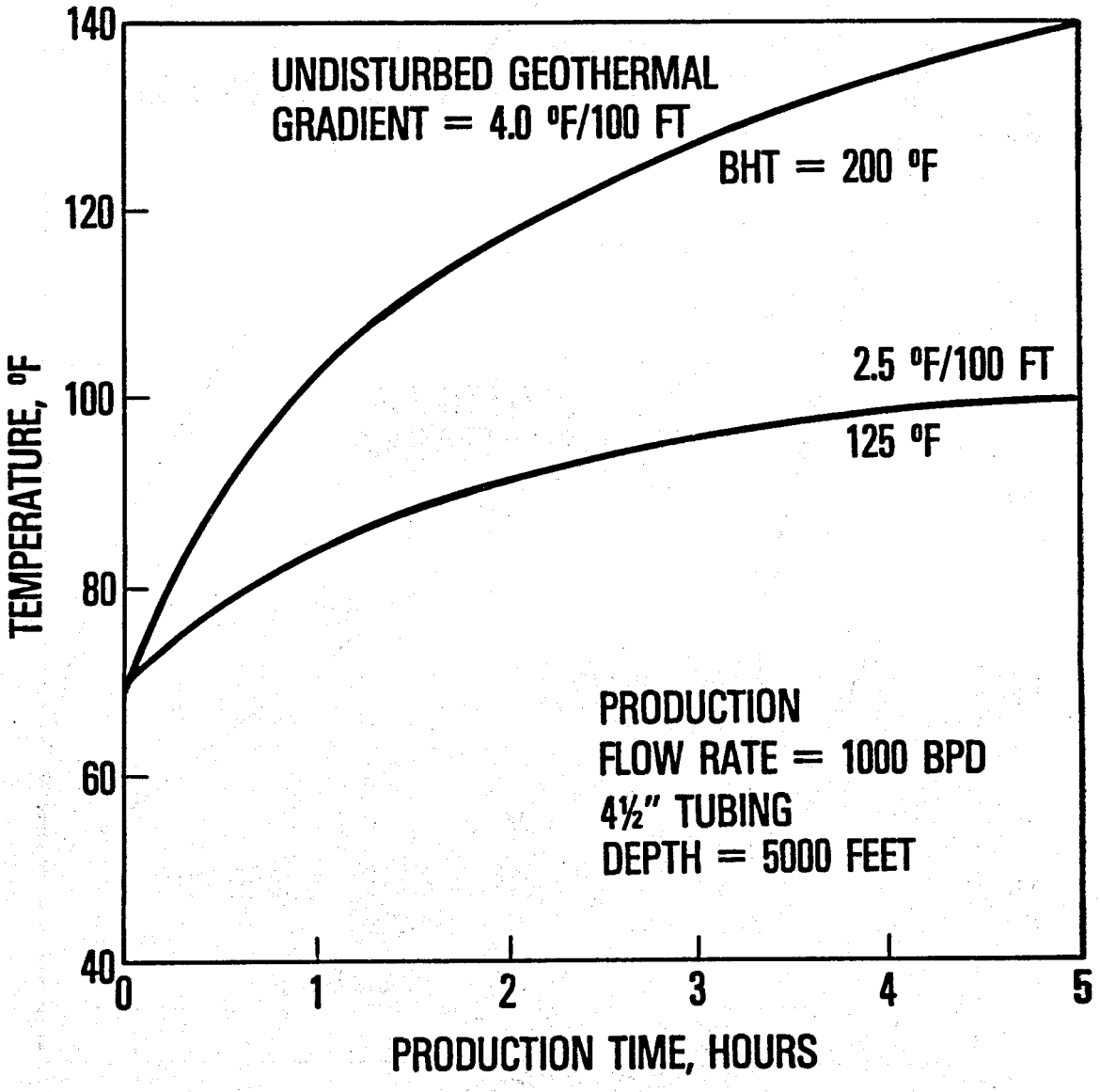

Figure 68

Sensitivity of Fluid Temperature Profile To Undisturbed Geothermal Gradient

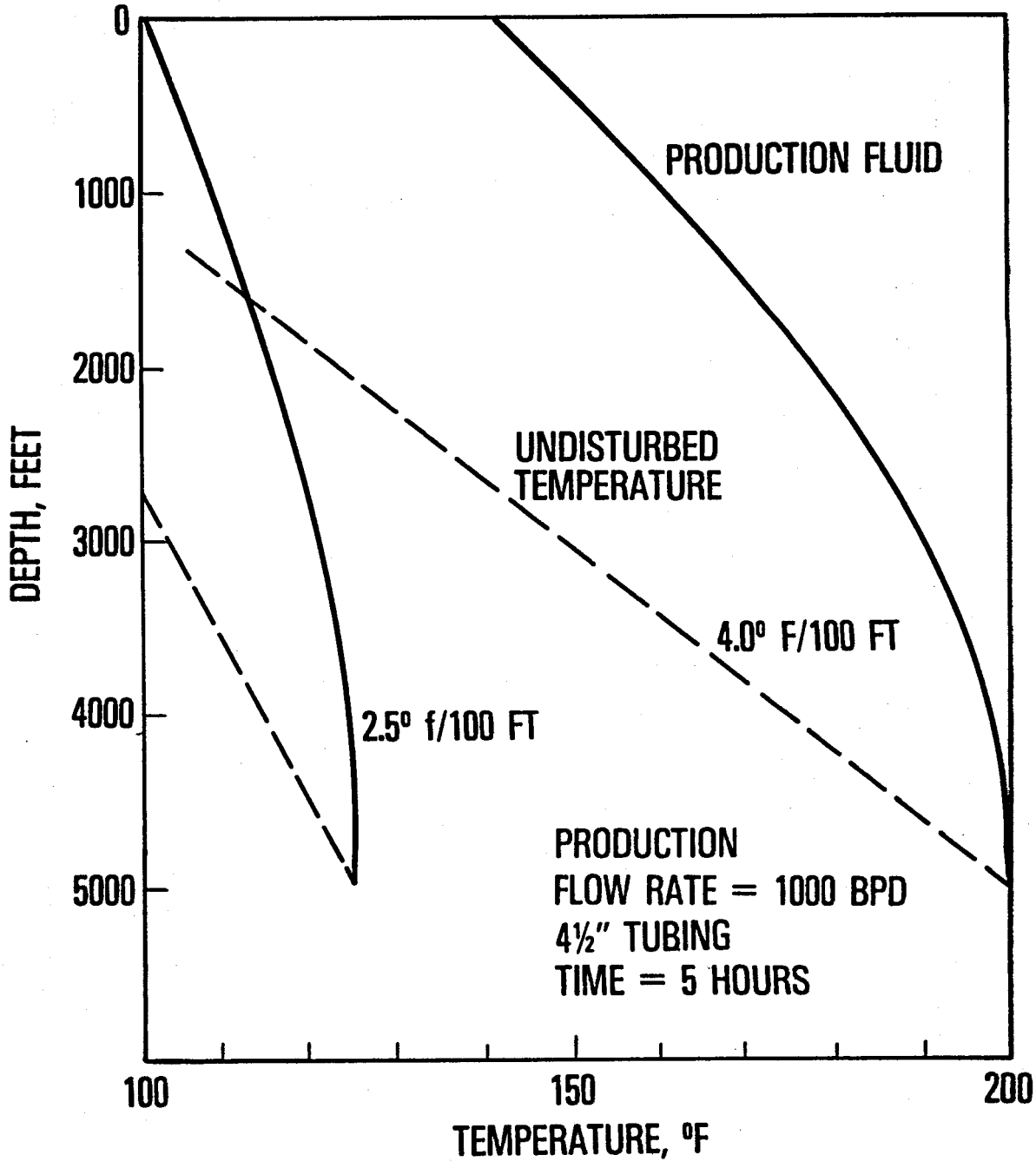

Figure 69

Sensitivity of Surface Temperature To Depth

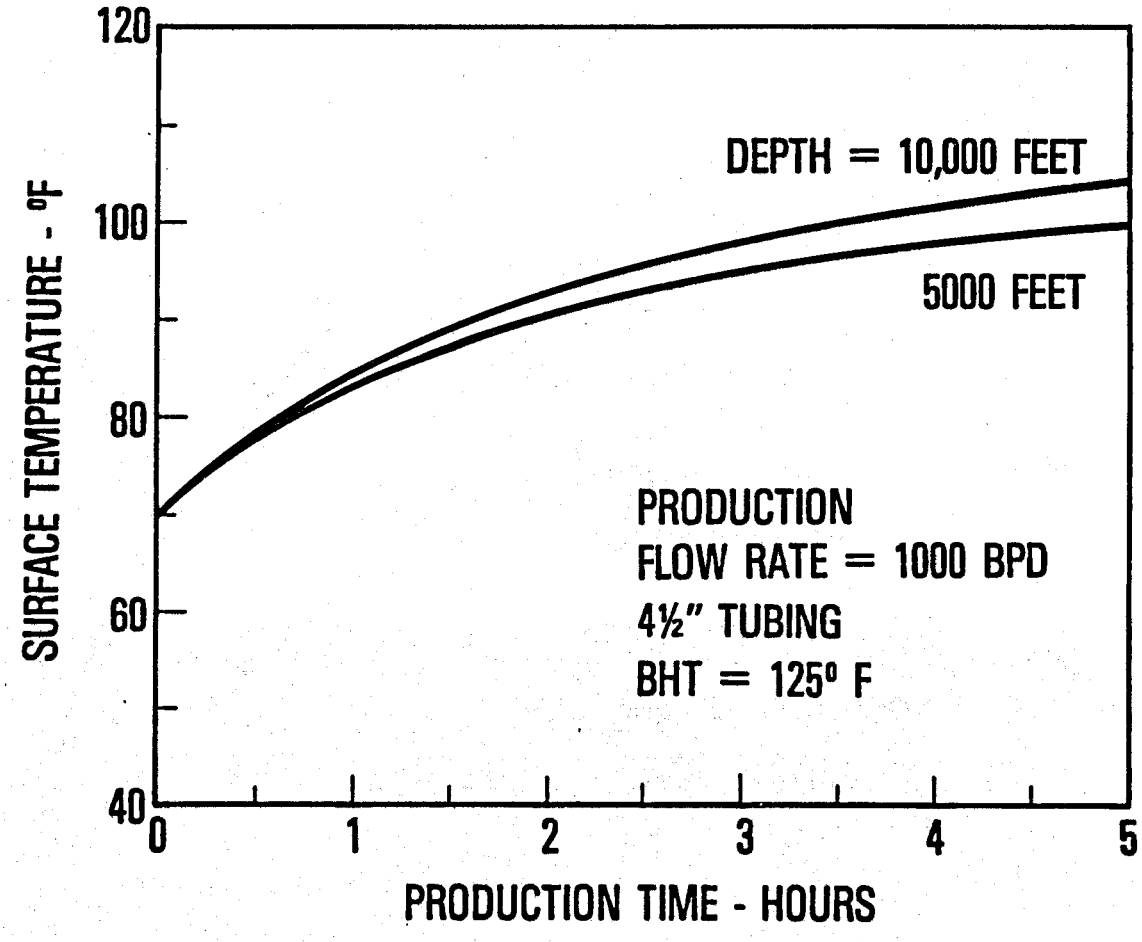

Figure 70

Sensitivity of Fluid Temperature Profile To Depth

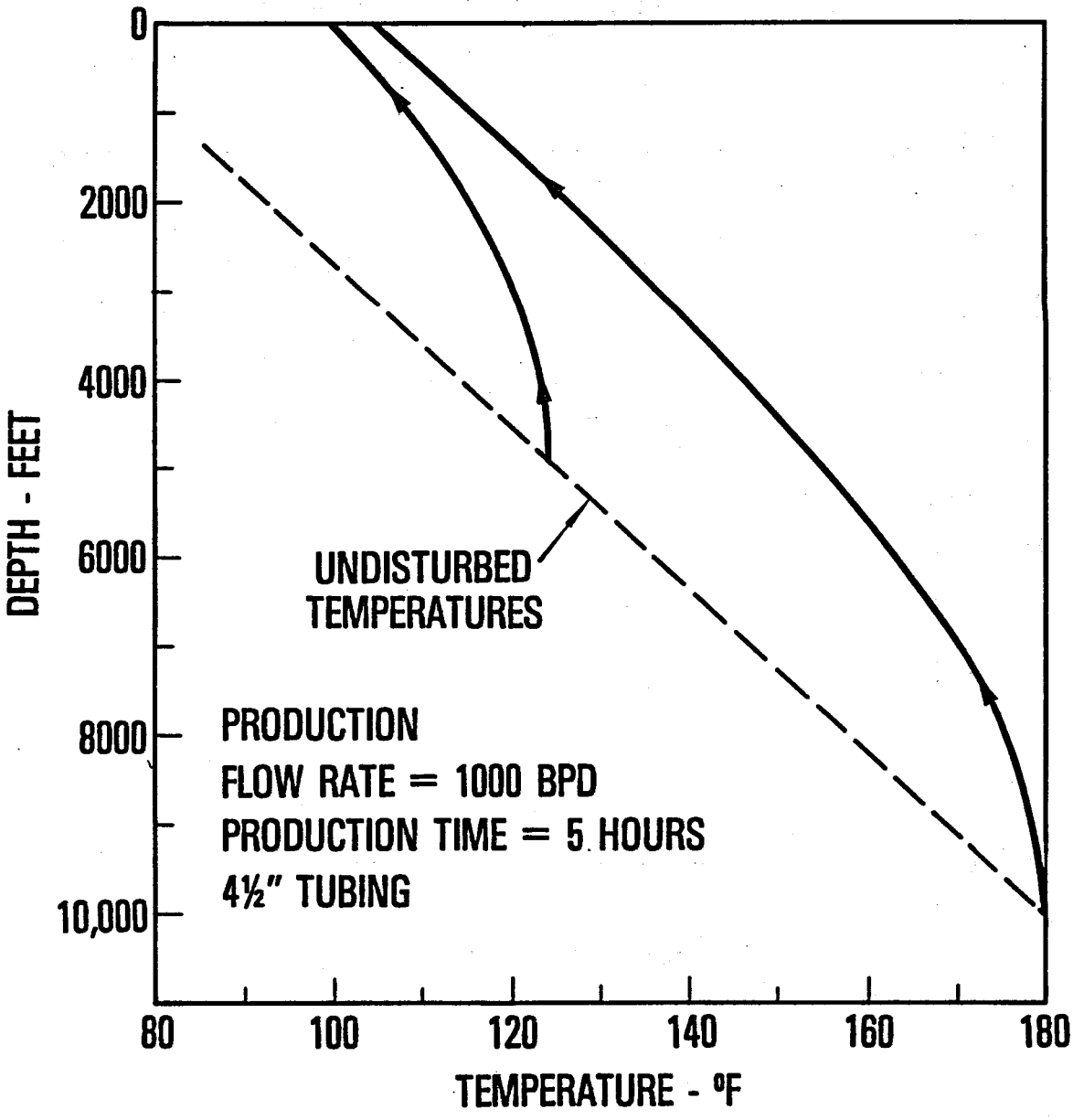

Distribution:
TID-4500-R66 UC-66c (567)

400	C. Winter*
1000	G. A. Fowler*
1100	C. D. Broyles*
1130	H. E. Viney*
2000	E. D. Reed*
2300	J. C. King*
2320	K. Gillespie*
2325	R. E. Fox*
2328	J. H. Barnette*
2500	J. C. Crawford*
2513	W. B. Leslie
4000	A. Narath*
4200	G. Yonas*
4300	R. L. Peurifoy, Jr.*
4400	A. W. Snyder*
4443	P. Yarrington*
4500	E. H. Beckner*
4700	J. H. Scott
4710	G. E. Brandvold*
4720	V. L. Dugan*
4730	H. M. Stoller
4740	R. K. Traeger
4741	S. G. Varnado (25)
4742	A. F. Veneruso
4743	H. C. Hardee
4744	H. M. Dodd
4744	C. C. Carson
5000	J. K. Galt*
5512	A. Ortega (10)
5530	W. Herrmann*
5532	B. M. Butcher*
5533	J. M. McGlaun
5600	D. B. Schuster*
5620	M. M. Newsom*
5800	R. S. Claassen
5810	R. G. Kepler*
5812	C. J. M. Northrup, Jr.*
5812	B. T. Kenna
5813	P. B. Rand
5830	M. J. Davis*
5831	N. J. Magnani*
5832	R. W. Rohde*
5832	R. J. Salzbrenner
5833	J. L. Ledman*
5833	J. L. Jellison
3140	T. L. Werner (5)
3151	W. L. Garner (3)
8266	E. A. Aas

* Only abstracts distributed. Full report available upon request if there is interest.